Chemical Engineering Journal

Supercritical fluid and cocrystallization technologies for designing antimicrobial food packaging PLA nanocomposite foams loaded with eugenol cocrystals with prolonged release

--Manuscript Draft--

Manuscript Number:	CEJ-D-23-20045R2
Article Type:	Research Paper
Keywords:	Antimicrobial packaging; eugenol-phenazine cocrystal; C30B; Cocrystallization; Supercritical fluid technology
Corresponding Author:	Adrián Rojas University of Santiago Chile Santiago de Chile, CHILE
First Author:	Adrián Rojas
Order of Authors:	Adrián Rojas
	Dusan Misic, PhD
	Irena Zizovic, PhD
	Carol López de Dicastillo, PhD
	Eliezer Velásquez, PhD
	Aleksandra Rajewska
	Bastián Rozas
	Luciano Catalán
	Cristian Patiño Vidal, PhD
	Abel Guarda
	María José Galotto
Abstract:	Searching for effective strategies to modify the release rate of essential oil derivatives is one of the main challenges in designing prolonged-release antimicrobial food packaging materials. Herein, supercritical fluid technology and cocrystallization engineering were used to develop novel eugenol (EU) prolonged-release poly (lactic acid) (PLA) nanocomposite foams. Eugenol-phenazine (EU-PHE) cocrystals, produced by a solvent-free mechanochemical method, were incorporated by supercritical solvent impregnation (SSI) inside PLA nanocomposite foams with different contents of Cloisite30B® (C30B). The effect of the cocrystallization process and C30B content on the EU release kinetics and its relation with their antimicrobial activity by direct contact (anti-attachment) and release in broth culture were studied. The deposition of isolated spherical-shaped micrometric EU-PHE cocrystal particles with 0.8 μm average diameter inside the pores of PLA foams was evidenced by XRD, SEM, DSC, and TGA analyses. The release mechanism of EU and its cocrystal was defined as a quasi-Fickian diffusion process successfully described by Korsmeyer-Peppas model with release rate constants up to 3.6-fold lower than the release rate constant of pure EU. The impregnated foam samples completely inhibited the attachment of Listeria monocytogenes and Salmonella Enteritidis and provided prolonged antimicrobial activity in broth culture against both food-borne pathogens. This study suggests a new, environmentally friendly method for designing sustained-release antimicrobial food packaging materials.
Response to Reviewers:	Response to the reviewers' comments The authors thank Reviewer 2 and the Editor for constructive suggestions and manuscript improvements. The mechanical tests were performed according to the advice of Reviewer 2. The changes in the manuscript are colored red in the revised version. Comment of Reviewer 2: Please add mechanical property tests to illustrate its feasibility as a packaging material. And the addition of C30B may enhance the

	mechanical properties. Editor's comment: I believe all issues are resolved with the exception of the mechanical property experimental data, which I agree is necessary to include in order to validate the use of the material for food packaging. While I appreciate this work may take some time, I have (as per your estimate) provided a 60-day response window for returning the paper with this data included as well as appropriate discussion around that data in the context of the practical application of your material. Answer: We are grateful for the additional time given and appreciate the comments about including the characterization of the mechanical properties of the PLA foams developed in our study. Therefore, the updated version of the paper includes the mechanical properties of the PLA foams according to ASTM D-882. These properties comprise the tensile modulus, tensile strength, and elongation at break of the tested samples. As the reviewer assumed, the addition of C30B at 5% enhanced the mechanical properties of the foams. The same was shown for the cocrystal addition. The feasibility of using the foams as a packaging material is included in the new Section 2.5.5. (lines 700-703): "PLAF control presented tensile strength (1.8 MPa) and elongation at break (31.9%) values similar to those reported in the literature for expanded polystyrene [84], which have encouraged the use of PLA foams at the industrial level for food packaging purposes, including its use for the fabrication of cups and trays [85,86]." The mechanical properties of foams were further improved by the C30B and cocrystal addition, as shown in the newly added Table 4, and Fig. S10. The changes in the manuscript are colored red and introduced in lines 287-293, 685-726, and 1083-1084. Fig. S9 and Fig. S10 were added to the Supplementary material.

Graphical abstract

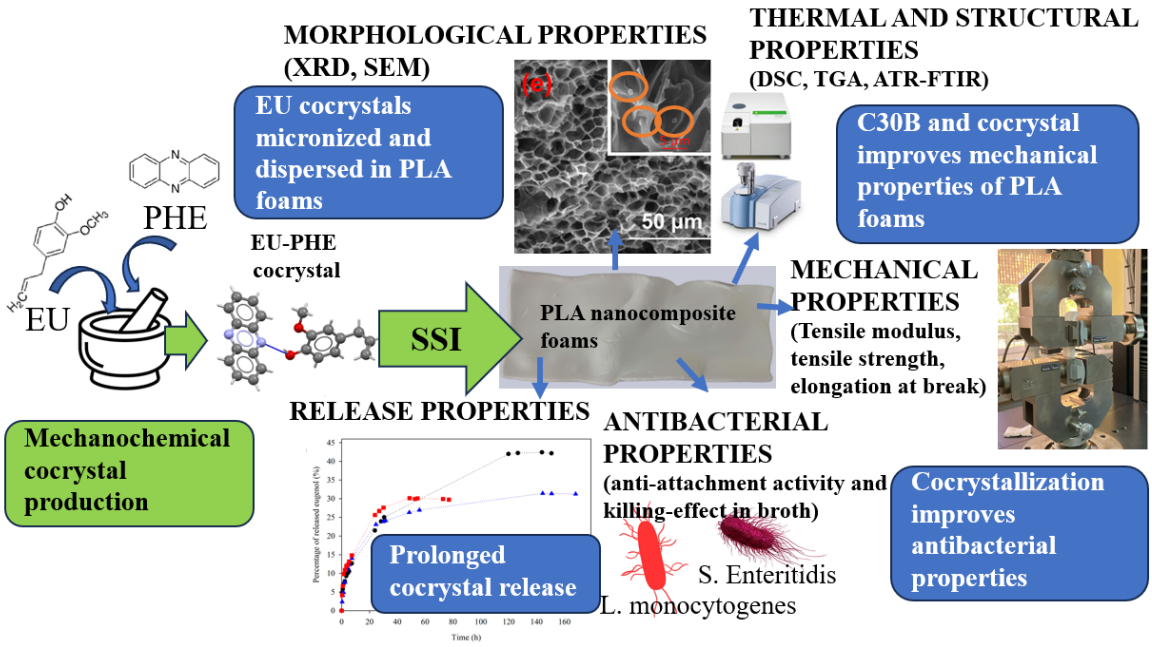

Highlights

- SSI process allowed the EU cocrystals' micronization and dispersion in PLA foams
- The release rate constants were up to 3.6-fold lower for cocrystals than for EU
- All impregnated PLA foams exhibited inhibition of bacterial attachment
- Cocrystal-impregnated PLA foams showed the strongest antibacterial activity after 48h
- C30B and cocrystal addition improves the mechanical properties of PLA foams

Supercritical fluid and cocrystallization technologies for designing antimicrobial food packaging PLA nanocomposite foams loaded with eugenol cocrystals with prolonged release

Adrián Rojas[1,2*], Dusan Misic[3], Irena Zizovic[4], Carol López de Dicastillo[5], Eliezer Velásquez[1,2], Aleksandra Rajewska[3], Bastián Rozas[1], Luciano Catalán[1], Cristian Patiño Vidal[6], Abel Guarda[1,2], María José Galotto[1,2*]

[1] Packaging Innovation Center (LABEN), Department of Science and Food Technology, Faculty of Technology, University of Santiago of Chile (USACH), Obispo Umaña 050, Santiago 9170201, Chile

[2] Center for the Development of Nanoscience and Nanotechnology (CEDENNA), Santiago 9170124, Chile

[3] Department of Functional Food Products Development, Faculty of Biotechnology and Food Sciences, Wrocław University of Environmental and Life Sciences, 51-630 Wrocław, Poland

[4] Faculty of Chemistry, Wroclaw University of Science and Technology, Wybrzeze Wyspianskiego 27, 50-370 Wroclaw, Poland.

[5] Packaging Laboratory, Institute of Agrochemistry and Food Technology IATA-CSIC, Av. Agustín Escardino 7, 46980 Paterna, Spain

[6] Universidad Nacional de Chimborazo, Facultad de Ingeniería, Carrera de Agroindustria, Grupo de Investigación Vegetal y Agroindustrial (INVAGRO), Av. Antonio José de Sucre Km 1 1/2, 060108, Riobamba, Ecuador.

* Corresponding authors: Packaging Innovation Center (LABEN), Department of Science and Food Technology, Faculty of Technology, University of Santiago of Chile (USACH), Obispo Umaña 050, Santiago 9170201, Chile
E-mail addresses: adrian.rojass@usach.cl (A. Rojas), maria.galotto@usach.cl (M.J. Galotto)

ABSTRACT

Searching for effective strategies to modify the release rate of essential oil derivatives is one of the main challenges in designing prolonged-release antimicrobial food packaging materials. Herein, supercritical fluid technology and cocrystallization engineering were used to develop novel eugenol (EU) prolonged-release poly (lactic acid) (PLA) nanocomposite foams. Eugenol-phenazine (EU-PHE) cocrystals, produced by a solvent-free mechanochemical method, were incorporated by supercritical solvent impregnation (SSI) inside PLA nanocomposite foams with different contents of Cloisite30B® (C30B). The effect of the cocrystallization process and C30B content on the EU release kinetics and its relation with their antimicrobial activity by direct contact (anti-attachment) and release in broth culture were studied. The deposition of isolated spherical-shaped micrometric EU-PHE cocrystal particles with 0.8 μm average diameter inside the pores of PLA foams was evidenced by XRD, SEM, DSC, and TGA analyses. The release mechanism of EU and its cocrystal was defined as a quasi-Fickian diffusion process successfully described by the Korsmeyer-Peppas model with release rate constants up to 3.6-fold lower than the release rate constant of pure EU. The impregnated foam samples completely inhibited the attachment of *Listeria monocytogenes* and *Salmonella* Enteritidis and provided prolonged antimicrobial activity in broth culture against both food-borne pathogens. This study suggests a new, environmentally friendly method for designing sustained-release antimicrobial food packaging materials.

Keywords: Antimicrobial packaging; eugenol-phenazine cocrystal; C30B; Cocrystallization; Supercritical fluid technology

1. Introduction

The food industry is faced with the issue of prolonging the food shelf-life and providing safe food free of food-borne pathogens and spoilage microorganisms without the addition of synthetic preservatives. One of the most promising strategies to meet this demand is the design of new active packaging materials with incorporated natural bioactive molecules [1]. As a result, controlled release packaging has arisen as a new concept for releasing systems, emphasizing the depth of understanding the mechanism and kinetics of an active compound's release from the polymer. Designing active packaging with proper release kinetics of the active substance is a prerequisite since these materials should release the active compound when needed when the food is packaged, and not before or after that [2,3].

Essential oils and their constituents are the most commonly used agents for developing active packaging materials because of their safety status, widespread acceptance by consumers, and multipurpose use due to their multiple biological effects, including antimicrobial and antioxidant activities. However, essential oils are highly volatile compounds characterized by high vapor pressure. Consequently, they have very high release rates from polymer structures designed for food packaging, even when different strategies are used to modify the polymer mass transfer properties, such as incorporating nanoclays [4,5], cellulose nanocrystals [6,7], and cyclodextrins [8,9] into the polymer matrix, or designing multi-layer structures [10,11].

A supercritical fluid (SCF) is a substance whose temperature and pressure exceed its critical values. In this state, the fluid is characterized by high diffusivities and low viscosities comparable to gases, while densities and solvating properties are similar to liquids [12]. In

addition, the absence of surface tension in the supercritical phase allows for easy penetration of SCF into the depth of the solid matrix. Exploiting this advantageous combination of thermodynamic and transport properties of SCFs, supercritical fluid technology has emerged as a highly attractive alternative to conventional processing in food, pharmaceutical, textile, and wood industries, material engineering, and biomass treatment [13,14]. The most utilized SCF is supercritical carbon dioxide ($scCO_2$) because of its favorable critical parameters (31 °C and 7.38 MPa) that allow the processing of thermally labile substances, nontoxicity, inflammability, availability, and inert nature. Moreover, $scCO_2$ usage allows for obtaining solvent-free materials by depressurizing the system and separating gaseous CO_2 from the final product. Another vital advantage of $scCO_2$ technology, especially for industrial applications, is the absence of effluent and solid waste generation. $ScCO_2$ is extensively used as a solvent for an active substance for impregnation of solids. The process is termed supercritical solvent impregnation (SSI) and was proven to be an efficient alternative to incorporating active agents in polymers aimed at food packaging, pharmaceutical, and textile applications [15–18]. Besides SSI, one of the most important applications of $scCO_2$ in polymer processing is its use as a blowing agent for foam production. Recently, $scCO_2$ foaming and impregnation were coupled to develop antibacterial polymeric foams for food packaging and tissue engineering applications [19–21].

Cocrystallization can be an innovative approach to modify the physicochemical properties of an active substance aimed at active food packaging and its release. A cocrystal corresponds to a multicomponent crystalline material with different molecular entities stoichiometrically together within the same crystal lattice as a consequence of supramolecular interactions between the active agent and the coformer, resulting from the combination of noncovalent

interactions, such as hydrogen bonds, π-π stacking or van der Waals forces [22,23]. In pharmaceutical research, cocrystallization has gained tremendous importance because of its ability to fine-tune the physicochemical properties of crystalline drugs without modifying their molecular structure. The sublimation rate of a solid depends on its vapor pressure, which corresponds to the escaping tendency of molecules from the solid phase. Recently, Hui Zu et al. studied the sublimation of thymol cocrystals, reporting that the sublimation rate of thymol-4,4'-dipyridyl (Thy-DP) cocrystals was 26 folds lower than the one of thymol and 3.3 folds larger than the sublimation rate of DP [24]. Mazzeo et al. reported that cocrystallization significantly modified the release profile of essential oil derivatives such as thymol, eugenol, and carvacrol, depending on the coformer [25]. In another work, Bianchi et al. reported the sustained release of cocrystallized thymol, eugenol, and carvacrol from a chitosan coating deposited on low-density polyethylene (LDPE) [26]. In this work, packaging prototypes were prepared by the adhesion of cocrystals on LDPE using chitosan solution. To the best of our knowledge, the mentioned study is the only report on the design of cocrystal-based active food packaging materials.

This study is the first report on a cocrystal behavior in $scCO_2$ and its impregnation into a polymeric matrix aimed at designing novel food packaging material with a prolonged active component release due to the intramolecular interactions between the selected active substance and coformer. The questions to be answered relate to the stability and solubility of the cocrystal in $scCO_2$ and SSI feasibility concerning the release kinetics and biological activity of the obtained materials. Phenazine (PHE, solid coformer) was considered in this study as a model coformer because it is prone to act as a strong hydrogen bond acceptor with wide use in designing cocrystals for pharmaceutical applications. Eugenol (EU, liquid), a

highly volatile bioactive substance, was selected as a model essential oil derivative due to its GRAS status given by the Food and Drug Administration (FDA) [27], extensive use in food packaging due to its well-known bioactivity against bacteria and fungi [28–31], and chemical structure that allows it to be used as a hydrogen-bond donor [25,26]. Polylactic acid (PLA) foams with or without nanoclay C30B were produced by foaming in $scCO_2$ and used as a substrate for EU-PHE cocrystal impregnation (SSI) in the next step. The impregnation of foams was also performed with pure EU for comparison reasons. As a biodegradable polymer, PLA has been extensively studied for packaging applications [19,32–34]. The monomer, LA, is recognized as a safe food preservative by the FDA, and its migration from PLA packing containers to food is also considered negligible. In addition, PLA has several beneficial properties that make it appropriate for use in contact with food, such as good oxygen and water barrier properties, resistance against oils and fats, resistance to UV radiation, transparency, and thermal processability [35]. Its favorable mechanical properties make PLA an appropriate replacement for polysulfone food packaging [36], which is one of the envisaged applications of the foams obtained in this study. C30B is a montmorillonite nanoclay with a high chemical affinity to PLA that can contribute to the intercalated nanocomposite structure. The nucleation and antibacterial properties of C30B were also reported, which is why it is frequently used in food packaging [37,38].

Finally, the antibacterial properties of the obtained materials were investigated against *Listeria monocytogenes* and *Salmonella* Enteritidis. The vast presence of *L. monocytogenes* in nature, including the surface layers of the soil, organisms of birds, mammals, and fish, increases the possibility of contamination of most food products with this microorganism. It is generally found on leaves of green vegetables (spinach, onion, leek) and rind of

watermelon and melon. It can be found in fish products, as well as in cheese and other dairy products [39]. *Salmonella* is a strictly pathogenic microorganism and is not as widespread as *Listeria*. Still, the possibility of contaminating almost any food product is always open. There have been recorded outbreaks of *salmonellosis* through peanut butter, tea, chocolate, chips, and peppers, in addition to eggs and meat, which traditionally represent the most common source of infection [40]. The capability of *L. monocytogenes* and *S.* Enteritidis to multiply between 4^0C to 45^0C and pH from 5.0 to 9.0 increases the risk of the contamination of the food products during the packing process or even in a retail network. Therefore, these two microorganisms were chosen for this study.

2. Materials and chemicals

2.1. Materials

Poly (lactic acid) (PLA), 2003D, with a specific gravity of 1.24 and an MFR of g/10min (210 °C, 2.16 kg) was supplied by Natureworks® Co. (Minnetonka, MN, USA). Merck provided the 99.9% HPLC-grade ethanol and methanol used in the study (Darmstadt, Germany). Aldrich® Chemistry supplied the following chemicals: phenazine (PHE) (98%) and eugenol (EU) (99.5%). (St. Louis, MO, USA). Southern Clay Products (Texas, United States) supplied the Cloisite® 30B (C30B) (100 meq/100 g) commercial organo-modified montmorillonite. Linde (Santiago, Chile) supplied carbon dioxide (CO_2). DMSO was purchased from Sigma-Aldrich (Darmstadt, Germany).

177 *2.2. Preparation of PLA nanocomposite films and synthesis of the EU-PHE cocrystal*

178 The following steps were taken to prepare the PLA foams. First, PLA powder and C30B
179 nanoclay were vacuum-dried at 60 °C for 24 h. Then, PLA nanocomposite films were
180 obtained using a LabTech LTE20 twin-screw extruder. Control PLA films (without the
181 nanoclay), and PLA nanocomposites with varying amounts of C30B nanoclay (5 and 10%
182 w/w) were extruded under a temperature range between 185 and 195 ºC with a screw speed
183 of 42 rpm and a chill roll speed of 0.9 rpm. The nanocomposite films were kept in a desiccator
184 until supercritical fluid processing.
185 The eugenol-phenazine (EU-PHE) cocrystal was prepared using a method previously
186 reported [25] consisting of manually grinding equimolar quantities of PHE and EU in an agar
187 mortar for approximately 20 min, yielding a yellow powder. The cocrystal was kept at a
188 temperature of -18 °C until the supercritical impregnation process.
189

190 *2.3. Polymer supercritical fluid processing: foaming of PLA films and foam impregnation*
191 *with EU and EU-PHE cocrystal*

192 The apparatus for the supercritical foaming of extruded PLA films is shown in **Fig.1**. Pure
193 PLA and nanocomposite sheets (1.5 cm x 4 cm, ~700 µm) were deposited inside a 100 mL
194 high-pressure cell (Thar Instruments, USA). The cell was filled with previously liquified CO_2
195 by cooling in an Alpha RA 8 refrigerator unit (Lauda, Germany). A high-pressure pump
196 Teledyne ISCO 260D (Teledyne, USA) was used to elevate the cell pressure. The
197 temperature was maintained by an electric resistance heater wrapped around the cell. The
198 foaming of all samples was performed at 120 °C and 25 MPa. The samples were maintained

199 at these conditions for 20 minutes. The CO_2 was then released within 2 s from the system.
200 The resulting foams were kept in a desiccator until supercritical impregnation.

201 The produced PLA foams with varying concentrations of C30B (0, 5, and 10 % w/w) were
202 impregnated with EU and EU-PHE cocrystal by SSI in the same equipment used for the
203 foaming (**Fig. 1)**. EU (0.64 g) or EU-PHE cocrystal (1.35 g) was put in a glass container and
204 placed at the bottom of the vessel. PLA nanocomposite foams (0.5 g) were deposited inside
205 the high-pressure vessel above the active substance, and the system was loaded with liquid
206 CO_2. The ISCO 260D syringe pump and the electric heater were used to attain the desired
207 conditions. The SSI conditions for EU, being the pressure of 15 MPa, temperature of 60 °C,
208 depressurization rate of 0.5 MPa/min, and impregnation time of 2 h, were adopted from the
209 literature as they were reported the best to incorporate EU into polyamide fibers [41,42]. The
210 impregnation process of the EU-PHE cocrystal was carried out at 15 MPa and 60 °C for 4 h.
211 The system was then left for natural cooling (from 60 to 25 °C for 2 h) to promote the
212 precipitation and recrystallization of EU-PHE cocrystals inside the PLA nanocomposite
213 foams [43,44]. After the cooling, the system was decompressed at a rate of 0.5 MPa/min. The
214 impregnation yield (*I*) was determined gravimetrically using an analytical balance with an
215 accuracy of ±0.0001 g and calculated as follows:

216 $$I = \frac{m_2 - m_1}{m_1} \cdot 100\ \% \qquad (1)$$

217 where m_1 is the initial mass of foam and m_2 is the foam mass after the impregnation [45].

218

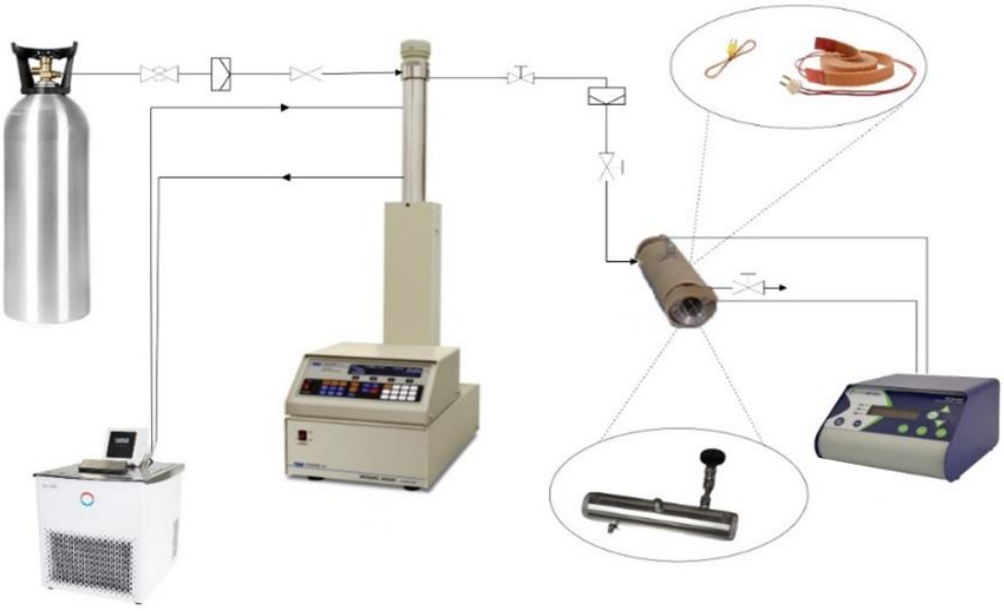

Fig. 1. Outline of the experimental setup for the CO_2-assited foaming and impregnation of the PLA nanocomposite foams.

2.4. Solubility determination

The solubility of pure substances EU and PHE and their cocrystal EU-PHE in $scCO_2$ under the conditions of interest (15 MPa and 60 °C) was performed by the previously published procedure [46] in a 25 mL high-pressure view cell (Eurotechnica GmbH, Bargteheide, Germany) equipped with two sapphire windows that allow for the process visualization and an electrical heating jacket. A glass vessel with around 0.4 g of substance (EU, PHE, or EU-PHE) was placed in the previously heated (60 °C) cell. A perforated cover was put on the top of the glass container to minimize the precipitation of the substance back to the vessel during the decompression. The vessel's surface (3 cm^2) was considerably smaller than the surrounding surface of the cell for the same reason. The CO_2 was introduced to the cell, and pressure was increased to 15 MPa by an air-driven gas booster (Eurotechnica GmbH). After 24 h, the system was decompressed at 0.5 MPa/min. The mass of the dissolved

235 substance was determined gravimetrically using an analytical balance with an accuracy of
236 ±0.00001 g. The $scCO_2$ density at 15 MPa and 60 °C used to calculate the solubility in (g
237 substance)/(g $scCO_2$) was 605.6927 kg/m^3 [47].

238

239 *2.5. Characterization of the PLA nanocomposite foams impregnated with EU and the EU-*
240 *PHE cocrystal*

241 *2.5.1. Morphological analysis*

242 Scanning electron microscope (SEM) VEGAN3 TESCAN with an accelerating voltage of
243 10 kV was used to examine the morphology of the neat and impregnated PLA foams with
244 EU and the EU-PHE cocrystal. Cross-sections of foams were obtained by nitrogen fracture.
245 The samples were coated with gold using a Sputtering System Hummer 6.2. Image-
246 processing Image J program was used to calculate the average values of the pore diameter
247 and cell density of the foams, applying equations 2 and 3, respectively.

248 $$d_{av} = \frac{\sum_{i=1}^{600} d_i}{600} \quad (2)$$

249 where d_{av} indicates the average pore diameter, i corresponds to the number of pores with the
250 pore size d_i, and 600 is the number of pores considered for the evaluation.

251 $$\rho_c = \left(\frac{nM^2}{A}\right)^{(3/2)} \quad (3)$$

252 where ρ_c indicates the cell density, n is the number of cells in the SEM image, M is the
253 magnification, and A is the micrograph area.

254

2.5.2. Thermal properties

Differential scanning calorimetry (DSC) tests were performed using a Mettler-Toledo model STAR 822e (Schwerzenbach, Switzerland) apparatus with a cooling system (HAAKE EK 90/MT, Newington, USA). 4-6 mg of sample was subjected to a single heating from 0 to 250 °C at a steady rate of 10 °C/min[1] under a nitrogen atmosphere. The glass transition temperature (T_g), melting temperature (T_m), cold crystallization temperature (T_{cc}), melting enthalpy (ΔH_m), and cold crystallization enthalpy (ΔH_{cc}) of foams were the thermal parameters analyzed. Equation 4 was used to determine the crystallinity:

$$X_C(\%) = 100 \cdot \left(\frac{\Delta H_m - \Delta H_{cc}}{\Delta H_m^0 \cdot (100-\omega)}\right) \quad (4)$$

where, ΔH_m^0 is the specific melting enthalpy of crystalline PLA (93,6 J g^{-1}) [19], and ω is the mass percentage of C30B.

Thermogravimetric analysis (TGA) was carried out using a Mettler Toledo Gas Controller GC20 Stare System TGA/DCS (Schwerzenbach, Switzerland). 7 mg of sample was placed in porcelain capsules, which were heated under a nitrogen atmosphere at a rate of 10 °C/min[1] over a temperature range of 30 to 600 °C (flow rate 50 mL/min[1]). The parameters obtained were the temperature of degradation at 2.5% of weight loss (T_{onset}), and the temperature of maximum degradation (T_d).

2.5.3. X-ray diffraction

The dispersion and exfoliation of C30B and EU-PHE cocrystal inside the structure of PLA nanocomposite foams were analyzed by using Bruker D8 Advance X-ray diffraction equipment (Marca, Ciudad, País). Scanning was performed over the sample surface. The patterns for profile fitting were obtained using CuKα radiation at the 2θ° scanning angle between 2 to 80 º, with a scanning step of 0.02 º, at a collection time of 10 s per step operating at 40 kV.

2.5.4. Attenuated Total Reflectance Fourier transform infrared (ATR-FTIR) spectroscopy

The chemical characterization of foams was performed using Bruker IFS 66V spectrometer in attenuated total reflection (ATR) mode. The 64 co-added interferograms at 4 cm^{-1} resolution and a 4000 to 400 cm^{-1} wavenumber range yielded the FTIR spectra. OPUS Software Version 7 was used to analyze them.

2.5.5. Mechanical Assays

Following ASTM D-882, a Zwick Roell model BDOFB 0.5TH Tensile Tester was used to measure each material's tensile modulus, tensile strength, and elongation at break at 23 ± 2 °C. Analyses were performed on PLA foams (8 x 2.5 cm), previously conditioned in a desiccator at 25 ºC and 53% relative humidity (a saturated salt solution of magnesium nitrate) for 48 h, with a 1 kN load cell. Considering the size of the specimens obtained by foaming/supercritical impregnation, the initial grip separation was 15 mm, and the crosshead speed was 500 mm/min. For each sample, 10 measurements were performed.

295 *2.5.6. Study of the release kinetics of the EU-PHE cocrystal*

296 EU and EU-PHE cocrystal migration tests from PLA nanocomposite foams were carried
297 out using EtOH 10% v/v solution as an aqueous food simulant to evaluate their release
298 kinetics and to describe the mass transfer. According to EU Regulations, migration tests were
299 performed in duplicate and in accordance with the European Committee for
300 Standardization's recommendations [48]. 130 mL of food simulant and a sample of 0.5 g
301 PLA nanocomposite foam impregnated with EU or EU-PHE cocrystal were placed in a glass
302 tube. For at least 6 days, these tubes were maintained at 40 °C, and the amount of EU released
303 was periodically quantified by UV spectroscopy at 298 nm.

304 Release assays were carried out up to the equilibrium point, i.e., when the EU content in
305 the food simulant was maintained constant in at least two continuous succeeding
306 measurements. The dimensionless distribution coefficient of EU between the PLA
307 nanocomposite foams and food simulant ($K_{P/FS}$), which is represented by the ratio of the EU
308 concentrations at the interface between the polymer and food simulant, was used to
309 characterize this thermodynamic equilibrium condition (Equation 5)

310 $$K_{P/FS} = \frac{C_{EU}^{P}}{C_{EU}^{FS}} \quad (5)$$

311 where C_{EU}^{P} is the equilibrium EU concentration in the PLA nanocomposite foams and C_{EU}^{FS}
312 corresponds to EU concentration values in the food simulant. The EU release kinetics were
313 modeled using the kinetic models of Higuchi and Korsmeyer-Peppas presented by equations
314 6 and 7, respectively.

315 $$\frac{M_t}{M_\infty} = k \cdot t^{1/2} \quad (6)$$

316

317 $$\frac{M_t}{M_\infty} = k \cdot t^n \quad (7)$$

318 where M_t is the amount of EU released at any given time *t*, M_∞ is the amount of EU released
319 at the infinite time, k is the release rate constant, and n is the diffusional exponent, which
320 indicates the type of release mechanism.

321

322 *2.5.7. Antimicrobial properties of PLA foams loaded with the EU-PHE cocrystal*

323 *2.5.7.1. Investigated strains*

324 *Listeria (L.) monocytogenes*, serotype 1/2a, isolated from frozen salmon, as well as
325 *Salmonella* (*S.*) Enteritidis (*S. enterica* subspecies *enterica* serovar Enteritidis) isolated from
326 chicken egg samples, as a typical foodborne pathogen, were used for the investigations.
327 Bacterial strains were isolated in routine microbiological activities and kept at - 80 °C in a
328 cryoprotective medium. In preliminary tests (results not published), a strong ability of both
329 strains to produce biofilms was demonstrated. Just before testing, the cultures were refreshed
330 in Tryptone soya broth (TSB, Oxoid, Basingstoke, UK) at 37 °C overnight, then spread on
331 5% sheep blood agar and incubated for 24 h.

332

333 *2.5.7.2. Determination of MIC (minimal inhibitory concentration) values of EU, PHE and*
334 *EU-PHE cocrystals*

335 The antibacterial activities of EU, PHE, and EU-PHE cocrystals were also analyzed
336 through the dilution antimicrobial susceptibility test [49] with the modification that instead
337 of antibiotics, EU, PHE, and EU-PHE cocrystals previously dissolved in dimethyl sulfoxide
338 (DMSO) were used. Investigated concentrations ranged from 5% to 0.00244 %. Although
339 completely dissolved in DMSO, PHE, and EU-PHE cocrystal in concentrations higher than

5% formed a deposit after mixing with Cation Adjusted Mueller Hinton broth, the reference medium for broth microdilution. Thus, the highest possible investigated concentration was 5%. The final bacterial inoculum density was approximately 5×10^5 CFU/mL. Microtiter plates were incubated for 18-24 h at 37 °C. The MIC was defined as the lowest concentration that inhibited the visible growth of bacteria.

2.5.7.2. Anti-attachment (contact inhibition) activity of PLA nanocomposite foams

The microbial assay has been applied to determine the inhibition of the bacterial adhesion to the polymer surface [50]. Strains were incubated in TSB with 1% (w/v) glucose for 24 h. Overnight cultures were diluted to approximately 1-2 x 10^8 CFU/mL. Polymeric samples with a surface of 1 cm^2 were prepared and sterilized in an autoclave at 121 °C for 15 min and subsequently immersed in 2 mL of diluted cultures and incubated for 24 and 48 at 37 °C in static condition. After an incubation, PLA foam samples were collected and washed thoroughly with sterile Phosphate Buffered Saline (PBS). Subsequently, each piece of foam was transferred into tubes filled with 10 mL of PBS and subjected to ultrasonication at 37,000 Hz (Elmasonic S60, Elma Schmidbauer GmbH, Singen, Germany) for 5 min to detach the cells. Serial dilutions were done to a final dilution of 10^{-8}. Each dilution was inoculated in three 10 μL aliquots on Tryptone soya agar, which were then incubated 24 h at 37 °C. After that, colonies were counted. The number of obtained CFU/mL was calculated according to the formula from 7218 ISO standard [51]:

$$NCFU= (\sum C)/ (V \times [n1+(0.1 \times n2)] \times d) \quad (8)$$

where $\sum C$ is the total number of colonies from two successive dilutions, V is the volume of inoculum applied to each Petri dish (mL), $n1$ is the number of replicates from the first

362 dilution, *n2* is the number of replicates from the second dilution, and *d* is the dilution factor
363 corresponding to the first dilution.

364 The calculation of the number of attached bacteria per cm^2 (*NP*) was done following the
365 equation 9 [52]:

366 $$NP = (NCFU \times V)/P \quad (9)$$

367 where *NCFU* is the total number of detached bacteria (previously determined as CFU/mL),
368 *V* is the volume of PBS where the ultrasonic detachment was done, and *P* is the total surface
369 in mm^2 of the PLA. The investigation was carried out in three independent experiments from
370 which the average numerical values were derived and shown in the results.

371 *2.5.7.3. Assay of antimicrobial activity in broth cultures of active foams – determination of*
372 *killing effect (KE)*

373 The killing effect of the polymer, as well as its durability in a liquid environment,
374 depends on the active substance release rate. It was determined under static incubation
375 following the previously described method [50]. Briefly, a test polymer with a surface area
376 of 1 cm^2 was added to 2 mL Mueller-Hinton broth with 1% glucose, suspension of the
377 investigated strain adjusted to an OD_{550} of 0.125 (approximately 2 x 10^8 CFU/mL, A_o), and
378 left to incubate for 24 h at 37 °C ($A_{\text{test tube}}$). Controls were culture without polymer (A_{control}),
379 culture with pure non-impregnated PLA foam (PLAF) as a neutral control polymer
380 ($A_{\text{controlPLAF}}$), and blank was a sterile broth. The test was repeated daily by transferring the
381 polymer to a freshly prepared culture broth as long as the OD values of the tested polymer
382 were lower than those of the control ($A_{\text{control}} \geq A_{\text{test tube}}$). When the two absorbances were
383 similar ($A_{\text{control}} \leq A_{\text{test tube}}$), the polymer sample could no longer inhibit bacterial growth.

384 Results were presented as the percentage of bacterial growth in the presence of polymers
385 compared to the bacterial growth in the presence of controls.

386 *2.5.7.5. Statistical analysis*

387 All data was analyzed using Statistical software version 13.0 (StatSoft Inc., Tulsa,
388 OK, USA). The quantitative bacterial counts of *L. monocytogenes* and *S.* Enteritidis strains
389 per centimeter square underwent a logarithmic transformation. To monitor the effect of the
390 investigated PLA foams on the adhesion of microorganisms to surfaces, a logarithmic
391 reduction was also calculated.

392

393

3. Results and discussion

3.1. PLA nanocomposite foam production and solubility determination

PLA nanocomposite films with different concentrations of C30B (0, 5, and 10 % w/w) were successfully obtained by extrusion and subsequently foamed using $scCO_2$ as a blowing agent. During the foaming process, the pressure, temperature, and soaking time were maintained at 25 MPa, 120 °C, and 20 min, respectively, based on previously reported processing conditions by Rojas et al. [19]. The presence of C30B at low concentration (5 % w/w) did not significantly change the expansion ratio (19.71 ± 3.84) and porosity (94.69 ± 0.82 %) of the PLA-nanocomposite foam compared to the values of expansion ratio (12.63 ± 2.59) and porosity (91.91 ± 1.66 %) obtained for the control PLA foam (PLAF). This result is in accordance with the data reported by Rojas et al. [19]. It is well known that the porosity and expansion ratio of PLA foams obtained using $scCO_2$ as a blowing agent depends on the conditions of pressure, temperature, and time, which govern the amount of sorbed $scCO_2$ in the polymer structure, and on the number of nucleation sites inside the polymer for cell formation [53]. Particularly, the promotion of the crystallization of PLA has been used as an effective strategy to improve its foaming ability, *i.e.,* improving the expansion ratio and the porosity of the resulting PLA foams. Namely, crystals reduce the cell nucleation energy barrier by providing numerous heterogeneous nucleation sites [54,55]. In this context, the similar expansion ratios and porosities of PLA foams without the clay and with 5 % w/w C30B were in agreement with the same crystallinity (part 3.4) and an exfoliated structure (part 3.2) of both samples. The exfoliation of C30B at 5 % w/w inside PLA has been previously reported [56–58].

418 **Table 1**. Pore diameters (d), cell density (ρ_c), and impregnation yield (*I*) of EU-PHE cocrystal

Sample	d_{min} (µm)	d_{max} (µm)	d_{aver} (µm)	ρ_c (10^{-8} pores cm^{-3}]	*I* (% w/w)
PLAF (control)	4.22	42.71	22.70 ± 6.65 [a]	2.40	-
PLAF-EU-PHE	3.69	50.85	15.97 ± 6.65[d]	3.31	8.62 ± 0.06[c]
PLAF-5%C30B	4.22	41.21	20.90 ± 6.35 [b]	2.80	-
PLAF-5%C30B/EU-PHE	3.83	33.14	15.55 ± 4.73 [d]	3.65	9.19 ± 0.12[d]
PLAF-10%C30B	3.84	37.16	15.39 ± 3.84 [c]	4.58	-
PLAF-10%C30B/EU-PHE	3.80	61.36	13.58 ± 3.80 [e]	14.06	9.25 ± 0.37[d]

419 Different superscripts indicate statistically significant differences in the crystallinity of the samples.
420

421 **Fig. 2** shows the representative images of PLA nanocomposite foams with different
422 C30B concentrations (0, 5, and 10 % w/w). The foams' average pore diameters (d_{aver}) and
423 cell density (ρ_c) values are presented in **Table 1**. As shown in **Fig. 2**, the incorporation of
424 C30B did not change the closed cell morphology present in the control PLAF. Nevertheless,
425 clay agglomerates were observed in the PLA nanocomposite foam with C30B at 10 % w/w
426 since the nanoparticles were less dispersed inside the polymer (**Fig. 2d**). This phenomenon
427 decreased the porosity (81.69%) and consequently, the expansion ratio (5.47) of the foam
428 with the high C30B concentration compared to the pristine PLA foam. Particularly, nanoclay
429 agglomerations could act as a physical barrier for the polymer expansion during the cell
430 growth stage [19,59], which explained the formation of polymer foams with lower average
431 pore diameter sizes (15.39 ± 3.84 µm) compared to the control PLAF (20.90 ± 6.35 µm) and
432 the foam with 5 % w/w C30B (22.70 ± 6.65 µm). Consequently, the PLA nanocomposite
433 foam with 10 % w/w C30B presented the highest cell density compared with the values
434 obtained for the control PLAF and PLA nanocomposite foam with 5% w/w C30B (**Table 1**).

435

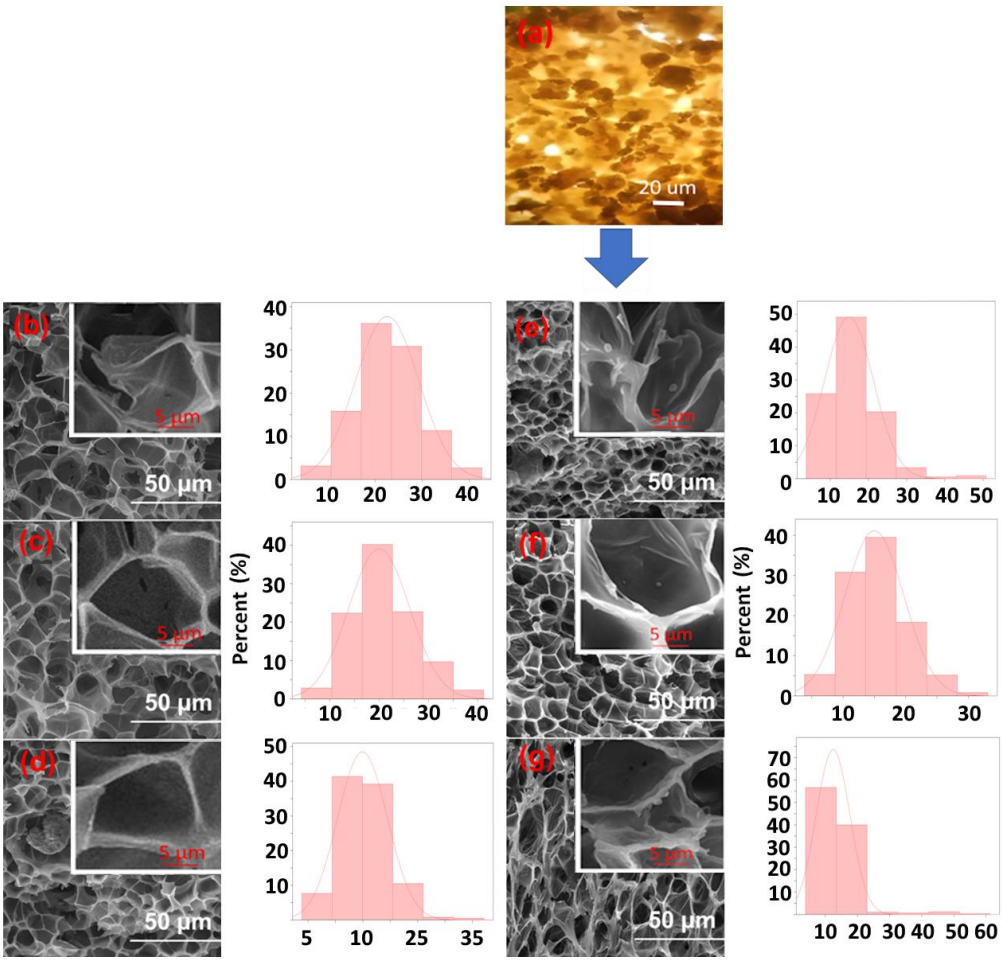

436

437 **Fig. 2.** Optical microscope image of the EU-PHE cocrystal powder (a), SEM images
438 and pore size distribution of PLA foams with 0, 5 and 10 % w/w of C30B (b, c, and d,
439 respectively), and SEM images and pore size distribution of the PLA foams impregnated
440 with EU-PHE cocrystals with 0, 5 and 10 % w/w of C30B (e, f, and g, respectively).

441

442 The experiments in the view cell confirmed the stability of the EU-PHE cocrystal
443 when exposed to $scCO_2$ under the conditions of interest (15 MPa and 60 °C). No phase
444 separation could be observed during the exposure or after the system decompression. The
445 determined solubilities of EU, EU-PHE cocrystal, and PHE in $scCO_2$ at 15 MPa and 60 °C
446 were 0.0370±0.0005, 0.0123±0.0002, and 0.00109±0.00006 g/g_{scCO2}, respectively. The
447 results indicated that the EU solubility in $scCO_2$ was considerably higher than that of PHE.

448 The EU-PHE cocrystal solubility was approximately ten times higher than the solubility of
449 pure PHE and three times lower compared to the EU. In the literature, data on EU solubility
450 in $scCO_2$ are usually derived from supercritical fluid extraction measurements for different
451 $scCO_2$ flow rates and particle sizes [60]. In contrast, the static solubility measurement data
452 are scarce. Chen et al. determined the VLE data for the system $scCO_2$-EU in a semi-flow type
453 apparatus and reported the maximal EU molar fraction value of $0.96x10^{-2}$ (corresponding to
454 0.035 g/g_{scCO2}) at 328.15K & 125.1 bar [61], which is similar to our value. The only report
455 on PHE solubility in $scCO_2$ is the work of Van Alsten et al. [62]. The authors obtained a PHE
456 molar fraction of 0.000225 (corresponding to 0.00092 g/g_{scCO2}) at 14.58 MPa and 50 °C,
457 which is comparable to our result. The determined EU-PHE cocrystal solubility (0.0123
458 g/g_{scCO2}) lies between the values of pure EU and PHE, and it is appropriate (high enough) to
459 allow for an effective SSI.

460 EU and EU-PHE cocrystals were successfully impregnated in PLA nanocomposite
461 foams by SSI under the conditions of 15 MPa and 60 °C and with a decompression rate of
462 0.5 MPa/min. To the best of our knowledge, there is no data on the impregnation of EU in
463 PLA by SSI or another method. The obtained impregnation yield of EU was in the range
464 between 20 to 22 % w/w and slightly increased (from 20 to 22%) with the C30B content.
465 This might be due to the hydrophobic nature of EU and possible interactions with the
466 nanoclay's silicate layers. The same phenomenon has been used to explain the slight impact
467 of C30B on the impregnation yield of cinnamaldehyde in PLA nanocomposite foams [19]
468 and films [63] with C30B content up to 5 % w/w. The impregnation yield of EU for PLA
469 foams obtained in this study is comparable to those reported for other essential oil derivatives.
470 Under similar processing conditions, Torres et al. stated that a thymol loading in PLA films
471 was 20.4% w/w [64].

Recently reported EU-impregnated polymeric materials utilizing $scCO_2$ include linear low-density polyethylene (LLDPE) with EU impregnation yield ranging between 1 and 6 % w/w [65], polyamide fibers with impregnation yield between 8 and 15 % w/w [41], and polyamide dental floss with impregnation yield ranging between 4 and 16 % w/w [42]. It is clear from comparing these studies with our findings that PLA exhibits higher EU impregnation yields than the aforementioned polymers. It is well-known that the SSI of bioactive substances in polymers depends on the balance between the affinity of the bioactive substance towards the polymer and $scCO_2$. Particularly, the high loading of active substances in PLA has been attributed to electrostatic interactions between functional groups of the bioactive substances and free carbonyl groups available in PLA chains. In the case of cinnamaldehyde, hydrogen bonds between the oxygen of the aldehyde belonging to the cinnamaldehyde and the PLA carbonyl group allow for incorporations of up to 13 % w/w [66]. According to reports, notable thymol incorporation in the polymeric matrix (up to 24 % w/w) was caused by a secondary interaction between the phenolic group of thymol and the free PLA's carbonyl groups [6]. In our study, the hydroxyl group of EU and its electrostatic interactions with carbonyl groups of PLA contributed to the high EU loadings.

The obtained impregnation yields for the EU-PHE cocrystal were notably high, ranging from 8.62 to 9.25 % w/w (**Table 1**). The presence of C30B slightly increased the cocrystal loading, similar to the observed with EU. **Fig. 2**. presents the images of EU-PHE cocrystal and neat and impregnated PLA foams along with their pore size distribution. The SEM images revealed a slight decrease in the average pore diameter of PLA nanocomposite foams due to the EU-PHE cocrystal incorporation (**Fig. 2e**, **2f**, and **2g**). This phenomenon has been previously observed for PLA nanocomposite foams impregnated with cinnamaldehyde [19] and starch foams impregnated with carvacrol [67,68]. The phenomenon

was explained by the plasticizing properties of these essential oil derivatives. **Fig. 2a** shows EU-PHE cocrystals generated manually by grinding according to the procedure described in part 2.2. The cocrystals appear as agglomerated granules of diameters up to 25 µm. However, EU-PHE cocrystals appeared inside the PLA nanocomposite foams as isolated spherical shape micrometric particles with an average diameter of around 0.8 µm (**Fig. 2e, f, and g**). Therefore, it can be concluded that the recrystallization of the EU-PHE complex from the supercritical phase occurred. SEM images with EU-PHE recrystallized particles and their dimensions are presented in Fig. S1 (Supplementary material). The micronization or nanonization of solid particles inside polymeric structures by means of the SSI process has been previously reported [43,44]. Ubellitogullary et al. reported the nanonization of phytosterol particles inside nanoporous starch aerogels by decreasing their solubility in $scCO_2$ during the last stage of the SSI process. The authors attributed the formation of isolated nanoparticles to favored nucleation rather than crystal growth during the fast-cooling stage previous to the depressurization of the system [43].

It is well-known that the solvation of solid particles in supercritical fluids involves the formation of clusters or aggregates of solvent molecules around the solute [69,70]. In this way, clusters of CO_2 molecules probably surrounded the EU-PHE cocrystal particles without destabilizing the supramolecular interactions between their components (EU and PHE) during the first stage of the SSI (solvation stage), allowing their dispersion and transport in the supercritical phase towards the polymer in the second stage of the process (diffusion stage). Finally, the incorporation/recrystalization of the EU-PHE cocrystals inside the polymer foam occurred in the third stage by cooling and the subsequent depressurization of the system.

519 It is well-known that $scCO_2$ solvent power is an important factor governing the
520 impregnation of bioactive substances in polymers [17,18]. In this way, the differences
521 between the impregnation yield obtained for EU and the EU-PHE cocrystal could be
522 associated with their different solubilities in $scCO_2$. There is no data in the open literature
523 about the solubility of cocrystallized derivative essential oils in supercritical fluids, and our
524 study is the first report on cocrystal solubility in $scCO_2$. The solubility values determined in
525 this work support the obtained SSI results and the feasibility of the proposed process.
526

527 *3.2. X-ray diffraction*

528 The X-ray diffraction analysis of PLA nanocomposite foams was performed to
529 identify if the nanoclay was exfoliated on the polymer matrix, that is, if C30B was uniformly
530 distributed, allowing correct intercalation of PLA chains in nanoclay sheets. As **Fig. 3a**
531 shows, XRD diffractograms of PLAF and PLAF-5%C30B did not evidence differences,
532 confirming the exfoliation of C30B by PLA [56,71]. On the other hand, a significant
533 difference was observed in the diffractogram of PLAF-10%C30B with the characteristic
534 band of C30B at approximately 5º that confirmed the low exfoliation in the material when
535 the clay was added at high concentration. This nanocomposite presented an agglomeration
536 of C30B consistent with SEM images and the previously explained phenomena related to the
537 porosity and the expansion coefficient. This effect has also been observed through TEM
538 analysis in a previous work that evidenced the agglomeration of C30B in PLA polymeric
539 structure when added at 10 % w/w [72].
540

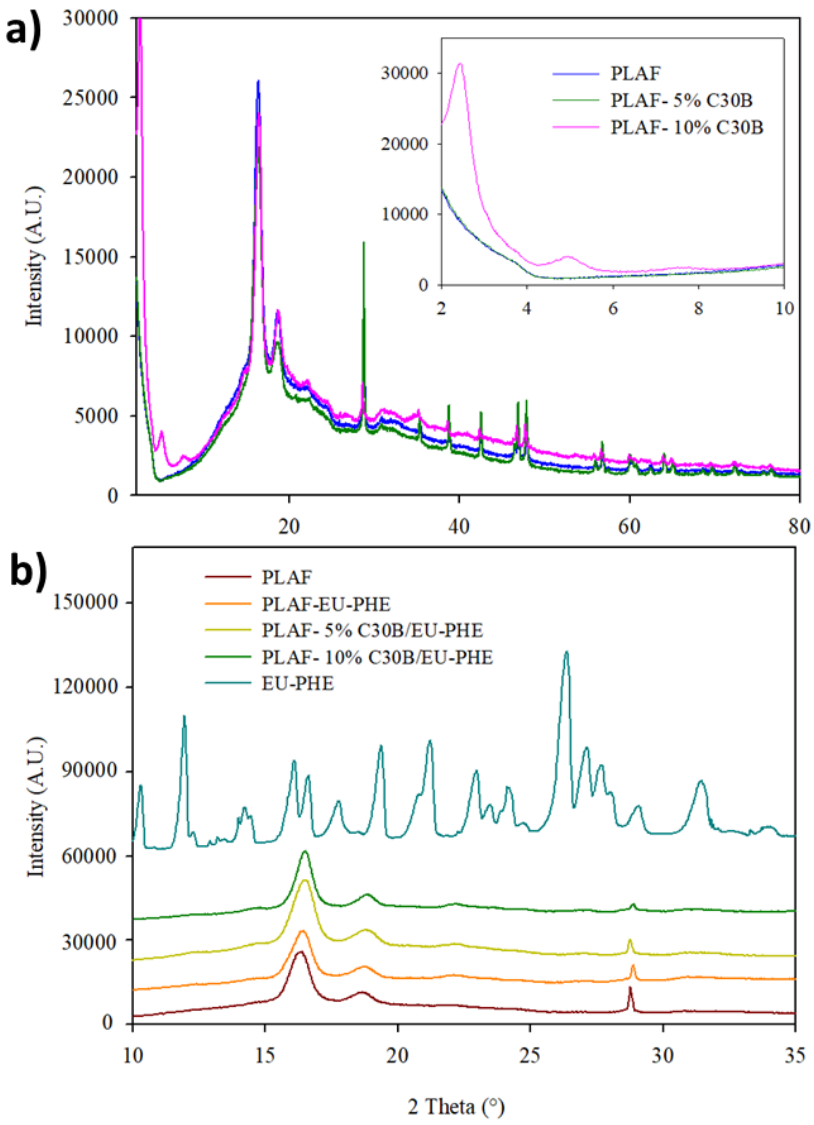

Fig. 3. DRX diffractograms of: a) foamed PLA nanocomposites with 0, 5 and 10 % w/w C30B; b) foamed PLA nanocomposites with 0, 5 and 10 % w/w C30B impregnated with EU/PHE cocrystals.

Fig. 3b presents the XRD diffractograms of foamed PLA nanocomposites impregnated with EU-PHE cocrystals. The diffractogram of EU-PHE confirmed the incorporation of the crystal structure in PLA, in agreement with the XRD previously reported by Mazzeo et al. [25]. The foamed PLA nanocomposites evidenced a shift in the main bands upon incorporating EU-PHE into the polymeric foams, which are present at 16º, 18.6º and

28.75º respectively, indicating an intercalation of EU-PHE with the polymer matrix. No cocrystal agglomeration was detected. New weak bands at 12.3, 22.1, and 27º also appeared upon impregnating the cocrystals, which were attributable to the incorporation/recrystallization of EU-PHE cocrystals in the polymeric matrix.

3.3. FTIR analysis

Fig. 4a shows the spectra of foamed PLA nanocomposites. The main characteristic peaks for PLA can be observed at 1750 and 1082 cm^{-1}, corresponding to the symmetric and asymmetric stretching of the C=O group, respectively; the bands at 1180 and 1127 cm^{-1} are associated to the asymmetric and symmetric stretching of the C-O bond, respectively; the CH_3 bending at 1454 cm^{-1} and the symmetric and asymmetric stretching of the C-H bond of CH_2 are seen as peaks at 1381 and 1360 cm^{-1}, respectively [19,73,74]. Finally, the amorphous and crystalline zones of PLA were observed at 870 and 754 cm^{-1}, respectively [75]. The presence of C30B nanoclay was observed in the range of wavenumbers between 2800 and 3050 cm^{-1}. The bands at 2920 and 2850 cm^{-1} are associated with the asymmetric and symmetric vibrations of the C-H group of the methylene group of C30B, respectively [76].

FTIR spectra of PLA foams impregnated with EU are presented in **Fig. S2** (Supplementary material). Comparing the spectra of neat and EU-impregnated foams, new bands were observed in the impregnated samples, confirming the presence of EU. The new peak at 1511 cm^{-1} is attributed to the stretching of the EU; two new bands at 818 and 793 cm^{-1} are associated with the vibration of the tetra-substituted aromatic ring. The characteristic bands for PLA were detected, and there was no shift in wavenumbers. However, compared to neat foams, a decrease in the absorbance for the characteristic frequencies of the functional

groups C=O and C-O was observed, evidencing an interaction of the hydrogen bond type between these groups and the incorporated EU.

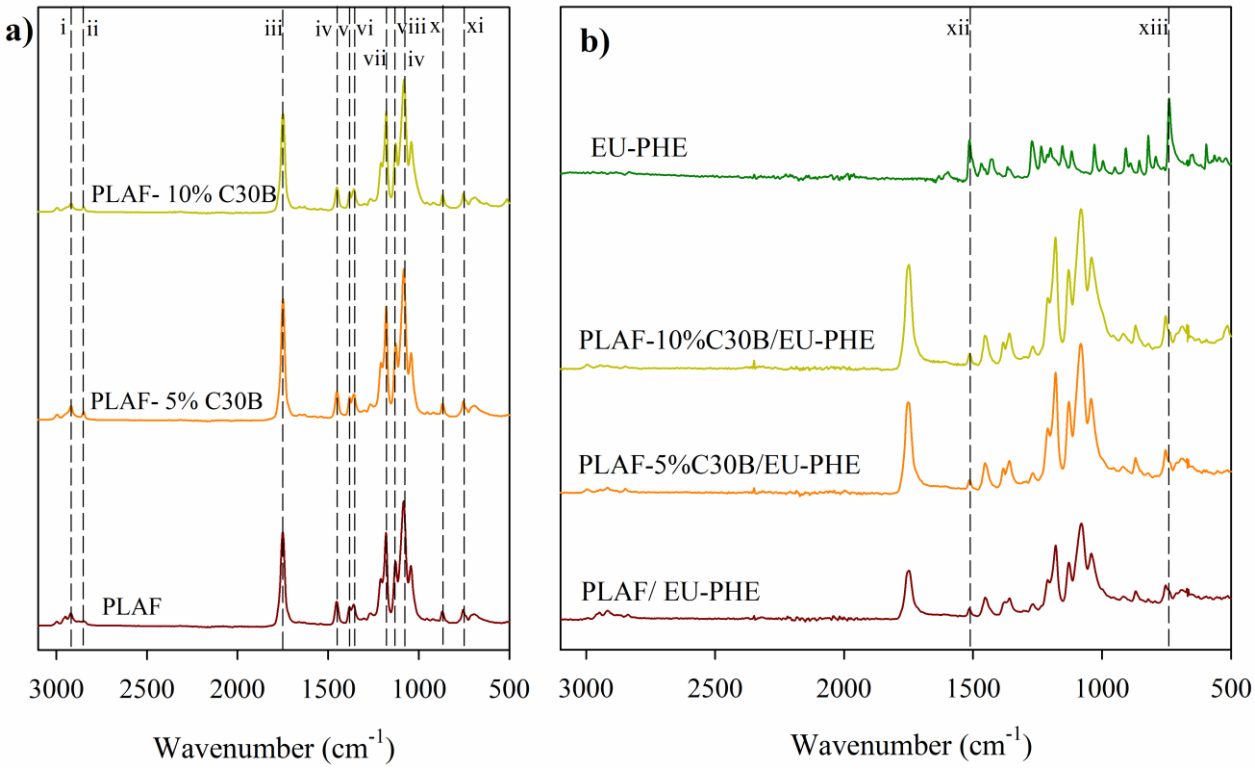

Fig. 4. ATR-FTIR spectra of a) foamed PLA nanocomposites; b) active foamed PLA nanocomposites impregnated with EU-PHE cocrystals.

Fig. 4b shows FTIR spectra of PLA foams impregnated with EU-PHE cocrystals. The PLA characteristic bands were detected, with no shift in wavenumbers. A decrease in the absorbance of the C=O and C-O functional groups was evidenced, showing hydrogen bond interactions between the EU-PHE cocrystals and the PLA polymeric structure [77]. On the other hand, the main peaks of EU-PHE were identified at 1514 cm^{-1}, corresponding to the vibration of the aromatic ring, and at 821 cm^{-1}, associated with the vibration of the tetra-substituted aromatic ring.

3.4. Thermal properties of the impregnated PLA nanocomposite foams

3.4.1. Differential scanning calorimetry

Table 2 shows the thermal properties of pure substances and nanocomposite foams obtained by the DSC analysis. DSC thermograms for EU-PHE cocrystal and PHE, and representative thermograms for the PLA nanocomposite foams, are shown in **Fig. S3** and **Fig. S4** (Supplementary material), respectively. The effective formation of the EU-PHE cocrystal by grinding was evidenced by the appearance of a single melting peak around 52 ºC, revealing that it had a different crystalline structure than that of PHE, which presented a single melting transition at 175 ºC (**Table 2** and **Fig. S3**).

The control PLAF presented a thermal transition at 69 °C associated with the polymer's glass transition temperature. T_g was not detected in PLA foams with EU, EU-PHE cocrystal, and clay, which had higher crystallinity values than the control PLAF. In addition, cold crystallization at 111 °C was registered in PLAF and the active-free PLA nanocomposite foams due to rearrangement of the amorphous regions during the DSC heating, as was reported for pristine PLA foams [78].

Table 2.

Thermal properties of the individual substances and PLA nanocomposite foams.

Sample	T_{cc} (ºC)	ΔH_{cc} (J g^{-1})	T_{m1} (ºC)	T_{m2} (ºC)	T_{m3} (ºC)	ΔH_{m1} (J g^{-1})	ΔH_{m2-3} (J g^{-1})	X_c (%)
PLAF (control)	111	3.8	-	149	-	-	34.6	33 ± 1^{a}
PLAF - EU	-	-	-	104	135	-	33.4	$36 \pm 2^{b,c}$
PLAF - EU-PHE	-	-	33	125	142	0.34	44.2	48 ± 1^{f}
PLAF - 5% C30B	118	5.8	-	150	-	-	32.0	$34 \pm 1^{a,b}$
PLAF - 5% C30B/EU	-	-	-	106	134	-	33.5	38 ± 1^{c}
PLAF - 5% C30B/EU-PHE	-	-	33	126	142	0.25	36.2	41 ± 1^{d}
PLAF - 10% C30B	118	2.1	-	148	157	-	31.0	$34 \pm 2^{a,b}$
PLAF - 10% C30B/EU	-	-	-	107	134	-	27.6	33 ± 1^{a}
PLAF - 10% C30B/EU-PHE	-	-	33	130	143	0.84	37.2	44 ± 1^{e}
EU-PHE	-	-	52	-	-	-	125.1	-
PHE	-	-	-	175	-	-	179.9	-

ANOVA analysis was carried out to find significant differences in the crystallinity values of the samples. Different superscripts indicate statistically significant differences.

The thermograms of PLAF and PLA nanocomposite foams show an endothermic transition at approximately 150 °C, associated with the melting of PLA (**Fig. S4**, Supplementary material). Similar T_m values have been reported for PLA foams obtained by foaming with $scCO_2$ at 147 °C [79] and 150 °C [78]. However, in EU-impregnated PLA foam thermograms (~21 % w/w EU), a broad endothermic transition is observed with two distinct peaks, indicating the melting of two crystalline structures with different degrees of ordering, α' structures less ordered and polymeric structures thermodynamically more stable that melted around 104 °C and 135 °C, respectively (**Fig. S4** and **Table 2**). Similar was observed for PLA foams with different porosities and PLA foams with clay/cinnamaldehyde by Bocz et al. [78] and Rojas et al. [19], respectively. Thermograms of PLAF and its nanocomposite foams impregnated with EU-PHE cocrystal (~9 % w/w of EU-PHE cocrystal) showed a broad melting, which indicated the formation of two crystal structures with different ordering. T_m was shifted to higher temperature values despite the lower proportion of impregnated EU-PHE (compared to EU), reaching values up to 130 °C (T_{m1}) and 143 °C

(T_{m2}) for the PLAF-10%C30B/EU-PHE sample. This is consistent with a more crystalline (41-48%) and stable foam due to EU-PHE cocrystal impregnation compared to those impregnated with EU (33-38%). However, both values were above the crystallinity of the PLAF (33%) (**Table 2**). A crystallinity of 35% was reported for PLA pellets and PLA foams formed by extrusion with 10 % w/w rice husks [80].

The lower melting temperatures (T_{m2} and T_{m3}) of the PLA foams impregnated with EU or EU-PHE cocrystal with respect to those of their corresponding PLA foam controls are explained by a plasticizing effect of the active component. Besides, the melting temperatures of the foams with EU and EU-PHE cocrystal presented differences attributed to the different interactions of the incorporated components with the polymer. For PLAF with EU, hydrogen bond interaction could be established between the hydroxyl group and oxygen of EU and the carbonyl and terminal chains hydroxyl groups of the PLA, obtaining a crystalline structure that was destabilized and melted at lower temperatures than EU-PHE cocrystal-impregnated foams. This result suggested that more stable hydrogen bonding interactions between the pyrazine nitrogen groups and the terminal hydroxyl groups of PLA chains would also be formed. Hydrogen-bonding interactions have been reported in thymol-impregnated polyamide membranes using $scCO_2$ [81]. In addition, in the case of PLA nanocomposite foams, interactions could be formed between the hydroxyl groups of the clay and the organic modifier with EU or EU-PHE molecules. Therefore, a tendency for higher T_m values was observed (**Table 2**). Regarding these observations, Bianchi et al. recently analyzed the inhibition of *Escherichia coli*, *Salmonella* Typhimurium, and *Staphylococcus aureus* using different cocrystals based on carvacrol, thymol, and cinnamaldehyde as essential oils and hexamethylenetetramine and 4-hydroxybenzoic acid as coformers incorporated into the surface of low-density polyethylene (LDPE) films using a chitosan solution. The authors

concluded that the most determining factor for the active compound's stability and time-sustained release is the hydrogen bond's strength between the polymeric matrix and the coformer of the cocrystal [26]. Importantly, PLA foam impregnated with EU-PHE cocrystals showed a low-intensity transition between 30 °C and 50 °C attributed to the melting of the cocrystals, confirming their incorporation into PLAF **(Table 2** and **Fig. S4**).

3.4.2. Thermogravimetric analysis

The results of thermogravimetric analysis are presented in **Table 3** and **Figs. S5-S8** (Supplementary material). PLAF initiated to decompose at 344 °C and had a T_d at 362 °C, similar to that reported in the literature [19,74]. Meanwhile, foams impregnated with EU or EU-PHE presented two degradation stages at T_{d1} and T_{d2}. The first stage was associated with the degradation of the impregnated compound (EU or EU-PHE), whose T_{d1} values were close to that of the individual substances, which confirmed the incorporation of EU and EU-PHE cocrystal in the foams. The second stage was related to PLA degradation (**Table 3** and **Figs. S6** and **S7**).

The T_{onset} and T_d of the PLA foam impregnated with EU-PHE cocrystal, without and with clay, were between the temperature values of the control PLAF and the values obtained for the PLA foam impregnated with EU (**Figs. S5-S8** and **Table 3**). This is in agreement with the higher thermal stability found for the cocrystal compared to the EU but lower with respect to that of the PHE, in terms of the onset decomposition and the maximum degradation rate temperatures (**Table 3**).

Furthermore, it was observed that the nanoclay and EU tended to diminish T_{onset} of the PLA foams, attributed to the lower thermal stability of the organic modifier of the clay and the EU compared to PLA [82,83]. However, the incorporation of EU-PHE cocrystal

counteracted this effect and increased the thermal stability of the active foams, which were more crystalline. However, T_d was not significantly modified, similar to the report of Rojas et al., who found that the addition of C30B did not affect the T_d of PLA nanocomposites with cinnamaldehyde [19].

Table 3
TGA analysis of the individual substances and the impregnated PLA nanocomposite foams.

Sample	T_{onset} (ºC)	T_{d1} (ºC)	T_{d2} (ºC)
PLAF (control)	344 ± 1.0^{a}	$362 \pm 0.5^{a,b}$	-
PLAF - EU	156 ± 1.0^{f}	186 ± 1.0^{f}	$362 \pm 1.0^{a,b}$
PLAF - EU-PHE	165 ± 1.0^{e}	$200 \pm 1.0^{c,d}$	$362 \pm 1.0^{a,b}$
PLAF - 5% C30B	341 ± 1.0^{b}	360 ± 0.5^{a}	-
PLAF - 5% C30B/EU	148 ± 1.0^{g}	$186 \pm 1.0^{e,f}$	357 ± 1.0^{c}
PLAF - 5% C30B/EU-PHE	170 ± 1.0^{d}	202 ± 1.0^{c}	363 ± 1.0^{b}
PLAF - 10% C30B	340 ± 1.0^{b}	362 ± 2.0^{b}	-
PLAF - 10% C30B/EU	156 ± 0.1^{f}	188 ± 0.5^{e}	$362 \pm 0.5^{a,b}$
PLAF - 10% C30B/EU-PHE	172 ± 0.5^{c}	199 ± 0.5^{d}	361 ± 0.5^{a}
EU-PH	172 ± 1.0^{c}	236 ± 1.0	-
PHE	200 ± 1.0	256 ± 1.0	-
EU	103 ± 1.0	186 ± 2.0	-

Different superscripts indicated statistically significant differences in the properties among the foams determined by ANOVA analysis.

3.5. Mechanical assays

The effect of C30B and EU-PHE cocrystal addition on the mechanical properties of PLAF was analyzed following the method described in part 2.5.5. The 10% C30B PLA foam samples were omitted for this analysis because the C30B agglomerated inside the polymer (part 3.2), negatively affecting the materials' physical properties (part 3.1). Therefore, neat PLAF and PLAF with 5% C30B foams (8 x 2.5 cm) were prepared and impregnated with EU and EU-PHE (**Fig. S9**, Supplementary material). In the next step, foams impregnated with

692 EU were excluded from the assays because they hadn't preserved their shape after the
693 impregnation (**Fig. S9**). This phenomenon is due to the extensive plasticizing effect of EU
694 on the polymeric matrix. On the contrary, EU-PHE-impregnated PLA foams maintained their
695 shape and size (**Fig. S9**).

696 Results of tensile modulus, tensile strength, and elongation at break for the non-
697 impregnated foams (PLAF and PLAF - 5% C30B) and the EU-PHE cocrystal impregnated
698 foams (PLAF - EU-PHE and PLAF - 5% C30B/EU-PHE) are shown in Table 4. Uniaxial
699 Stress-strain curves for the materials prepared in this study are shown in **Fig. S10**
700 (Supplementary material). PLAF control presented tensile strength (1.8 MPa) and elongation
701 at break (31.9%) values similar to those reported in the literature for expanded polystyrene
702 [84], which have encouraged the use of PLA foams at the industrial level for food packaging
703 purposes, including its use for the fabrication of cups and trays [85,86]. The presence of
704 C30B or the incorporation of EU-PHE did not significantly alter tensile modulus or tensile
705 strength. Nevertheless, C30B addition at 5% slightly increased the elongation at break of the
706 material from 31.9% (PLAF) to 48.2% (PLAF-5%C30B), which could be related to the full
707 exfoliation of C30B (part 3.2) which probably improved the polymeric matrix cohesion by
708 the electrostatic interactions established between C30B and the polymer chains, consequently
709 improving ductility. This behavior has been previously reported for montmorillonite clays
710 fully exfoliated in a polymeric matrix. Chen et al. reported an increase in the elongation at
711 break from 71.8% to 118% for poly(L-lactide)/poly(butylene succinate) blends using Cloisite
712 25A. The authors attributed the increase in ductility of the films to the electrostatic
713 interactions between C25A and the polymer chains promoted by C25A exfoliation [87].
714 Elongation at break was increased by EU-PHE cocrystal addition from 31.9% (PLAF control)

to 90.3% (PLAF-EU-PHE) due to its plasticizing effect on the polymeric matrix, which increased the material's ductility. This effect has been reported previously for PLA films impregnated with essential oil derivatives such as thymol [64] and cinnamaldehyde [66]. Consequently, the nanocomposite impregnated with the EU-PHE cocrystal (PLAF-5%C30B/EU-PHE) presented the highest elongation at break value (141%) due to the concomitant effect of C30B presence and higher EU-PHE cocrystal incorporation (9.19 % w/w) than in PLAF/EU-PHE (8.62 % w/w).

Table 4
Tensile properties parameters of the materials.

Material Sample	Tensile modulus [MPa]	Tensile Strength [MPa]	Elongation at break [%]
PLAF (control)	14.0 ± 5.3^{a}	1.8 ± 0.7^{a}	31.9 ± 7.8^{a}
PLAF - 5% C30B	17.5 ± 9.3^{a}	2.3 ± 0.9^{a}	48.2 ± 18.8^{a}
PLAF - EU-PHE	18.3 ± 10.4^{a}	3.0 ± 1.0^{a}	90.3 ± 32.9^{b}
PLAF - 5% C30B/EU-PHE	18.4 ± 8.9^{a}	4.9 ± 1.2^{b}	141.0 ± 25.0^{c}

Different superscripts indicate statistically significant differences.

3.6. The release kinetics

The release of EU in its pure and cocrystallized forms from PLAF with different C30B contents was studied through specific migration assays using EtOH 10% as an aqueous food simulant. The partition coefficient of EU ($K_{P/FS}$), a thermodynamic parameter that represents the ratio between the concentration of the bioactive substance in the polymer (P) and the food simulant (FS), was used to express the equilibrium condition. The mathematical modeling employing Korsmeyer-Peppas and Higuchi kinetic models was used to identify the

735 release mechanism of pure EU and cocrystallized EU from the PLA nanocomposite foams.
736 **Table 5** shows the values of the regression coefficient (R^2) obtained from the Higuchi and
737 Korsmeyer-Peppas models. Likewise, the diffusional exponent "n" for the Korsmeyer-
738 Peppas model and the release rate constant "k" were determined. The parameter "n" indicates
739 the type of active substance release mechanism: $n < 0.5$ for a quasi-Fickian diffusion, $n = 0.5$
740 for a Fickian diffusion, and $n > 0.5$ for an anomalous transport [88,89].

741
742 **Table 5.**
743 Partition coefficient ($K_{P/FS}$), regression coefficient (R^2), diffusional exponent (n), and release
744 rate constant (k) of Higuchi and Korsmeyer-Peppas kinetic models.
745

Kinetic Release Models		**Higuchi**			**Korsmeyer-Peppas**		
Sample	**$K_{P/FS}$**	**R^2**	**n**	**k**	**R^2**	**n**	**k**
PLAF-EU	947	0.421	0.5	0.075	0.961	0.055	0.223
PLAF- 5%C30B/EU	1248	0.299	0.5	0.049	0.944	0.033	0.200
PLAF-10%C30B/EU	1017	0.762	0.5	0.073	0.974	0.046	0.188
PLAF-EU-PHE	48	0.990	0.5	0.038	0.994	0.396	0.061
PLAF-5%C30B/EU-PHE	98	0.868	0.5	0.030	0.927	0.293	0.076
PLAF-10%C30B/EU-PHE	131	0.929	0.5	0.042	0.970	0.315	0.085

746

747 The highest R^2 values obtained using the Korsmeyer-Peppas model evidenced its
748 better performance compared to the Higuchi model to fit the experimental release data of EU
749 and EU-PHE cocrystal from the PLA nanocomposite foams. Therefore, the "k" and "n"
750 values determined using the Korsmeyer-Peppas model were used to study the release
751 mechanisms of EU and EU-PHE from PLA foams. **Table 5** shows that the different PLA

752 foams impregnated with EU and EU-PHE showed "n" values lower than 0.5, evidencing that
753 both EU and EU-PHE showed a quasi-Fickian diffusion release mechanism in these
754 materials. Previous studies on active polymeric foams have also reported a quasi-Fickian
755 diffusion mechanism for different substances. For instance, "n" values between 0.14 and 0.31
756 revealed that the release of chloramphenicol from polymeric blended foams based on
757 chitosan followed a quasi-Fickian diffusion-driven sustained release [90]. Likewise, the
758 release of cinnamaldehyde from PLA nanocomposite foams towards EtOH 50% also
759 followed a quasi-Fickian diffusion process since the "n" value was near 0.20 [19]. Spent
760 coffee phenolic compounds also followed a quasi-Fickian diffusion release mechanism from
761 starch foam composites in water and EtOH 10 and 50% as food simulants, with "n" values
762 between 0.18 and 0.49 [91].

763 Most research on designing antimicrobial food packaging materials has been done
764 considering the use of essential oils or some of their derivatives. The main challenge
765 identified so far is decreasing the release rate of these highly volatile compounds from
766 polymeric structures through different strategies [92]. Interestingly, the release kinetics of
767 eugenol from food packaging materials has been scarcely studied [93–95]. **Fig. 5** shows the
768 experimental EU release data from the different PLA foams. **Fig. 5a** indicates EU exhibited
769 a fast release, reaching the equilibrium condition independent of the C30B content after 2 h.
770 A similar fast-release behavior was reported for cinnamaldehyde from PLA nanocomposite
771 foams with different concentrations of C30B using EtOH 50% as food simulant [19]. Fitting
772 the experimental release data using the Korsmeyer-Peppas model showed that the release rate
773 constant (k) for EU in PLAF was 0.223. A similar release rate constant for EU (0.17) was
774 reported for poly (hydroxybutyrate-co-hydroxyvalerate) films and EtOH 10% as a food

775 simulant, evidencing a fast release of EU independent of the polymeric structure used to
776 design the active material [94]. On the contrary, the EU release curves for the PLA foams
777 impregnated with the EU-PHE cocrystal (**Fig. 5b**) exhibited a more prolonged EU release
778 than those impregnated with pure EU. In particular, the time (120 h) necessary to reach the
779 equilibrium condition for the release of cocrystallized EU from PLAF was 60-fold higher
780 than the value for pure EU (2 h). This result confirmed that the EU cocrystallization promoted
781 a prolonged EU release since the diffusion through the porous matrix was carried out in
782 association with a crystalline solid state instead of the liquid state (case of pure EU). In
783 another study, Celebioglu et al. reported a 10-fold decrease in the time necessary to reach the
784 equilibrium condition in water for EU released from pullulan nanofibers due to its
785 encapsulation in cyclodextrins (CDs) [93]. Particularly, the encapsulation of essential oil
786 derivatives in CDs has been one of the most effective reported strategies to prolong their
787 release [96–98]. Therefore, the comparison of the results obtained in this study with the
788 literature data indicates the advantage of cocrystallization engineering over conventional
789 methods to develop antimicrobial polymeric materials with more prolonged release
790 properties. New questions also arose about modifying release kinetic for a specific
791 application regarding the coformer choice, which would influence intermolecular interaction
792 between the coformer and active substance.

793 The sustained release of the EU-PHE cocrystal was also observed in the PLA
794 nanocomposite foams but with less intensity than in PLAF. Nevertheless, the time required
795 to reach the equilibrium condition for the release of the EU-PHE cocrystal decreased with
796 C30B content (**Fig. 5b).** Fitting the experimental release data using the Korsmeyer-Peppas
797 model allowed us to determine that the release rate constants of EU-PHE in PLAF-5%C30B

(0.076) and PLAF-10%C30B (0.085) were 1.25 and 1.39-fold higher than the value obtained for EU-PHE cocrystal in PLAF, respectively. The negative impact of the addition of C30B at 10% on the sustained release of the EU-PHE cocrystals could be associated with the agglomeration of C30B (part 3.2) and the generation of a nanocomposite foam with low porosity and expansion ratio which promoted a shorter release path in comparison with the other materials.

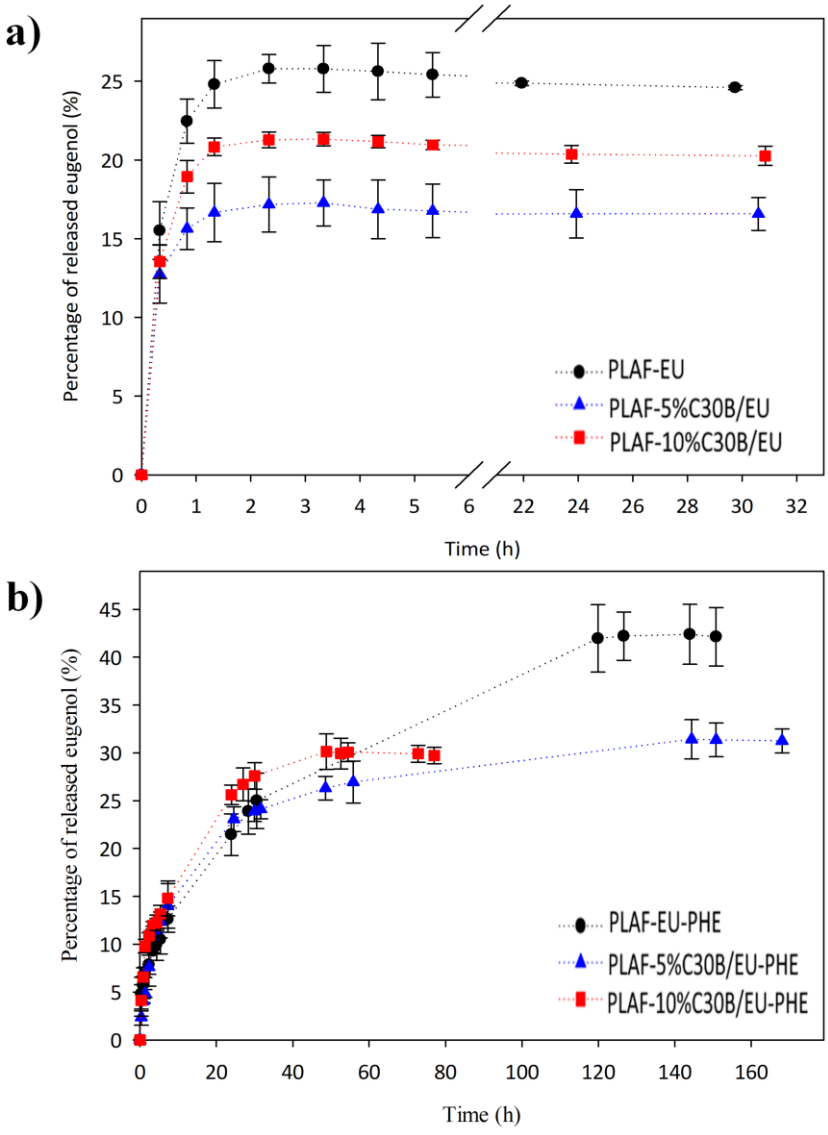

Fig. 5. Release curves of EU from a) EU-impregnated foams and b) EU-PHE cocrystal-impregnated foams towards EtOH 10% at 40 °C.

The sustained release of the EU-PHE cocrystal was also observed in the PLA nanocomposite foams but with less intensity than in PLAF. Nevertheless, the time required to reach the equilibrium condition for the release of the EU-PHE cocrystal significantly decreased with C30B content (**Fig. 5b).** Fitting the experimental release data using the Korsmeyer-Peppas model allowed us to determine that the release rate constants of EU-PHE in PLAF-5%C30B (0.076) and PLAF-10%C30B (0.085) were 1.25 and 1.39-fold higher than the value obtained for EU-PHE cocrystal in PLAF, respectively. The negative impact of the addition of C30B at 10% on the sustained release of the EU-PHE cocrystals could be associated with the agglomeration of C30B (part 3.2) and the generation of a nanocomposite foam with low porosity and expansion ratio, which promoted a shorter release path in comparison with the other materials.

Table 5 also summarizes the distribution coefficients ($K_{P/FS}$) that characterize the equilibrium condition for the release of EU and EU-PHE from the different PLA nanocomposite foams. Among the polymeric foam samples impregnated with pure EU, PLAF showed the lowest $K_{P/FS}$ value, evidencing the highest percent released of EU to the food simulant at the equilibrium condition (**Fig. 5a**). The $K_{P/FS}$ value increased with the concentration of C30B. This fact could be related to the interaction between the free hydroxyl groups of C30B and the EU hydroxyl groups that increased the affinity of EU towards the polymeric phase, decreasing its release to the simulant. The same phenomenon was also observed for the release of thymol from LDPE extruded films with C30B at 5 % w/w [4] and LLDPE extruded films loaded with C20A [99]. In these studies, the high retention of thymol in the polymer was associated to interactions between the nanoclays and the active compounds. In our study, the lowest EU release was obtained from PLA nanocomposite foam

with C30B at 5 % w/w. In this case, the exfoliation of the nanoclays in the foam favored the retention of EU in the foams. Instead, the poor dispersion of the nanoclay sheets in the PLA nanocomposite foam with C30B at 10 % w/w promoted the easier release of the active compound to the food simulant, evidenced by lower $K_{P/FS}$ values than for the PLA nanocomposite foam with C30B at 5 % w/w.

Table 5 shows that the highest percentages of released EU were obtained from PLA foams impregnated with the EU-PHE cocrystal. Particularly, $K_{P/FS}$ values for the release of EU from PLAF impregnated with the EU-PHE were 20-fold lower than the value obtained for the PLAF impregnated with pure EU. This fact is related to the lower initial EU content (4.14 % w/w) in the samples impregnated with EU-PHE cocrystal compared to the initial EU content (20 % w/w) in the PLAF impregnated with pure EU. As was obtained for the EU-impregnated samples, the $K_{P/FS}$ for EU increased by the C30B presence due to the interactions developed between C30B and the EU-PHE cocrystal.

3.7. Microbiological studies

The obtained MIC value of EU for *L. monocytogenes* and *S. Enteritidis* was 1.25%. The obtained MIC values of PHE and the EU-PHE cocrystal were >5%.

The log CFU/cm^2 reduction values of the anti-attachment assay on *L. monocytogenes* compared to the PLAF control are shown in **Fig. 6**. *L. monocytogenes* growth expressed as CFU/cm^2 is displayed in **Table S1** (Supplementary material). Total attachment inhibition of *L. monocytogenes* occurred after 24 h on PLA-5%C30B/EU-PHE, PLAF-5%C30B/EU, PLAF-10%C30B/EU, PLAF-EU/PHE, and PLAF-EU with zero attached cells (**Fig. 6a)**.

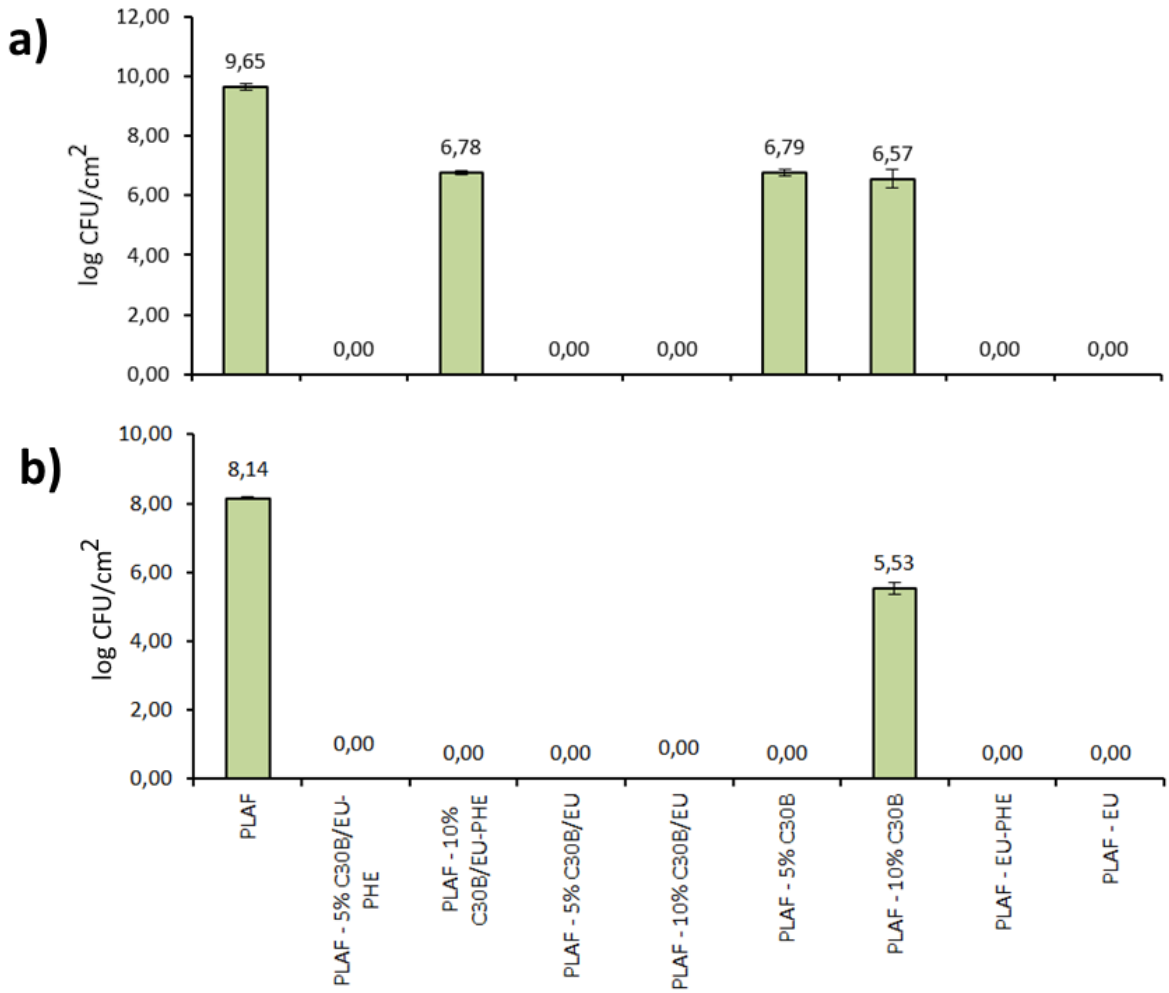

Fig. 6. Inhibition of adhesion of *L. monocytogenes* on PLAF nanocomposite foams after a) 24 h and b) 48 h of incubation in TSB with 1 % glucose. Legend: The results were expressed as log CFU/cm^2 of attached cells.

The tested strain, after 24 h, successfully attached to the PLAF control surface with a total number of 9.65±0.13 log CFU/cm^2, and to the PLA nanocomposite foams surfaces (PLAF-5%C30B and PLAF-10%C30B) in a number of 6.79±0.12 log CFU/cm^2 and 6.50±0.30 log CFU/cm^2, respectively. Regardless of the successful attachment to PLAF-5%C30B and PLAF-10%C30B, the significant logarithmic reduction between 2.87 – 3.0 log CFU/cm^2 ($p<0,05$) in the number of attached *Listeria* is noticeable in comparison with the

865 control PLAF (**Table S1**). The antibacterial activity of C30B against *L. monocytogenes* has
866 been reported previously for LDPE/C30B films [100] and polyethylene)/thermoplastic
867 starch/C30B films [101], and it has been attributed to the action of the quaternary ammonium
868 cations in the C30B silicate layers. In our study, the detected number of attached *L.*
869 *monocytogenes* of 6.78±0.07 log CFU/cm^2 to PLAF-10%C30B-EU-PHE was similar to log
870 CFU values detected on non-impregnated nanocomposites, PLAF-5%C30B and PLAF-
871 10%C30B (**Fig. 6a**), which indicated that during the first 24 h of incubation, the EU-PHE
872 cocrystal was still not available to exert an additional antibacterial activity against *L.*
873 *monocytogenes*. This result could be explained in terms of the higher retention capacity of
874 the EU cocrystal as the C30B content increases, as evidenced by the release assays using a
875 food simulant.

876 A prolonged incubation period of 48 h provided a complete adhesion inhibition of *L.*
877 *monocytogenes* on the surface of all tested PLAF samples, except the control PLAF and
878 PLAF-10% C30B, where the strain attached in the number of 8.14±0.07 log CFU/cm^2 and
879 5.53±0.16 log CFU/cm^2, respectively (**Fig. 6b**). Particularly, the weaker anti-attachment
880 activity of PLAF-10%C30B, compared with the activity of PLAF-5%C30B, could be
881 associated with the thermal degradation of its quaternary ammonium modifiers during the
882 extrusion process [100]. This degradation phenomenon was evidenced by XRD only for the
883 PLA nanocomposite foam sample with C30B at 10% and not for the nanocomposite foam
884 with C30B at 5%.

885

886 The log CFU/cm^2 reduction values obtained in the anti-attachment assay of *S.*
887 Enteritidis compared to the PLAF control are shown in **Figure 7**. *S.* Enteritidis growth
888 expressed as CFU/cm^2 is shown in **Table S2**.
889

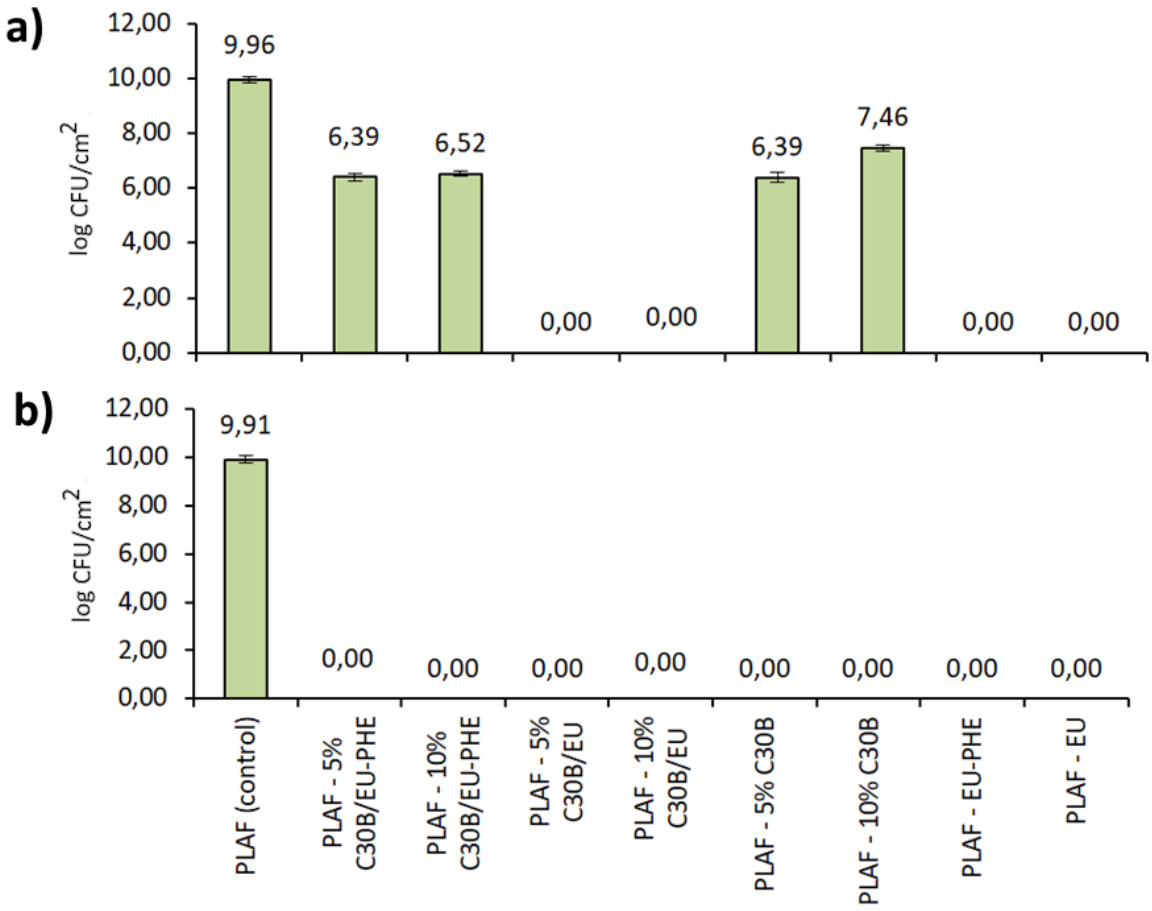

890

891 **Fig. 7.** Inhibition of adhesion of *S.* Enteritidis on PLAF nanocomposite foams after a) 24 h
892 and b) 48 h of incubation in TSB with 1% glucose. Legend: The results are expressed as log
893 CFU/cm^2 of attached cells.
894

After 24 h of incubation, total adhesion inhibition of *S.* Enteritidis occurred on PLAF-5%C30B/EU, PLAF-10%C30B/EU, PLAF-EU-PHE, and PLAF-EU, (>9,0 log CFU reduction compared to PLAF control, $p<0.05$) (**Table 2S**). *S.* Enteritidis showed stronger resistance to contact inhibition compared to *L. monocytogenes* and after 24 hours it successfully attached to the PLAF control and to the PLA nanocomposite foams impregnated with the EU-PHE cocrystal (PLAF-5%C30B/EU-PHE and PLAF-10%30B/EU-PHE) in a total number of 9.96 ±0.10 log CFU/cm^2, 6.39±0.15 log CFU/cm^2, 6.52±0.10 log CFU/cm^2, respectively (**Fig. 7a**). These results could be related, to the higher MIC values of the EU-PHE cocrystal compared with the pure EU. Also, C30B retains the cocrystal in the PLAF structure better than PLAF without C30B. This was evidenced from the release assays using a food simulant (part 3.6) through the 3-fold increase for the cocrystal distribution coefficient due to the presence of 10%C30B compared with the cocrystal distribution coefficient for the PLAF without C30B. As expected, *S.* Enteritidis successfully attached to PLAF-5%C30B and PLAF-10%C30B, in a total number of 6.39±0.18 log CFU/cm^2, 7.46±0.11 log CFU/cm^2, respectively. Despite the successful attachment, both nanocomposite PLA foams significantly reduced the total number of attached cells compared to the PLAF control (log CFU/cm^2 reduction 2.49 -3.45, $p<0.05$) (**Table 2S**).

After 48 hours of incubation, all impregnated PLAF films exhibited a complete adhesion inhibition effect on *S.* Enteritidis, with zero cells detected on the surface of the films, which is a 100% reduction compared to the PLAF control ($p<0.05$) (**Fig. 7b**). These results show that C30B did not reduce the antimicrobial potential of the EU-PHE cocrystal but slowed down its manifestation. PLAF with C30B alone (without impregnated EU or EU-PHE cocrystal) also exhibited antimicrobial activity against *S.* Enteritidis due to the release of quaternary ammonium cations from C30B silicate layers.

Regarding the determination of killing effect (KE), bacterial growth control ($A_{control}$), and culture with PLAF non-impregnated polymer ($A_{control\ PLAF}$) had very similar OD values (statistically and microbiologically, the differences were insignificant), which was expected for PLAF to be microbiologically inert. Therefore, due to the easier and clearer presentation of the results, in **Table 6** and **Table 7**, results are presented as % of the growth of *Listeria* and *Salmonella*, respectively, in the broth with impregnated foams compared to their growth with the control PLAF which was taken as a 100% growth.

Table 6
Killing effect [KE%] during 96 h incubation of *Listeria monocytogenes.*

Sample	KE [%]			
	After 24h	After 48h	After 72h	After 96h
PLAF - 5% C30B/EU-PHE	99.24 ± 0.06	48.71 ± 0.30	103.70 ± 0.45	95.34 ± 0.46
PLAF - 10% C30B/EU-PHE	98.88 ± 0.06	65.44 ± 1.23	81.91. ± 0.31	80.31 ± 0.01
PLAF - 5% C30B/EU	95.42 ± 0.05	108.73 ± 0.53	78.85 ± 0.28	95.91 ± 0.35
PLAF - 10% C30B/EU	95.79 ± 0.11	64.71 ± 0.36	87.45 ± 0.49	78.28 ± 0.04
PLAF - 5% C30B	99.97 ± 0.06	83.90 ± 0.07	102.74 ± 0.49	111.81 ± 0.01
PLAF - 10% C30B	99.34 ± 0.15	109.39 ± 0.01	100.09 ± 0.27	71.84 ± 0.05
PLAF - EU-PHE	99.41 ± 0.10	85.40 ± 0.44	96.83 ± 0.30	69.31 ± 0.21
PLAF - EU	95.82 ± 0.05	95.48 ± 0.53	93.42 ± 0.18	50.12 ± 0.03
PLAF	100.00 ± 0.00	100.00 ± 0.00	100.00 ± 0.00	100.00 ± 0.00

Legend: Percentage of bacterial growth in the presence of impregnated PLAF films compared to the PLAF control, which was taken as 100% growth.

The broth killing effect results, which were directly proportional to the release of the active substances into the environment, indicated that the release of the antimicrobial substances from all the foams needed to be triggered by the previous soaking of the PLA foams in a liquid medium for approximately 24 h. This result is very relevant for antibacterial food packaging because the antibacterial substances need to be released to the food only when it is necessary, i.e., once the food is packaged and not before, by means of a trigger

937 mechanism for the release of the antimicrobial substances, such as the water vapor emitted
938 from some foods, such as fruits and vegetables, to the package headspace [92,102,103].
939 After 48 h of contact, all active PLA foams, except PLAF-10%C30B and PLAF-
940 5%C30B-EU, showed antibacterial activity against *L. monocytogenes*, reducing the growth
941 between 4.52% and 51.29%. Particularly, PLAF impregnated with EU manifested only
942 4.52% growth reduction of *L. monocytogenes*, which could be related to the low solubility of
943 EU in an aqueous medium. The growth reduction of *L. monocytogenes* slightly increased to
944 6.58% after 72 h and 49.88% after 96 h
945 A significantly higher growth reduction of *L. monocytogenes* was obtained for the
946 PLAF impregnated with the EU-PHE cocrystal (14.6%) after 48 h. This result is very
947 interesting, considering that phenazine (the other component of the cocrystal) itself didn't
948 exert strong antibacterial activity against *L. monocytogenes.* Moreover, the initial amount of
949 EU-PHE cocrystal in PLAF-EU-PHE (8.62% w/w) was lower than the initial content of EU
950 in PLAF-EU (21% w/w), which implied a lower active compound concentration gradient for
951 the release of the cocrystal compared with EU. Considering both facts, the notable increase
952 in the capacity of EU to inhibit the growth of *L. monocytogenes* could be related to the
953 synergistic antibacterial activity between EU and PHE in the broth culture and to the
954 improvement of the EU solubility in the aqueous medium due to its cocrystallization.
955 Different solutes have been found to become more soluble in aqueous media thanks to their
956 cocrystallization [89,104,105].
957 Probably the highest solubility of EU in its cocrystallized form allowed the PLAF-
958 EU-PHE sample to reach the maximal growth reduction of *L. monocytogenes* (30.69%) after
959 96 h, not so far from the growth reduction reached by PLAF-EU (49.88%), even considering
960 the notable differences in the initial amount of EU between PLAF-EU (21% w/w) and PLAF-

EU-PHE (4.14 % w/w). This is a relevant result because the design of antibacterial food packaging materials should consider the use of minimal amounts of essential oil derivatives to exert the desired antibacterial effect on food with minimal impact on the physical properties of the plastic films [106,107] and the organoleptic properties and food quality [88,108].

Interestingly, after 48 h, both nanocomposite PLAF samples impregnated with the EU-PHE cocrystal, PLAF-5%C30B-EU-PHE, and PLAF-10%C30B-EU-PHE, showed stronger *L. monocytogenes* growth reduction values (51.29% and 34.56%, respectively) comparing to the sum of the individual growth reduction rates obtained for PLAF-5%C30B (16.1%), PLAF-10%C30B (0%) and PLAF-EU-PHE (14.6%), indicating that C30B and EU-PHE had synergistic antibacterial activity against *L. monocytogenes*. Particularly, the lower inhibition growth of PLAF-10%C30B-EU-PHE compared with the activity of PLAF-5%C30B-EU-PHE, which agrees with the attachment inhibition assay results for *L. monocytogenes* obtained using both samples, could be associated with the decrease of the C30B antibacterial activity due to partial thermal degradation of its quaternary ammonium modifiers during the extrusion process and to the lower amount of EU-PHE cocrystal released from the PLAF sample with the highest C30B content after 48 h. Considering that both nanocomposite foams presented a similar initial amount of EU-PHE cocrystal, the lower release of the cocrystal from PLAF-10%C30B could be related to the increase in the cocrystal retention capacity of PLAF as C30B content increased, which even allowed the PLAF-10%C30B-EU-PHE sample to supply cocrystal to the broth culture after 96 h in a controlled manner to exert an approximately 20% growth reduction of *L. monocytogenes*. Meanwhile, PLAF-5%C30B-EU-PHE loses completely its antibacterial properties against *L. monocytogenes* between 48 h and 72 h due to its lower EU-PHE cocrystal retention capacity.

The high EU-PHE retention capacity for the nanocomposite PLAF with the highest C30B content was evidenced from the release assays using a food simulant (part 3.5) through the 1.34-fold increase in the cocrystal distribution coefficient by the increase in C30B content from 5% to 10%.

Table 7
Killing effect [KE%] during 96h incubation of ***Salmonella*** **Enteritidis.**

Samples	KE [%]			
	After 24h	After 48h	After 72h	After 96h
PLAF - 5% C30B/EU-PHE	97.98 ± 0.13	68.91 ± 1.52	94.11 ± 0.80	94.80 ± 0.02
PLAF - 10% C30B/EU-PHE	92.07 ± 0.04	84.40 ± 2.14	96.27 ± 0.31	90.49 ± 0.04
PLAF - 5% C30B/EU	59.52 ± 0.08	49.41 ± 1.30	83.99 ± 0.28	90.13 ± 0.06
PLAF - 10% C30B/EU	67.95 ± 0.06	54.56 ± 1.18	56.76 ± 0.41	68.87 ± 0.17
PLAF - 5% C30B	99.42 ± 0.08	38.36 ± 0.92	100.66 ± 0.76	99.16 ± 0.42
PLAF - 10% C30B	101.58 ± 0.14	62.71 ± 1.45	102.07 ± 0.47	101.04 ± 0.04
PLAF - EU-PHE	91.02 ± 0.08	20.59 ± 0.46	92.49 ± 0.52	94.89 ± 0.00
PLAF - EU	77.35 ± 0.05	19.45 ± 0.46	82.67 ± 0.51	88.04 ± 0.04
PLAF	100.00 ± 0.00	100.00 ± 0.00	100.00 ± 0.00	100.00 ± 0.00

Legend: Percentage of bacterial growth in the presence of experimental, impregnated PLAF films compared to the PLAF control, which was taken as 100% growth.

Table 7 shows that the samples impregnated with EU were more effective than EU-PHE cocrystal-impregnated samples to inhibit the growth of *S.* Enteritidis. In the first 24 h. PLAF-5%C30B/EU. PLAF-10%C30B/EU and PLAF-EU showed a relatively strong killing effect, reducing the growth of *S.* Enteritidis by approximately 40%, 30%, and 25%, respectively. Meanwhile. in the first 24 h. the nanocomposite PLAF samples (PLAF-5%C30B and PLAF-10%C30B) did not reduce the growth of *S.* Enteritidis.

All polymers strongly reduced the growth of *Salmonella* after 48h, of which PLAF-EU and PLAF-EU-PHE were particularly strong, reducing growth by 80%, while PLAF-5%C30B. PLAF-5%C30B/EU and PLAF-10%C30B/EU were also relatively strong with a

reduction in growth of approximately 45-60%. Particularly, the weaker growth inhibition of *Salmonella* using PLAF with C30B could be the effect of increasing the retaining EU and EU-PHE capacity with the simultaneous increase in C30B content, which reduced the release of both substances into the broth culture. This was also evidenced by the release assays using a food simulant (part 3.6). Unlike in antibacterial assays against *L. monocytogenes*, where several foams showed the strongest killing effect after 96 h, only PLAF-10%C30B/EU retained the killing effect against *Salmonella* Enteritidis in the 96th hour (with approximately 30% growth reduction) due to more prolonged release of EU from this sample.

3.8. Relevance of the obtained results and future prospective

3.8.1. Relevance for the food industry

Unlike most infectious diseases that have been eradicated or suppressed significantly in the last few decades, *salmonellosis* and *listeriosis* are continuously present in all countries, regardless of the region's geographical, cultural, and climate characteristics [109,110]. In recent decades, parallel to the development of molecular research methods, there is more and more evidence that certain *L. monocytogenes* strains and *Salmonella* serovars can persist for months and even years in food production facilities. Equipment and all kinds of surfaces made of plastic, stainless steel, wood, glass, and gum may be a substrate for successful surface adherence of *S.* Enteritidis and *L. monocytogenes* and for the development of biofilms that become a source of repeated contamination of final food products [111]. According to data from the *European Food Safety Authority* (EFSA), in 2019, there were 87,923 cases of *salmonellosis* recorded in the territory of European countries, the source of which was food [112]. The incidence of *listeriosis* is significantly lower and amounted to 0.46 and 0.24 cases per 100,000 population in 2015 in the European Union and the United States, respectively

[111]. Despite the reduced incidence during the last decade, cases of *salmonellosis* and *listeriosis* are still relatively frequent, leading to a certain number of deaths and high economic costs for hospitalized affected consumers [113]. There is also the perspective of the significant economic losses of the food industry, which, after the outbreaks of *salmonellosis* or *listeriosis,* is obliged to withdraw from the sale and destroy all contaminated products or to stop production completely.

Based on the obtained results, in theory, materials developed in this study that showed the strongest antimicrobial activity and significantly reduced the total number of *Salmonella* and *Listeria* (such as PLAF-EU-PHE, which reduced the total number of *Salmonella* by approximately 80%) would significantly reduce the incidence of *salmonellosis* and *listeriosis* if applied on the industrial level. Besides the envisaged application to substitute PS trays, we should not rule out the possible use of obtained materials for packaging food for animals, especially for intensively breeding animals on farms. The animal food can also be contaminated with *Salmonella* and lead to outbreaks of diseases in farms with substantial economic consequences. We should not forget that the initial number of microorganisms in our study was very high, 10^8 CFU/mL. In comparison, the number of *Salmonella* and *Listeria* in contaminated food can be significantly lower (10^3 CFU/mL, 10^2 CFU/mL, or even smaller). Therefore, the actual effect of the *in situ* PLAF material in which the contaminated food is packed could be increased to 100%.

From the microbiological point of view, a new question arose. Is it possible to design an active food packaging aimed at protection from a target bacterial strain? We reported obviously different (individual) degrees of sensitivity of *Salmonella* and *Listeria* to the same material designed in this study. Therefore, a new hypothesis was developed that designing

specialized active packaging with the maximal antimicrobial activity against *Listeria* or *Salmonella* was possible.

3.8.2. Relevance for the pharmaceutical industry

The crystallization to obtain the smallest possible crystals of active pharmaceutical ingredients (API) with improved bioavailability is very important for the pharmaceutical industry. Consequently, micronization techniques have been developed applying $scCO_2$ as a green solvent or antisolvent [114]. As mentioned in the introduction, cocrystallization has gained tremendous importance in the pharmaceutical industry because of its ability to fine-tune the physicochemical properties of crystalline drugs without modifying their molecular structure [115]. There are reports and efforts to establish API cocrystallization from the $scCO_2$ phase [116,117]. The proposed process (CSS - cocrystallization from supercritical solution) is based on the dissolution of pure API and conformer in $scCO_2$ and their posterior cocrystallization from the supercritical phase during the cooling and decompression. However, the main limitation of this process is the necessity of similar solubilities of the API and conformer in $scCO_2$ [117]. In this study, we demonstrated a possibility to overcome this limitation. We produced micronized EU-PHE cocrystals (average diameter of 0.8 μm) in an environmentally friendly manner without organic solvents, though EU and PHE have significantly different solubilities in $scCO_2$ (0.037 and 0.00109 g/g_{scCO2}, respectively). We introduced the re-cocrystallization (or cocrystal recrystallization) based on the dissolution of previously formed large cocrystals in $scCO_2$ (average diameter of 25 μm) with the subsequent micronization from the supercritical phase. The prerequisites for this process are cocrystal stability (*e.g.*, no liquid EU separation from the cocrystal when exposed to $scCO_2$) and good solubility in $scCO_2$. To our knowledge, this study is the first report on re-cocrystallization

from the $scCO_2$. Therefore, the obtained results are relevant for the pharmaceutical industry as well.

4. Conclusions

The EU-PHE cocrystal was produced by a simple mechanical method. The cocrystal was stable in $scCO_2$ under the conditions of interest, with the solubility in $scCO_2$ approximately ten times larger than the cofomer's solubility (PHE). Nanocomposite PLA films with 0, 5, and 10 % w/w of nanoclay were produced by extrusion. In the next step, the films were foamed by $scCO_2$. The foams were successfully impregnated with EU (impregnation yields from 20 to 22 % w/w) and EU-PHE cocrystal (impregnation yields from 8.62 to 9.25 % w/w) via SSI. The presence of C30B and cocrystal improved the mechanical properties of PLA foams. The SEM, DCS, TGA, and XRD analyses confirmed the EU-PHE cocrystal re-crystallization within the PLA foams. Consequently, the foams impregnated with PHE-EU cocrystal had significantly slower release kinetics of the active compound than EU-impregnated ones. The impregnated foams completely inhibited the attachment of *Listeria monocytogenes* and *Salmonella* Enteritidis strains. PLAF-EU-PHE sample reduced the total number of *Salmonella* in broth by approximately 80% after 48 h. PLAF - 5% C30B/EU-PHE and PLAF-10% C30B/EU-PHE foams showed the strongest reduction of *Listeria monocytogenes* in 48 h. The release and microbiological assays showed that PLAF-C30B/EU-PHE polymeric foams had prolonged EU release and extended bioactivity.

This study proposes a green approach to designing antimicrobial food packaging materials based on the coupling of the concepts of supercritical fluid technology and cocrystallization engineering. The successful EU-PHE cocrystal micronization by $scCO_2$ is of interest to materials engineering and pharmaceutical technology.

CRediT authorship contribution statement

Adrián Rojas: Conceptualization. Methodology. Formal analysis. Supervision. Writing original draft. Writing– review & editing. Project administration. Funding acquisition. **Dusan Misic:** Methodology. Investigation. Formal analysis. Writing original draft. Writing– review & editing. **Irena Zizovic**: Methodology. Investigation. Writing original draft. Writing– review & editing. **Carol López de Dicastillo:** Formal analysis. Writing original draft. Writing– review. **Aleksandra Rajewska:** Methodology. Investigation. Formal analysis. **Eliezer Velásquez:** Formal analysis. Writing original draft. Writing– review & editing. **Bastián Rozas:** Investigation. Formal analysis. **Luciano Catalán:** Investigation. Formal analysis. **Cristian Vidal Patiño:** Writing original draft.. **Abel Guarda:** Supervision. Resources. **María José Galotto:** Supervision. Resources. Project administration. Funding acquisition.

Declaration of Competing Interest

The authors declare that they have no known competing financial interests or personal relationships that could have appeared to influence the work reported in this paper.

Acknowledgment

M.J. Galotto and A. Rojas thank the support of Agencia Nacional de Investigación y Desarrollo through the Fondecyt regular Project N°1201301 and to the "Programa de Financiamiento Basal para Centros Científicos y Tecnológicos de Excelencia" (Project AFB220001). A. Rojas thanks the support of the University of Santiago de Chile through the Postdoctoral Fellowship DICYT Código 082371GL_Postdoc. C. López de Dicastillo acknowledges the "Ramon y Cajal" Fellowship RYC2020-029874-I/AEI/10.13039/501100011033 financed by the Spanish Ministry of Science and Innovation. D. Misic and I. Zizovic thank the support of Narodowe Centrum Nauki. (Poland), Grant number 2019/35/B/NZ9/02774.

References

[1] B. Malhotra, A. Keshwani, H. Kharkwal, Antimicrobial food packaging: Potential and pitfalls, Front Microbiol. 6 (2015) 1–9. https://doi.org/10.3389/fmicb.2015.00611.

[2] X. Chen, M. Chen, C. Xu, K.L. Yam, Critical review of controlled release packaging to improve food safety and quality, Crit Rev Food Sci Nutr. 59 (2019) 2386–2399. https://doi.org/10.1080/10408398.2018.1453778.

[3] L. Kuai, F. Liu, B. Sen Chiou, R.J. Avena-Bustillos, T.H. McHugh, F. Zhong, Controlled release of antioxidants from active food packaging: A review, Food Hydrocoll. 120 (2021) 106992. https://doi.org/10.1016/J.FOODHYD.2021.106992.

[4] A. Rojas, A. Torres, A. Añazco, C. Villegas, M.J. Galotto, A. Guarda, J. Romero, Effect of pressure and time on scCO<inf>2</inf>-assisted incorporation of thymol into LDPE-based nanocomposites for active food packaging, Journal of CO2 Utilization. 26 (2018) 434–444. https://doi.org/10.1016/j.jcou.2018.05.031.

[5] A. Rojas, A. Torres, F. Martínez, L. Salazar, C. Villegas, M.J. Galotto, A. Guarda, J. Romero, Assessment of kinetic release of thymol from LDPE nanocomposites obtained by supercritical impregnation: Effect of depressurization rate and nanoclay content, Eur Polym J. 93 (2017). https://doi.org/10.1016/j.eurpolymj.2017.05.049.

[6] N. Alvarado, J. Romero, A. Torres, C. López de Dicastillo, A. Rojas, M.J. Galotto, A. Guarda, Supercritical impregnation of thymol in poly(lactic acid) filled with electrospun poly(vinyl alcohol)-cellulose nanocrystals nanofibers: Development an active food packaging material, J Food Eng. 217 (2018). https://doi.org/10.1016/j.jfoodeng.2017.08.008.

[7] M.S. Razavi, A. Golmohammadi, A. Nematollahzadeh, C. Rovera, S. Farris, Cinnamon Essential Oil Encapsulated into a Fish Gelatin-Bacterial Cellulose Nanocrystals Complex and Active Films Thereof, Food Biophys. 17 (2022) 38–46. https://doi.org/10.1007/s11483-021-09696-6.

[8] M. Li, F. Zhang, Z. Liu, X. Guo, Q. Wu, L. Qiao, Controlled Release System by Active Gelatin Film Incorporated with β-Cyclodextrin-Thymol Inclusion Complexes, Food Bioproc Tech. 11 (2018) 1695–1702. https://doi.org/10.1007/s11947-018-2134-1.

[9] A. Adjali, A.R.N. Pontillo, E. Kavetsou, A. Katopodi, A. Tzani, S. Grigorakis, S. Loupassaki, A. Detsi, Clove Essential Oil–Hydroxypropyl-β-Cyclodextrin Inclusion Complexes: Preparation, Characterization and Incorporation in Biodegradable Chitosan Films, Micro. 2 (2022) 212–224. https://doi.org/10.3390/micro2010014.

[10] M. Krepker, C. Zhang, N. Nitzan, O. Prinz-Setter, N. Massad-Ivanir, A. Olah, E. Baer, E. Segal, Antimicrobial LDPE/EVOH layered films containing carvacrol fabricated by multiplication extrusion, Polymers (Basel). 10 (2018) 3–4. https://doi.org/10.3390/polym10080864.

[11] W. Zhang, C. Shu, Q. Chen, J. Cao, W. Jiang, The multi-layer film system improved the release and retention properties of cinnamon essential oil and its application as coating in inhibition to penicillium expansion of apple fruit, Food Chem. 299 (2019) 125109. https://doi.org/10.1016/J.FOODCHEM.2019.125109.

[12] G. Mensitieri, Supercritical fluids, Supercritical Fluid Science and Technology. 9 (2021) 55–68. https://doi.org/10.1016/B978-0-444-63724-6.00004-4.
[13] Ž. Knez, M. Škerget, M. Knez Hrnčič, D. Čuček, Chapter 2 - Particle Formation Using Sub- and Supercritical Fluids, in: V. Anikeev, M.B.T.-S.F.T. for E. and E.A. Fan (Eds.), Elsevier, Boston, 2014: pp. 31–67. https://doi.org/https://doi.org/10.1016/B978-0-444-62696-7.00002-2.
[14] E. Weidner, Impregnation via supercritical CO2–What we know and what we need to know, J Supercrit Fluids. 134 (2018) 220–227. https://doi.org/10.1016/J.SUPFLU.2017.12.024.
[15] G.A. Sutil, K.S. Andrade, E.A. Rebelatto, M. Lanza, Effects of incorporation of pure or multicomponent active agents in biopolymers for food packaging using supercritical CO2, Trends Food Sci Technol. 120 (2022) 349–362. https://doi.org/10.1016/J.TIFS.2022.01.025.
[16] N.D. Machado, J.E. Mosquera, R.E. Martini, M.L. Goñi, N.A. Gañán, Supercritical CO2-assisted impregnation/deposition of polymeric materials with pharmaceutical, nutraceutical, and biomedical applications: A review (2015–2021), J Supercrit Fluids. 191 (2022) 105763. https://doi.org/10.1016/J.SUPFLU.2022.105763.
[17] A. Rojas, A. Torres, M.J. Galotto, A. Guarda, R. Julio, Supercritical impregnation for food applications: a review of the effect of the operational variables on the active compound loading, Crit Rev Food Sci Nutr. 60 (2020) 1290–1301. https://doi.org/10.1080/10408398.2019.1567459.
[18] M. Champeau, J.M. Thomassin, T. Tassaing, C. Jérôme, Drug loading of polymer implants by supercritical CO2 assisted impregnation: A review, Journal of Controlled Release. 209 (2015) 248–259. https://doi.org/10.1016/J.JCONREL.2015.05.002.
[19] A. Rojas, A. Torres, C.L. de Dicastillo, E. Velásquez, C. Villegas, S. Faba, P. Rivera, A. Guarda, J. Romero, M.J. Galotto, Foaming with scCO2 and Impregnation with Cinnamaldehyde of PLA Nanocomposites for Food Packaging, Processes. 10 (2022). https://doi.org/10.3390/pr10020376.
[20] A. Satpayeva, A. Rojas, M. Tyrka, E. Ksepko, M.J. Galotto, I. Zizovic, Supercritical Foaming and Impregnation of Polycaprolactone and Polycaprolactone-Hydroxyapatite Composites with Carvacrol, Processes. 10 (2022) 482. https://doi.org/10.3390/pr10030482.
[21] S. Milovanovic, D. Markovic, A. Mrakovic, R. Kuska, I. Zizovic, S. Frerich, J. Ivanovic, Supercritical CO 2 - assisted production of PLA and PLGA foams for controlled thymol release, Materials Science and Engineering C. 99 (2019) 394–404. https://doi.org/10.1016/j.msec.2019.01.106.
[22] M. Guo, X. Sun, J. Chen, T. Cai, Pharmaceutical cocrystals: A review of preparations, physicochemical properties and applications, Acta Pharm Sin B. 11 (2021) 2537–2564. https://doi.org/10.1016/J.APSB.2021.03.030.
[23] J.L. Dias, M. Lanza, S.R.S. Ferreira, Cocrystallization: A tool to modulate physicochemical and biological properties of food-relevant polyphenols, Trends Food Sci Technol. 110 (2021) 13–27. https://doi.org/10.1016/J.TIFS.2021.01.035.

[24] H. Zu, R.F. Henry, G.G.Z. Zhang, L.R. MacGillivray, Inhibiting Sublimation of Thymol by Cocrystallization, J Pharm Sci. 112 (2023) 350–353. https://doi.org/10.1016/J.XPHS.2022.10.019.
[25] P.P. Mazzeo, C. Carraro, A. Monica, D. Capucci, P. Pelagatti, F. Bianchi, S. Agazzi, M. Careri, A. Raio, M. Carta, F. Menicucci, M. Belli, M. Michelozzi, A. Bacchi, Designing a Palette of Cocrystals Based on Essential Oil Constituents for Agricultural Applications, ACS Sustain Chem Eng. 7 (2019) 17929–17940. https://doi.org/10.1021/acssuschemeng.9b04576.
[26] F. Bianchi, F. Fornari, N. Riboni, C. Spadini, C.S. Cabassi, M. Iannarelli, C. Carraro, P.P. Mazzeo, A. Bacchi, S. Orlandini, S. Furlanetto, M. Careri, Development of novel cocrystal-based active food packaging by a Quality by Design approach, Food Chem. 347 (2021) 129051. https://doi.org/10.1016/J.FOODCHEM.2021.129051.
[27] H. Services, 54960 Federal Register / Vol . 81 , No . 159 / Wednesday , August 17 , 2016 / Rules and Regulations AGENCY : ACTION :, 81 (2016) 54960–55055.
[28] E. Orlo, C. Nerín, M. Lavorgna, M. Wrona, C. Russo, M. Stanzione, R. Nugnes, M. Isidori, Antioxidant activity of coatings containing eugenol for flexible aluminium foils to preserve food shelf-life, Food Packag Shelf Life. 39 (2023) 101145. https://doi.org/10.1016/J.FPSL.2023.101145.
[29] M.T. Yilmaz, W.S. Hassanein, A.S. Alkabaa, Z. Ceylan, Electrospun eugenol-loaded gelatin nanofibers as bioactive packaging materials to preserve quality characteristics of beef, Food Packag Shelf Life. 34 (2022) 100968. https://doi.org/10.1016/J.FPSL.2022.100968.
[30] J. Cheng, H. Wang, S. Kang, L. Xia, S. Jiang, M. Chen, S. Jiang, An active packaging film based on yam starch with eugenol and its application for pork preservation, Food Hydrocoll. 96 (2019) 546–554. https://doi.org/10.1016/J.FOODHYD.2019.06.007.
[31] L. Lin, C. Mei, C. Shi, C. Li, M.A. Abdel-Samie, H. Cui, Preparation and characterization of gelatin active packaging film loaded with eugenol nanoparticles and its application in chicken preservation, Food Biosci. 53 (2023) 102778. https://doi.org/10.1016/J.FBIO.2023.102778.
[32] R. Scaffaro, A. Maio, F.E. Gulino, C. Di Salvo, A. Arcarisi, Bilayer biodegradable films prepared by co-extrusion film blowing: Mechanical performance, release kinetics of an antimicrobial agent and hydrolytic degradation, Compos Part A Appl Sci Manuf. 132 (2020) 105836. https://doi.org/10.1016/J.COMPOSITESA.2020.105836.
[33] R. Scaffaro, E.F. Gulino, M.C. Citarrella, A. Maio, Green Composites Based on Hedysarum coronarium with Outstanding FDM Printability and Mechanical Performance, Polymers (Basel). 14 (2022) 1198. https://doi.org/10.3390/polym14061198.
[34] R. Scaffaro, L. Settanni, E.F. Gulino, Release Profiles of Carvacrol or Chlorhexidine of PLA/Graphene Nanoplatelets Membranes Prepared Using Electrospinning and Solution Blow Spinning: A Comparative Study, Molecules. 28 (2023) 1967. https://doi.org/10.3390/molecules28041967.
[35] T.A. Swetha, A. Bora, K. Mohanrasu, P. Balaji, R. Raja, K. Ponnuchamy, G. Muthusamy, A. Arun, A comprehensive review on polylactic acid (PLA) – Synthesis,

processing and application in food packaging, Int J Biol Macromol. 234 (2023) 123715. https://doi.org/10.1016/J.IJBIOMAC.2023.123715.
[36] Goodao ©, PLA Trays and Containers, (2017) 1. https://www.gl-bz.com/new-environmentally-friendly-pla-material-biodegradable-trays-and-containers-for-packing-fruit-meat-food-product/.
[37] S. Punia Bangar, W.S. Whiteside, V. Chaudhary, P. Parambil Akhila, K.V. Sunooj, Recent functionality developments in Montmorillonite as a nanofiller in food packaging, Trends Food Sci Technol. 140 (2023) 104148. https://doi.org/10.1016/J.TIFS.2023.104148.
[38] D. Cheikh, H. Majdoub, M. Darder, An overview of clay-polymer nanocomposites containing bioactive compounds for food packaging applications, Appl Clay Sci. 216 (2022) 106335. https://doi.org/10.1016/J.CLAY.2021.106335.
[39] L.R. Beuchat, Listeria monocytogenes: incidence on vegetables, Food Control. 7 (1996) 223–228. https://doi.org/10.1016/S0956-7135(96)00039-4.
[40] F.M. Sánchez-Vargas, M.A. Abu-El-Haija, O.G. Gómez-Duarte, Salmonella infections: An update on epidemiology, management, and prevention, Travel Med Infect Dis. 9 (2011) 263–277. https://doi.org/10.1016/J.TMAID.2011.11.001.
[41] J.E. Mosquera, M.L. Goñi, R.E. Martini, N.A. Gañán, Mass transfer kinetics of CO2 and eugenol in the supercritical impregnation of polyamide fibers: Experimental data and modeling, J Supercrit Fluids. 166 (2020) 105030. https://doi.org/10.1016/J.SUPFLU.2020.105030.
[42] J.E. Mosquera, M.L. Goñi, R.E. Martini, N.A. Gañán, Supercritical carbon dioxide assisted impregnation of eugenol into polyamide fibers for application as a dental floss, Journal of CO2 Utilization. 32 (2019) 259–268. https://doi.org/10.1016/J.JCOU.2019.04.016.
[43] A. Ubeyitogullari, O.N. Ciftci, Generating phytosterol nanoparticles in nanoporous bioaerogels via supercritical carbon dioxide impregnation: Effect of impregnation conditions, J Food Eng. 207 (2017) 99–107. https://doi.org/10.1016/j.jfoodeng.2017.03.022.
[44] A. Ubeyitogullari, O.N. Ciftci, Phytosterol nanoparticles with reduced crystallinity generated using nanoporous starch aerogels, RSC Adv. 6 (2016) 108319–108327. https://doi.org/10.1039/c6ra20675a.
[45] F. Muratore, M.L. Goñi, M.C. Strumia, S.E. Barbosa, N.A. Gañan, R.E. Martini, Eugenol As An Active Component In Food Packaging Materials, Eugenol: Biosynthesis, Toxicity and Uses. (2019) 1–48.
[46] S. Milovanovic, M. Stamenic, D. Markovic, M. Radetic, I. Zizovic, Solubility of thymol in supercritical carbon dioxide and its impregnation on cotton gauze, J Supercrit Fluids. 84 (2013) 173–181. https://doi.org/10.1016/J.SUPFLU.2013.10.003.
[47] José Aniceto, Supercritical carbon dioxide density and viscosity calculation, (2023). https://www.egichem.com/tools/calculators/carbon-dioxide/.
[48] C. Simoneau, Guidelines on testing conditions for articles in contact with foodstuffs (with a focus on kitchenware) - EUR 23814 EN 2009, 2015.
[49] CLSI, Clinical and Laboratory Standards Institute Methods for Dilution Antimicrobial Susceptibility Tests for Bacteria That Grow Aerobically Standard,, Approval CDM-A.;,

M07 Methods for Dilution Antimicrobial Susceptibility Tests for Bacteria That Grow Aerobically. (2018) 91.
[50] G. Donelli, Microbial Biofilms Methods and Protocols, 2014. https://doi.org/10.1007/978-1-4939-0467-9_3.
[51] ISO:7218, Microbiology of food and animal feeding stuffs — General requirements and guidance for microbiological examinations, Iso. 2013 (2013). www.iso.org.
[52] M. Tyrka, M. Nowak, D. Misic, T. Półbrat, S. Koter, A. Trusek, I. Zizovic, Cellulose Acetate Membranes Modification by Aminosilane Grafting in Supercritical Carbon Dioxide towards Antibiofilm Properties, Membranes (Basel). 12 (2021) 33. https://doi.org/10.3390/membranes12010033.
[53] E. Di Maio, E. Kiran, Foaming of polymers with supercritical fluids and perspectives on the current knowledge gaps and challenges, J Supercrit Fluids. 134 (2018) 157–166. https://doi.org/10.1016/J.SUPFLU.2017.11.013.
[54] B. Li, G. Zhao, G. Wang, L. Zhang, J. Gong, Fabrication of high-expansion microcellular PLA foams based on pre-isothermal cold crystallization and supercritical CO2 foaming, Polym Degrad Stab. 156 (2018) 75–88. https://doi.org/10.1016/J.POLYMDEGRADSTAB.2018.08.009.
[55] P. Xiang, L. Gou, Y. Zou, B. Chen, S. Bi, X. Chen, P. Yu, A facile strategy for preparation of strong tough poly(lactic acid) foam with a unique microfibrillated bimodal micro/nano cellular structure, Int J Biol Macromol. 199 (2022) 264–274. https://doi.org/10.1016/J.IJBIOMAC.2021.12.187.
[56] F.B. Ali, A.S. Azmi, H. Anuar, J. Jamaluddin, Characterization of Polylactic Acid/Organoclay Nanocomposites BT - Advances in Nanotechnology and Its Applications, in: A.T. Jameel, A.Z. Yaser (Eds.), Springer Singapore, Singapore, 2020: pp. 107–114. https://doi.org/10.1007/978-981-15-4742-3_7.
[57] J. Trifol, D. Plackett, C. Sillard, O. Hassager, A.E. Daugaard, J. Bras, P. Szabo, A comparison of partially acetylated nanocellulose, nanocrystalline cellulose, and nanoclay as fillers for high-performance polylactide nanocomposites, J Appl Polym Sci. 133 (2016). https://doi.org/https://doi.org/10.1002/app.43257.
[58] W. Chávez-Montes, G. González-Sánchez, E. López-Martínez, P. de Lira-Gómez, L. Ballinas-Casarrubias, S. Flores-Gallardo, Effect of Artificial Weathering on PLA/Nanocomposite Molecular Weight Distribution, Polymers (Basel). 7 (2015) 760–776. https://doi.org/10.3390/polym7040760.
[59] M. Keshtkar, M. Nofar, C.B. Park, P.J. Carreau, Extruded PLA/clay nanocomposite foams blown with supercritical CO2, Polymer (Guildf). 55 (2014) 4077–4090. https://doi.org/https://doi.org/10.1016/j.polymer.2014.06.059.
[60] N.H. Arsad, N.R. Putra, Z. Idham, N.S.M. Norodin, M.A. Che Yunus, A.H. Abdul Aziz, Solubilization of eugenol from Piper betle leaves to supercritical carbon dioxide: Experimental and modelling, Results in Engineering. 17 (2023) 100914. https://doi.org/10.1016/J.RINENG.2023.100914.
[61] K.W. Cheng, S.J. Kuo, M. Tang, Y.P. Chen, Vapor–liquid equilibria at elevated pressures of binary mixtures of carbon dioxide with methyl salicylate, eugenol, and diethyl phthalate, J Supercrit Fluids. 18 (2000) 87–99. https://doi.org/10.1016/S0896-8446(00)00056-5.

[62] J. G. Van Alsten, C. A. Eckert, Effect of entrainers and of solute size and polarity in supercritical fluid solutions, Journal of Chemical & Engineering Data. 38 (2002) 605–610. https://doi.org/10.1021/je00012a034.
[63] C. Villegas, M.P. Arrieta, A. Rojas, A. Torres, S. Faba, M.J. Toledo, M.A. Gutierrez, E. Zavalla, J. Romero, M.J. Galotto, X. Valenzuela, PLA/organoclay bionanocomposites impregnated with thymol and cinnamaldehyde by supercritical impregnation for active and sustainable food packaging, Compos B Eng. 176 (2019) 107336. https://doi.org/10.1016/j.compositesb.2019.107336.
[64] A. Torres, E. Ilabaca, A. Rojas, F. Rodríguez, M.J. Galotto, A. Guarda, C. Villegas, J. Romero, Effect of processing conditions on the physical, chemical and transport properties of polylactic acid films containing thymol incorporated by supercritical impregnation, Eur Polym J. 89 (2017). https://doi.org/10.1016/j.eurpolymj.2017.01.019.
[65] M.L. Goñi, N. Gañan, V. A., Q. N., A. A., R. Martini, Supercritical carbon dioxide impregnation of LLDPE films with eugenol. Influence of process conditions and film characterization, 2016.
[66] C. Villegas, A. Torres, M. Rios, A. Rojas, J. Romero, C.L. de Dicastillo, X. Valenzuela, M.J. Galotto, A. Guarda, Supercritical impregnation of cinnamaldehyde into polylactic acid as a route to develop antibacterial food packaging materials, Food Research International. 99 (2017) 650–659. https://doi.org/10.1016/j.foodres.2017.06.031.
[67] F. Lopresti, L. Botta, R. Scaffaro, V. Bilello, L. Settanni, R. Gaglio, Antibacterial biopolymeric foams: Structure–property relationship and carvacrol release kinetics, Eur Polym J. 121 (2019) 109298. https://doi.org/https://doi.org/10.1016/j.eurpolymj.2019.109298.
[68] R. Gaglio, L. Botta, G. Garofalo, A. Miceli, L. Settanni, F. Lopresti, Carvacrol activated biopolymeric foam: An effective packaging system to control the development of spoilage and pathogenic bacteria on sliced pumpkin and melon, Food Packag Shelf Life. 28 (2021) 100633. https://doi.org/https://doi.org/10.1016/j.fpsl.2021.100633.
[69] K.W. Cheng, M. Tang, Y.P. Chen, Calculations of solid solubility in supercritical fluids using a simplified cluster solvation model, Fluid Phase Equilib. 214 (2003) 169–186. https://doi.org/10.1016/S0378-3812(03)00350-9.
[70] C.J. Benmore, B.L. Tomberli, The structure of carbon dioxide around naphthalene investigated using H/D substitution in neutron diffraction, Ind Eng Chem Res. 39 (2000) 4491–4495. https://doi.org/10.1021/ie000150i.
[71] E.J. Velásquez, L. Garrido, A. Guarda, M.J. Galotto, C. López de Dicastillo, Increasing the incorporation of recycled PET on polymeric blends through the reinforcement with commercial nanoclays, Appl Clay Sci. 180 (2019) 105185. https://doi.org/10.1016/J.CLAY.2019.105185.
[72] M. Pluta, M.-A. Paul, M. Alexandre, P. Dubois, Plasticized polylactide/clay nanocomposites. I. The role of filler content and its surface organo-modification on the physico-chemical properties, J Polym Sci B Polym Phys. 44 (2006) 299–311. https://doi.org/https://doi.org/10.1002/polb.20694.

[73] P.A. Ulloa, J. Vidal, C. Dicastillo, F. Rodriguez, A. Guarda, R.M.S. Cruz, M.J. Galotto, Development of poly(lactic acid) films with propolis as a source of active compounds: Biodegradability, physical, and functional properties, J Appl Polym Sci. 136 (2019) 47090. https://doi.org/10.1002/app.47090.
[74] E. Velásquez, A. Rojas, C. Piña, M.J. Galotto, C.L. de Dicastillo, Development of bilayer biodegradable composites containing cellulose nanocrystals with antioxidant properties, Polymers (Basel). 11 (2019) 1945. https://doi.org/10.3390/polym11121945.
[75] M. Przybysz-Romatowska, J. Haponiuk, K. Formela, Poly(ε-Caprolactone)/Poly(Lactic Acid) Blends Compatibilized by Peroxide Initiators: Comparison of Two Strategies, Polymers (Basel). 12 (2020) 228. https://doi.org/10.3390/polym12010228.
[76] J.M. Cervantes-Uc, J. V. Cauich-Rodríguez, H. Vázquez-Torres, L.F. Garfias-Mesías, D.R. Paul, Thermal degradation of commercially available organoclays studied by TGA–FTIR, Thermochim Acta. 457 (2007) 92–102. https://doi.org/10.1016/J.TCA.2007.03.008.
[77] S.G. Kazarian, G.G. Martirosyan, Spectroscopy of polymer/drug formulations processed with supercritical fluids: in situ ATR–IR and Raman study of impregnation of ibuprofen into PVP, Int J Pharm. 232 (2002) 81–90. https://doi.org/10.1016/S0378-5173(01)00905-X.
[78] K. Bocz, T. Tábi, D. Vadas, M. Sauceau, J. Fages, G. Marosi, Characterisation of natural fibre reinforced PLA foams prepared by supercritical CO2 assisted extrusion, Express Polym Lett. 10 (2016) 771–779. https://doi.org/10.3144/expresspolymlett.2016.71.
[79] L. Wei, H. Shicheng, Z. Hongfu, Effect of octa(epoxycyclohexyl) POSS on thermal, rheology property, and foaming behavior of PLA composites, J Appl Polym Sci. 135 (2018) 46399. https://doi.org/https://doi.org/10.1002/app.46399.
[80] R. Mort, E. Peters, G. Curtzwiler, S. Jiang, K. Vorst, Biofillers Improved Compression Modulus of Extruded PLA Foams, Sustainability. 14 (2022) 5521. https://doi.org/10.3390/su14095521.
[81] I. Zizovic, A. Trusek, M. Tyrka, I. Moric, L. Senerovic, Functionalization of polyamide microfiltration membranes by supercritical solvent impregnation, Journal of Supercritical Fluids. 174 (2021). https://doi.org/10.1016/j.supflu.2021.105250.
[82] D. Matykiewicz, K. Skórczewska, Characteristics and Application of Eugenol in the Production of Epoxy and Thermosetting Resin Composites: A Review, Materials. 15 (2022) 4824. https://doi.org/10.3390/ma15144824.
[83] E. Velásquez, S. Espinoza, X. Valenzuela, L. Garrido, M.J. Galotto, A. Guarda, C. López de Dicastillo, Effect of Organic Modifier Types on the Physical–Mechanical Properties and Overall Migration of Post-Consumer Polypropylene/Clay Nanocomposites for Food Packaging, Polymers . 13 (2021) 1502. https://doi.org/10.3390/polym13091502.
[84] S. Doroudiani, M.T. Kortschot, Polystyrene foams: II. Structure-impact properties relationships, J Appl Polym Sci. 90 (2003) 1421–1426. https://doi.org/10.1002/app.12805.

[85] Ivheeco, Supermarket Biodegradable Disposable Take Away Customized Tray Food Grade Cornstarch Frozen Food Packaging Container, Ivheeco. (2023). https://www.lvheeco.com/Plate/supermarket-biodegradable-disposable-take-away-customized-tray-food-grade-cornstarch-frozen-food-packaging-container?gclid=CjwKCAiAvoqsBhB9EiwA9XTWGSXn-uHzQvtb0e74GCVP726_Qp8fhiVtMUhjaUwWTBGNQlTFcQgmsBoCSvgQAvD_BwE.
[86] J.H. Schut, Foamed PLA shows promise in biodegradable meat trays, Plastics Technology. 53 (2007) 39–43. https://www.ptonline.com/articles/foamed-pla-shows-promise-in-biodegradable-meat-trays.
[87] G.X. Chen, H.S. Kim, E.S. Kim, J.S. Yoon, Compatibilization-like effect of reactive organoclay on the poly(l-lactide)/poly(butylene succinate) blends, Polymer (Guildf). 46 (2005) 11829–11836. https://doi.org/10.1016/j.polymer.2005.10.056.
[88] A.R. Mukurumbira, R.A. Shellie, R. Keast, E.A. Palombo, S.R. Jadhav, Encapsulation of essential oils and their application in antimicrobial active packaging, Food Control. 136 (2022) 108883. https://doi.org/10.1016/J.FOODCONT.2022.108883.
[89] J.Y. Chen, H. Wu, C.Y. Guo, B. Zhu, G. Bin Ren, Enhancing the solubility of natural compound xanthotoxin by modulating stability via cocrystallization engineering, Int J Pharm. 572 (2019) 118776. https://doi.org/10.1016/J.IJPHARM.2019.118776.
[90] G. Michailidou, E. Christodoulou, S. Nanaki, P. Barmpalexis, E. Karavas, S. Vergkizi-Nikolakaki, D.N. Bikiaris, Super-hydrophilic and high strength polymeric foam dressings of modified chitosan blends for topical wound delivery of chloramphenicol, Carbohydr Polym. 208 (2019) 1–13. https://doi.org/10.1016/J.CARBPOL.2018.12.050.
[91] K. Trongchuen, A. Ounkaew, P. Kasemsiri, S. Hiziroglu, W. Mongkolthanaruk, R. Wannasutta, U. Pongsa, P. Chindaprasirt, Bioactive Starch Foam Composite Enriched With Natural Antioxidants from Spent Coffee Ground and Essential Oil, Starch - Stärke. 70 (2018) 1700238. https://doi.org/10.1002/star.201700238.
[92] A. Rojas, D. Misic, C.L. de Dicastillo, I. Zizovic, E. Velásquez, D. Gutiérrez, G. Aguila, C.P. Vidal, A. Guarda, M.J. Galotto, A review on thymol-based bioactive materials for food packaging, Ind Crops Prod. 202 (2023) 116977. https://doi.org/10.1016/J.INDCROP.2023.116977.
[93] A. Celebioglu, T. Uyar, Electrohydrodynamic encapsulation of eugenol-cyclodextrin complexes in pullulan nanofibers, Food Hydrocoll. 111 (2021) 106264. https://doi.org/10.1016/J.FOODHYD.2020.106264.
[94] R. Requena, M. Vargas, A. Chiralt, Release kinetics of carvacrol and eugenol from poly(hydroxybutyrate-co-hydroxyvalerate) (PHBV) films for food packaging applications, Eur Polym J. 92 (2017) 185–193. https://doi.org/10.1016/J.EURPOLYMJ.2017.05.008.
[95] M.L. Goñi, N.A. Gañán, M.C. Strumia, R.E. Martini, Eugenol-loaded LLDPE films with antioxidant activity by supercritical carbon dioxide impregnation, J Supercrit Fluids. 111 (2016) 28–35. https://doi.org/10.1016/J.SUPFLU.2016.01.012.
[96] F. Velázquez-Contreras, N. García-Caldera, J.D.P. de la Rosa, D. Martínez-Romero, E. Núñez-Delicado, J.A. Gabaldón, Effect of pla active packaging containing

monoterpene-cyclodextrin complexes on berries preservation, Polymers (Basel). 13 (2021). https://doi.org/10.3390/polym13091399.
[97] M.I. Rodríguez-López, M.T. Mercader-Ros, J.A. Pellicer, V.M. Gómez-López, D. Martínez-Romero, E. Núñez-Delicado, J.A. Gabaldón, Evaluation of monoterpene-cyclodextrin complexes as bacterial growth effective hurdles, Food Control. 108 (2020) 106814. https://doi.org/10.1016/j.foodcont.2019.106814.
[98] C. Shen, M. Wu, C. Sun, J. Li, D. Wu, C. Sun, Y. He, K. Chen, Chitosan/PCL nanofibrous films developed by SBS to encapsulate thymol/HPβCD inclusion complexes for fruit packaging, Carbohydr Polym. 286 (2022). https://doi.org/10.1016/j.carbpol.2022.119267.
[99] A. Torres, C.L. De Dicastillo, M. Ríos, I. Bastias, A. Guarda, M.J. Galotto, Effect of organoclay incorporation on thermal, physical and morphological properties of LLDPE nanocomposites for active food packaging applications, Journal of the Chilean Chemical Society. 59 (2015) 2681–2685. https://doi.org/10.4067/s0717-97072014000400011.
[100] S.I. Hong, J.W. Rhim, Preparation and properties of melt-intercalated linear low density polyethylene/clay nanocomposite films prepared by blow extrusion, LWT - Food Science and Technology. 48 (2012) 43–51. https://doi.org/10.1016/J.LWT.2012.03.009.
[101] S.I. Hong, L.F. Wang, J.W. Rhim, Preparation and characterization of nanoclays-incorporated polyethylene/thermoplastic starch composite films with antimicrobial activity, Food Packag Shelf Life. 31 (2022) 100784. https://doi.org/10.1016/J.FPSL.2021.100784.
[102] W. Zhang, R. Liu, X. Sun, H. An, T. Min, Z. Zhu, Y. Wen, Leaf-stomata-inspired packaging nanofibers with humidity-triggered thymol release based on thymol/EVOH coaxial electrospinning, Food Research International. 162 (2022) 112093. https://doi.org/10.1016/J.FOODRES.2022.112093.
[103] Z. Wang, F. Zhan, D. Zhang, Y. Wang, Y. Qiu, J. Zhang, L. Wang, L. Zhao, Relative humidity-triggered polyamide 4/Cinnamaldehyde core-shell nanofibers for antibacterial packaging, J Food Eng. 357 (2023) 111635. https://doi.org/10.1016/J.JFOODENG.2023.111635.
[104] J. Pantwalawalkar, H. More, D. Bhange, U. Patil, N. Jadhav, Novel curcumin ascorbic acid cocrystal for improved solubility, J Drug Deliv Sci Technol. 61 (2021) 102233. https://doi.org/10.1016/J.JDDST.2020.102233.
[105] P. Roy, N. Pandey, N. Kumari, R. Baidya, Y.S. Mary, Y.S. Mary, A. Ghosh, Development of sulfamethoxazole-succinimide cocrystal by mechanochemical cocrystallization – An insight into spectroscopic, electronic, chemical conformation and physicochemical properties, Chemical Engineering Research and Design. 185 (2022) 446–457. https://doi.org/10.1016/J.CHERD.2022.07.012.
[106] A. Rojas, E. Velásquez, C.P. Vidal, A. Guarda, M.J. Galotto, C.L. de Dicastillo, Active PLA packaging films: Effect of processing and the addition of natural antimicrobials and antioxidants on physical properties, release kinetics, and compostability, Antioxidants. 10 (2021). https://doi.org/10.3390/antiox10121976.

[107] E. Velásquez, C. Patiño Vidal, A. Rojas, A. Guarda, M.J. Galotto, C. López de Dicastillo, Natural antimicrobials and antioxidants added to polylactic acid packaging films. Part I: Polymer processing techniques, Compr Rev Food Sci Food Saf. 20 (2021) 3388–3403. https://doi.org/10.1111/1541-4337.12777.
[108] S. Sharma, S. Barkauskaite, A.K. Jaiswal, S. Jaiswal, Essential oils as additives in active food packaging, Food Chem. 343 (2021) 128403. https://doi.org/10.1016/J.FOODCHEM.2020.128403.
[109] S. Report, Salmonellosis, (2022) 1–9.
[110] S. Report, Listeriosis. AER 2021, (2022).
[111] P. Rodríguez-López, J. Rodríguez-Herrera, D. Vázquez-Sánchez, M. López Cabo, Current Knowledge on Listeria monocytogenes Biofilms in Food-Related Environments: Incidence, Resistance to Biocides, Ecology and Biocontrol, Foods. 7 (2018) 85. https://doi.org/10.3390/foods7060085.
[112] P. Korzeniowski, P. Śliwka, M. Kuczkowski, D. Mišić, A. Milcarz, M. Kuźmińska-Bajor, Bacteriophage Cocktail Can Effectively Control Salmonella Biofilm in Poultry Housing, Front Microbiol. 13 (2022) 1–11. https://doi.org/10.3389/fmicb.2022.901770.
[113] A.W.M. Suijkerbuijk, M. Bouwknegt, M.J.J. Mangen, G.A. De Wit, W. Van Pelt, P. Bijkerk, I.H.M. Friesema, The economic burden of a Salmonella Thompson outbreak caused by smoked salmon in the Netherlands, 2012-2013, Eur J Public Health. 27 (2017) 325–330. https://doi.org/10.1093/eurpub/ckw205.
[114] A. Martín, M.J. Cocero, Micronization processes with supercritical fluids: Fundamentals and mechanisms, Adv Drug Deliv Rev. 60 (2008) 339–350. https://doi.org/10.1016/J.ADDR.2007.06.019.
[115] S.N. Madanayake, A. Manipura, R. Thakuria, N.M. Adassooriya, Opportunities and Challenges in Mechanochemical Cocrystallization toward Scaled-Up Pharmaceutical Manufacturing, Org Process Res Dev. 27 (2023) 409–422. https://doi.org/10.1021/ACS.OPRD.2C00314.
[116] L. Padrela, M.A. Rodrigues, S.P. Velaga, H.A. Matos, E.G. de Azevedo, Formation of indomethacin–saccharin cocrystals using supercritical fluid technology, European Journal of Pharmaceutical Sciences. 38 (2009) 9–17. https://doi.org/10.1016/J.EJPS.2009.05.010.
[117] L. MacEachern, A. Kermanshahi-Pour, M. Mirmehrabi, Supercritical carbon dioxide for pharmaceutical co-crystal production, Cryst Growth Des. 20 (2020) 6226–6244. https://doi.org/10.1021/acs.cgd.0c00571.

Supercritical fluid and cocrystallization technologies for designing antimicrobial food packaging PLA nanocomposite foams loaded with eugenol cocrystals with prolonged release

Adrián Rojas[1,2*], Dusan Misic[3], Irena Zizovic[4], Carol López de Dicastillo[5], Eliezer Velásquez[1,2], Aleksandra Rajewska[3], Bastián Rozas[1], Luciano Catalán[1], Cristian Patiño Vidal[6], Abel Guarda[1,2], María José Galotto[1,2*]

[1] Packaging Innovation Center (LABEN), Department of Science and Food Technology, Faculty of Technology, University of Santiago of Chile (USACH), Obispo Umaña 050, Santiago 9170201, Chile

[2] Center for the Development of Nanoscience and Nanotechnology (CEDENNA), Santiago 9170124, Chile

[3] Department of Functional Food Products Development, Faculty of Biotechnology and Food Sciences, Wrocław University of Environmental and Life Sciences, 51-630 Wrocław, Poland

[4] Faculty of Chemistry, Wroclaw University of Science and Technology, Wybrzeze Wyspianskiego 27, 50-370 Wroclaw, Poland.

[5] Packaging Laboratory, Institute of Agrochemistry and Food Technology IATA-CSIC, Av. Agustín Escardino 7, 46980 Paterna, Spain

[6] Universidad Nacional de Chimborazo, Facultad de Ingeniería, Carrera de Agroindustria, Grupo de Investigación Vegetal y Agroindustrial (INVAGRO), Av. Antonio José de Sucre Km 1 1/2, 060108, Riobamba, Ecuador.

* Corresponding authors: Packaging Innovation Center (LABEN), Department of Science and Food Technology, Faculty of Technology, University of Santiago of Chile (USACH), Obispo Umaña 050, Santiago 9170201, Chile
E-mail addresses: adrian.rojass@usach.cl (A. Rojas), maria.galotto@usach.cl (M.J. Galotto)

ABSTRACT

Searching for effective strategies to modify the release rate of essential oil derivatives is one of the main challenges in designing prolonged-release antimicrobial food packaging materials. Herein, supercritical fluid technology and cocrystallization engineering were used to develop novel eugenol (EU) prolonged-release poly (lactic acid) (PLA) nanocomposite foams. Eugenol-phenazine (EU-PHE) cocrystals, produced by a solvent-free mechanochemical method, were incorporated by supercritical solvent impregnation (SSI) inside PLA nanocomposite foams with different contents of Cloisite30B® (C30B). The effect of the cocrystallization process and C30B content on the EU release kinetics and its relation with their antimicrobial activity by direct contact (anti-attachment) and release in broth culture were studied. The deposition of isolated spherical-shaped micrometric EU-PHE cocrystal particles with 0.8 μm average diameter inside the pores of PLA foams was evidenced by XRD, SEM, DSC, and TGA analyses. The release mechanism of EU and its cocrystal was defined as a quasi-Fickian diffusion process successfully described by the Korsmeyer-Peppas model with release rate constants up to 3.6-fold lower than the release rate constant of pure EU. The impregnated foam samples completely inhibited the attachment of *Listeria monocytogenes* and *Salmonella* Enteritidis and provided prolonged antimicrobial activity in broth culture against both food-borne pathogens. This study suggests a new, environmentally friendly method for designing sustained-release antimicrobial food packaging materials.

Keywords: Antimicrobial packaging; eugenol-phenazine cocrystal; C30B; Cocrystallization; Supercritical fluid technology

1. Introduction

The food industry is faced with the issue of prolonging the food shelf-life and providing safe food free of food-borne pathogens and spoilage microorganisms without the addition of synthetic preservatives. One of the most promising strategies to meet this demand is the design of new active packaging materials with incorporated natural bioactive molecules [1]. As a result, controlled release packaging has arisen as a new concept for releasing systems, emphasizing the depth of understanding the mechanism and kinetics of an active compound's release from the polymer. Designing active packaging with proper release kinetics of the active substance is a prerequisite since these materials should release the active compound when needed when the food is packaged, and not before or after that [2,3].

Essential oils and their constituents are the most commonly used agents for developing active packaging materials because of their safety status, widespread acceptance by consumers, and multipurpose use due to their multiple biological effects, including antimicrobial and antioxidant activities. However, essential oils are highly volatile compounds characterized by high vapor pressure. Consequently, they have very high release rates from polymer structures designed for food packaging, even when different strategies are used to modify the polymer mass transfer properties, such as incorporating nanoclays [4,5], cellulose nanocrystals [6,7], and cyclodextrins [8,9] into the polymer matrix, or designing multi-layer structures [10,11].

A supercritical fluid (SCF) is a substance whose temperature and pressure exceed its critical values. In this state, the fluid is characterized by high diffusivities and low viscosities comparable to gases, while densities and solvating properties are similar to liquids [12]. In

addition, the absence of surface tension in the supercritical phase allows for easy penetration of SCF into the depth of the solid matrix. Exploiting this advantageous combination of thermodynamic and transport properties of SCFs, supercritical fluid technology has emerged as a highly attractive alternative to conventional processing in food, pharmaceutical, textile, and wood industries, material engineering, and biomass treatment [13,14]. The most utilized SCF is supercritical carbon dioxide ($scCO_2$) because of its favorable critical parameters (31 °C and 7.38 MPa) that allow the processing of thermally labile substances, nontoxicity, inflammability, availability, and inert nature. Moreover, $scCO_2$ usage allows for obtaining solvent-free materials by depressurizing the system and separating gaseous CO_2 from the final product. Another vital advantage of $scCO_2$ technology, especially for industrial applications, is the absence of effluent and solid waste generation. $ScCO_2$ is extensively used as a solvent for an active substance for impregnation of solids. The process is termed supercritical solvent impregnation (SSI) and was proven to be an efficient alternative to incorporating active agents in polymers aimed at food packaging, pharmaceutical, and textile applications [15–18]. Besides SSI, one of the most important applications of $scCO_2$ in polymer processing is its use as a blowing agent for foam production. Recently, $scCO_2$ foaming and impregnation were coupled to develop antibacterial polymeric foams for food packaging and tissue engineering applications [19–21].

Cocrystallization can be an innovative approach to modify the physicochemical properties of an active substance aimed at active food packaging and its release. A cocrystal corresponds to a multicomponent crystalline material with different molecular entities stoichiometrically together within the same crystal lattice as a consequence of supramolecular interactions between the active agent and the coformer, resulting from the combination of noncovalent

interactions, such as hydrogen bonds, π-π stacking or van der Waals forces [22,23]. In pharmaceutical research, cocrystallization has gained tremendous importance because of its ability to fine-tune the physicochemical properties of crystalline drugs without modifying their molecular structure. The sublimation rate of a solid depends on its vapor pressure, which corresponds to the escaping tendency of molecules from the solid phase. Recently, Hui Zu et al. studied the sublimation of thymol cocrystals, reporting that the sublimation rate of thymol-4,4'-dipyridyl (Thy-DP) cocrystals was 26 folds lower than the one of thymol and 3.3 folds larger than the sublimation rate of DP [24]. Mazzeo et al. reported that cocrystallization significantly modified the release profile of essential oil derivatives such as thymol, eugenol, and carvacrol, depending on the coformer [25]. In another work, Bianchi et al. reported the sustained release of cocrystallized thymol, eugenol, and carvacrol from a chitosan coating deposited on low-density polyethylene (LDPE) [26]. In this work, packaging prototypes were prepared by the adhesion of cocrystals on LDPE using chitosan solution. To the best of our knowledge, the mentioned study is the only report on the design of cocrystal-based active food packaging materials.

This study is the first report on a cocrystal behavior in $scCO_2$ and its impregnation into a polymeric matrix aimed at designing novel food packaging material with a prolonged active component release due to the intramolecular interactions between the selected active substance and coformer. The questions to be answered relate to the stability and solubility of the cocrystal in $scCO_2$ and SSI feasibility concerning the release kinetics and biological activity of the obtained materials. Phenazine (PHE, solid coformer) was considered in this study as a model coformer because it is prone to act as a strong hydrogen bond acceptor with wide use in designing cocrystals for pharmaceutical applications. Eugenol (EU, liquid), a

highly volatile bioactive substance, was selected as a model essential oil derivative due to its GRAS status given by the Food and Drug Administration (FDA) [27], extensive use in food packaging due to its well-known bioactivity against bacteria and fungi [28–31], and chemical structure that allows it to be used as a hydrogen-bond donor [25,26]. Polylactic acid (PLA) foams with or without nanoclay C30B were produced by foaming in $scCO_2$ and used as a substrate for EU-PHE cocrystal impregnation (SSI) in the next step. The impregnation of foams was also performed with pure EU for comparison reasons. As a biodegradable polymer, PLA has been extensively studied for packaging applications [19,32–34]. The monomer, LA, is recognized as a safe food preservative by the FDA, and its migration from PLA packing containers to food is also considered negligible. In addition, PLA has several beneficial properties that make it appropriate for use in contact with food, such as good oxygen and water barrier properties, resistance against oils and fats, resistance to UV radiation, transparency, and thermal processability [35]. Its favorable mechanical properties make PLA an appropriate replacement for polysulfone food packaging [36], which is one of the envisaged applications of the foams obtained in this study. C30B is a montmorillonite nanoclay with a high chemical affinity to PLA that can contribute to the intercalated nanocomposite structure. The nucleation and antibacterial properties of C30B were also reported, which is why it is frequently used in food packaging [37,38].

Finally, the antibacterial properties of the obtained materials were investigated against *Listeria monocytogenes* and *Salmonella* Enteritidis. The vast presence of *L. monocytogenes* in nature, including the surface layers of the soil, organisms of birds, mammals, and fish, increases the possibility of contamination of most food products with this microorganism. It is generally found on leaves of green vegetables (spinach, onion, leek) and rind of

watermelon and melon. It can be found in fish products, as well as in cheese and other dairy products [39]. *Salmonella* is a strictly pathogenic microorganism and is not as widespread as *Listeria*. Still, the possibility of contaminating almost any food product is always open. There have been recorded outbreaks of *salmonellosis* through peanut butter, tea, chocolate, chips, and peppers, in addition to eggs and meat, which traditionally represent the most common source of infection [40]. The capability of *L. monocytogenes* and *S.* Enteritidis to multiply between 4^0C to 45^0C and pH from 5.0 to 9.0 increases the risk of the contamination of the food products during the packing process or even in a retail network. Therefore, these two microorganisms were chosen for this study.

2. Materials and chemicals

2.1. Materials

Poly (lactic acid) (PLA), 2003D, with a specific gravity of 1.24 and an MFR of g/10min (210 °C, 2.16 kg) was supplied by Natureworks® Co. (Minnetonka, MN, USA). Merck provided the 99.9% HPLC-grade ethanol and methanol used in the study (Darmstadt, Germany). Aldrich® Chemistry supplied the following chemicals: phenazine (PHE) (98%) and eugenol (EU) (99.5%). (St. Louis, MO, USA). Southern Clay Products (Texas, United States) supplied the Cloisite® 30B (C30B) (100 meq/100 g) commercial organo-modified montmorillonite. Linde (Santiago, Chile) supplied carbon dioxide (CO_2). DMSO was purchased from Sigma-Aldrich (Darmstadt, Germany).

177 *2.2. Preparation of PLA nanocomposite films and synthesis of the EU-PHE cocrystal*

178 The following steps were taken to prepare the PLA foams. First, PLA powder and C30B
179 nanoclay were vacuum-dried at 60 °C for 24 h. Then, PLA nanocomposite films were
180 obtained using a LabTech LTE20 twin-screw extruder. Control PLA films (without the
181 nanoclay), and PLA nanocomposites with varying amounts of C30B nanoclay (5 and 10%
182 w/w) were extruded under a temperature range between 185 and 195 ºC with a screw speed
183 of 42 rpm and a chill roll speed of 0.9 rpm. The nanocomposite films were kept in a desiccator
184 until supercritical fluid processing.
185 The eugenol-phenazine (EU-PHE) cocrystal was prepared using a method previously
186 reported [25] consisting of manually grinding equimolar quantities of PHE and EU in an agar
187 mortar for approximately 20 min, yielding a yellow powder. The cocrystal was kept at a
188 temperature of -18 °C until the supercritical impregnation process.
189

190 *2.3. Polymer supercritical fluid processing: foaming of PLA films and foam impregnation*
191 *with EU and EU-PHE cocrystal*

192 The apparatus for the supercritical foaming of extruded PLA films is shown in **Fig.1**. Pure
193 PLA and nanocomposite sheets (1.5 cm x 4 cm, ~700 µm) were deposited inside a 100 mL
194 high-pressure cell (Thar Instruments, USA). The cell was filled with previously liquified CO_2
195 by cooling in an Alpha RA 8 refrigerator unit (Lauda, Germany). A high-pressure pump
196 Teledyne ISCO 260D (Teledyne, USA) was used to elevate the cell pressure. The
197 temperature was maintained by an electric resistance heater wrapped around the cell. The
198 foaming of all samples was performed at 120 °C and 25 MPa. The samples were maintained

199 at these conditions for 20 minutes. The CO_2 was then released within 2 s from the system.
200 The resulting foams were kept in a desiccator until supercritical impregnation.

201 The produced PLA foams with varying concentrations of C30B (0, 5, and 10 % w/w) were
202 impregnated with EU and EU-PHE cocrystal by SSI in the same equipment used for the
203 foaming (**Fig. 1)**. EU (0.64 g) or EU-PHE cocrystal (1.35 g) was put in a glass container and
204 placed at the bottom of the vessel. PLA nanocomposite foams (0.5 g) were deposited inside
205 the high-pressure vessel above the active substance, and the system was loaded with liquid
206 CO_2. The ISCO 260D syringe pump and the electric heater were used to attain the desired
207 conditions. The SSI conditions for EU, being the pressure of 15 MPa, temperature of 60 °C,
208 depressurization rate of 0.5 MPa/min, and impregnation time of 2 h, were adopted from the
209 literature as they were reported the best to incorporate EU into polyamide fibers [41,42]. The
210 impregnation process of the EU-PHE cocrystal was carried out at 15 MPa and 60 °C for 4 h.
211 The system was then left for natural cooling (from 60 to 25 °C for 2 h) to promote the
212 precipitation and recrystallization of EU-PHE cocrystals inside the PLA nanocomposite
213 foams [43,44]. After the cooling, the system was decompressed at a rate of 0.5 MPa/min. The
214 impregnation yield (*I*) was determined gravimetrically using an analytical balance with an
215 accuracy of ±0.0001 g and calculated as follows:

216 $$I = \frac{m_2 - m_1}{m_1} \cdot 100\ \% \qquad (1)$$

217 where m_1 is the initial mass of foam and m_2 is the foam mass after the impregnation [45].

218

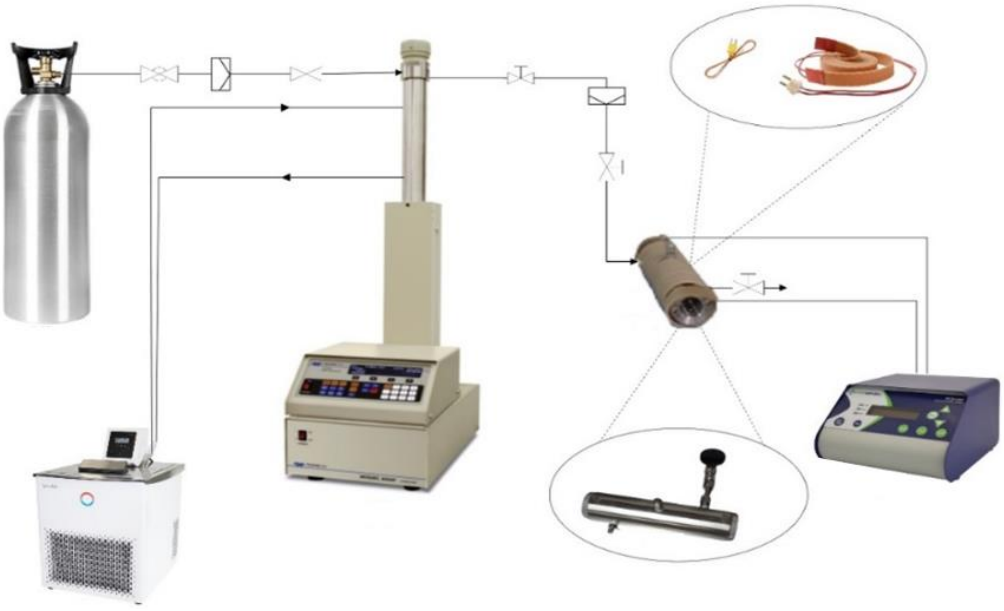

Fig. 1. Outline of the experimental setup for the CO_2-assited foaming and impregnation of the PLA nanocomposite foams.

2.4. Solubility determination

The solubility of pure substances EU and PHE and their cocrystal EU-PHE in $scCO_2$ under the conditions of interest (15 MPa and 60 °C) was performed by the previously published procedure [46] in a 25 mL high-pressure view cell (Eurotechnica GmbH, Bargteheide, Germany) equipped with two sapphire windows that allow for the process visualization and an electrical heating jacket. A glass vessel with around 0.4 g of substance (EU, PHE, or EU-PHE) was placed in the previously heated (60 °C) cell. A perforated cover was put on the top of the glass container to minimize the precipitation of the substance back to the vessel during the decompression. The vessel's surface (3 cm^2) was considerably smaller than the surrounding surface of the cell for the same reason. The CO_2 was introduced to the cell, and pressure was increased to 15 MPa by an air-driven gas booster (Eurotechnica GmbH). After 24 h, the system was decompressed at 0.5 MPa/min. The mass of the dissolved

235 substance was determined gravimetrically using an analytical balance with an accuracy of
236 ±0.00001 g. The $scCO_2$ density at 15 MPa and 60 °C used to calculate the solubility in (g
237 substance)/(g $scCO_2$) was 605.6927 kg/m^3 [47].

238

239 *2.5. Characterization of the PLA nanocomposite foams impregnated with EU and the EU-*
240 *PHE cocrystal*

241 *2.5.1. Morphological analysis*

242 Scanning electron microscope (SEM) VEGAN3 TESCAN with an accelerating voltage of
243 10 kV was used to examine the morphology of the neat and impregnated PLA foams with
244 EU and the EU-PHE cocrystal. Cross-sections of foams were obtained by nitrogen fracture.
245 The samples were coated with gold using a Sputtering System Hummer 6.2. Image-
246 processing Image J program was used to calculate the average values of the pore diameter
247 and cell density of the foams, applying equations 2 and 3, respectively.

248 $$d_{av} = \frac{\sum_{i=1}^{600} d_i}{600} \quad (2)$$

249 where d_{av} indicates the average pore diameter, i corresponds to the number of pores with the
250 pore size d_i, and 600 is the number of pores considered for the evaluation.

251 $$\rho_c = \left(\frac{nM^2}{A}\right)^{(3/2)} \quad (3)$$

252 where ρ_c indicates the cell density, n is the number of cells in the SEM image, M is the
253 magnification, and A is the micrograph area.

254

2.5.2. Thermal properties

Differential scanning calorimetry (DSC) tests were performed using a Mettler-Toledo model STAR 822e (Schwerzenbach, Switzerland) apparatus with a cooling system (HAAKE EK 90/MT, Newington, USA). 4-6 mg of sample was subjected to a single heating from 0 to 250 °C at a steady rate of 10 °C/min[1] under a nitrogen atmosphere. The glass transition temperature (T_g), melting temperature (T_m), cold crystallization temperature (T_{cc}), melting enthalpy (ΔH_m), and cold crystallization enthalpy (ΔH_{cc}) of foams were the thermal parameters analyzed. Equation 4 was used to determine the crystallinity:

$$X_C(\%) = 100 \cdot \left(\frac{\Delta H_m - \Delta H_{cc}}{\Delta H_m^0 \cdot (100-\omega)}\right) \quad (4)$$

where, ΔH_m^0 is the specific melting enthalpy of crystalline PLA (93,6 J g^{-1}) [19], and ω is the mass percentage of C30B.

Thermogravimetric analysis (TGA) was carried out using a Mettler Toledo Gas Controller GC20 Stare System TGA/DCS (Schwerzenbach, Switzerland). 7 mg of sample was placed in porcelain capsules, which were heated under a nitrogen atmosphere at a rate of 10 °C/min[1] over a temperature range of 30 to 600 °C (flow rate 50 mL/min[1]). The parameters obtained were the temperature of degradation at 2.5% of weight loss (T_{onset}), and the temperature of maximum degradation (T_d).

2.5.3. X-ray diffraction

The dispersion and exfoliation of C30B and EU-PHE cocrystal inside the structure of PLA nanocomposite foams were analyzed by using Bruker D8 Advance X-ray diffraction equipment (Marca, Ciudad, País). Scanning was performed over the sample surface. The patterns for profile fitting were obtained using CuKα radiation at the 2θ° scanning angle between 2 to 80 º, with a scanning step of 0.02 º, at a collection time of 10 s per step operating at 40 kV.

2.5.4. Attenuated Total Reflectance Fourier transform infrared (ATR-FTIR) spectroscopy

The chemical characterization of foams was performed using Bruker IFS 66V spectrometer in attenuated total reflection (ATR) mode. The 64 co-added interferograms at 4 cm^{-1} resolution and a 4000 to 400 cm^{-1} wavenumber range yielded the FTIR spectra. OPUS Software Version 7 was used to analyze them.

2.5.5. Mechanical Assays

Following ASTM D-882, a Zwick Roell model BDOFB 0.5TH Tensile Tester was used to measure each material's tensile modulus, tensile strength, and elongation at break at 23 ± 2 °C. Analyses were performed on PLA foams (8 x 2.5 cm), previously conditioned in a desiccator at 25 ºC and 53% relative humidity (a saturated salt solution of magnesium nitrate) for 48 h, with a 1 kN load cell. Considering the size of the specimens obtained by foaming/supercritical impregnation, the initial grip separation was 15 mm, and the crosshead speed was 500 mm/min. For each sample, 10 measurements were performed.

295 *2.5.6. Study of the release kinetics of the EU-PHE cocrystal*

296 EU and EU-PHE cocrystal migration tests from PLA nanocomposite foams were carried
297 out using EtOH 10% v/v solution as an aqueous food simulant to evaluate their release
298 kinetics and to describe the mass transfer. According to EU Regulations, migration tests were
299 performed in duplicate and in accordance with the European Committee for
300 Standardization's recommendations [48]. 130 mL of food simulant and a sample of 0.5 g
301 PLA nanocomposite foam impregnated with EU or EU-PHE cocrystal were placed in a glass
302 tube. For at least 6 days, these tubes were maintained at 40 °C, and the amount of EU released
303 was periodically quantified by UV spectroscopy at 298 nm.

304 Release assays were carried out up to the equilibrium point, i.e., when the EU content in
305 the food simulant was maintained constant in at least two continuous succeeding
306 measurements. The dimensionless distribution coefficient of EU between the PLA
307 nanocomposite foams and food simulant ($K_{P/FS}$), which is represented by the ratio of the EU
308 concentrations at the interface between the polymer and food simulant, was used to
309 characterize this thermodynamic equilibrium condition (Equation 5)

310 $$K_{P/FS} = \frac{C_{EU}^{P}}{C_{EU}^{FS}} \quad (5)$$

311 where C_{EU}^{P} is the equilibrium EU concentration in the PLA nanocomposite foams and C_{EU}^{FS}
312 corresponds to EU concentration values in the food simulant. The EU release kinetics were
313 modeled using the kinetic models of Higuchi and Korsmeyer-Peppas presented by equations
314 6 and 7, respectively.

315 $$\frac{M_t}{M_\infty} = k \cdot t^{1/2} \quad (6)$$

316

317 $$\frac{M_t}{M_\infty} = k \cdot t^n \quad (7)$$

318 where M_t is the amount of EU released at any given time *t*, M_∞ is the amount of EU released
319 at the infinite time, k is the release rate constant, and n is the diffusional exponent, which
320 indicates the type of release mechanism.

321

322 *2.5.7. Antimicrobial properties of PLA foams loaded with the EU-PHE cocrystal*

323 *2.5.7.1. Investigated strains*

324 *Listeria (L.) monocytogenes*, serotype 1/2a, isolated from frozen salmon, as well as
325 *Salmonella* (*S.*) Enteritidis (*S. enterica* subspecies *enterica* serovar Enteritidis) isolated from
326 chicken egg samples, as a typical foodborne pathogen, were used for the investigations.
327 Bacterial strains were isolated in routine microbiological activities and kept at - 80 °C in a
328 cryoprotective medium. In preliminary tests (results not published), a strong ability of both
329 strains to produce biofilms was demonstrated. Just before testing, the cultures were refreshed
330 in Tryptone soya broth (TSB, Oxoid, Basingstoke, UK) at 37 °C overnight, then spread on
331 5% sheep blood agar and incubated for 24 h.

332

333 *2.5.7.2. Determination of MIC (minimal inhibitory concentration) values of EU, PHE and*
334 *EU-PHE cocrystals*

335 The antibacterial activities of EU, PHE, and EU-PHE cocrystals were also analyzed
336 through the dilution antimicrobial susceptibility test [49] with the modification that instead
337 of antibiotics, EU, PHE, and EU-PHE cocrystals previously dissolved in dimethyl sulfoxide
338 (DMSO) were used. Investigated concentrations ranged from 5% to 0.00244 %. Although
339 completely dissolved in DMSO, PHE, and EU-PHE cocrystal in concentrations higher than

5% formed a deposit after mixing with Cation Adjusted Mueller Hinton broth, the reference medium for broth microdilution. Thus, the highest possible investigated concentration was 5%. The final bacterial inoculum density was approximately 5×10^5 CFU/mL. Microtiter plates were incubated for 18-24 h at 37 °C. The MIC was defined as the lowest concentration that inhibited the visible growth of bacteria.

2.5.7.2. Anti-attachment (contact inhibition) activity of PLA nanocomposite foams

The microbial assay has been applied to determine the inhibition of the bacterial adhesion to the polymer surface [50]. Strains were incubated in TSB with 1% (w/v) glucose for 24 h. Overnight cultures were diluted to approximately 1-2 x 10^8 CFU/mL. Polymeric samples with a surface of 1 cm^2 were prepared and sterilized in an autoclave at 121 °C for 15 min and subsequently immersed in 2 mL of diluted cultures and incubated for 24 and 48 at 37 °C in static condition. After an incubation, PLA foam samples were collected and washed thoroughly with sterile Phosphate Buffered Saline (PBS). Subsequently, each piece of foam was transferred into tubes filled with 10 mL of PBS and subjected to ultrasonication at 37,000 Hz (Elmasonic S60, Elma Schmidbauer GmbH, Singen, Germany) for 5 min to detach the cells. Serial dilutions were done to a final dilution of 10^{-8}. Each dilution was inoculated in three 10 μL aliquots on Tryptone soya agar, which were then incubated 24 h at 37 °C. After that, colonies were counted. The number of obtained CFU/mL was calculated according to the formula from 7218 ISO standard [51]:

$$NCFU= (\sum C)/ (V \times [n1+(0.1 \times n2)] \times d) \quad (8)$$

where $\sum C$ is the total number of colonies from two successive dilutions, V is the volume of inoculum applied to each Petri dish (mL), $n1$ is the number of replicates from the first

362 dilution, *n2* is the number of replicates from the second dilution, and *d* is the dilution factor
363 corresponding to the first dilution.

364 The calculation of the number of attached bacteria per cm^2 (*NP*) was done following the
365 equation 9 [52]:

366 $$NP = (NCFU \times V)/P \quad (9)$$

367 where *NCFU* is the total number of detached bacteria (previously determined as CFU/mL),
368 *V* is the volume of PBS where the ultrasonic detachment was done, and *P* is the total surface
369 in mm^2 of the PLA. The investigation was carried out in three independent experiments from
370 which the average numerical values were derived and shown in the results.

371 *2.5.7.3. Assay of antimicrobial activity in broth cultures of active foams – determination of*
372 *killing effect (KE)*

373 The killing effect of the polymer, as well as its durability in a liquid environment,
374 depends on the active substance release rate. It was determined under static incubation
375 following the previously described method [50]. Briefly, a test polymer with a surface area
376 of 1 cm^2 was added to 2 mL Mueller-Hinton broth with 1% glucose, suspension of the
377 investigated strain adjusted to an OD_{550} of 0.125 (approximately 2 x 10^8 CFU/mL, A_o), and
378 left to incubate for 24 h at 37 °C ($A_{\text{test tube}}$). Controls were culture without polymer (A_{control}),
379 culture with pure non-impregnated PLA foam (PLAF) as a neutral control polymer
380 ($A_{\text{controlPLAF}}$), and blank was a sterile broth. The test was repeated daily by transferring the
381 polymer to a freshly prepared culture broth as long as the OD values of the tested polymer
382 were lower than those of the control ($A_{\text{control}} \geq A_{\text{test tube}}$). When the two absorbances were
383 similar ($A_{\text{control}} \leq A_{\text{test tube}}$), the polymer sample could no longer inhibit bacterial growth.

384 Results were presented as the percentage of bacterial growth in the presence of polymers
385 compared to the bacterial growth in the presence of controls.

386 *2.5.7.5. Statistical analysis*

387 All data was analyzed using Statistical software version 13.0 (StatSoft Inc., Tulsa,
388 OK, USA). The quantitative bacterial counts of *L. monocytogenes* and *S.* Enteritidis strains
389 per centimeter square underwent a logarithmic transformation. To monitor the effect of the
390 investigated PLA foams on the adhesion of microorganisms to surfaces, a logarithmic
391 reduction was also calculated.

392

393

3. Results and discussion

3.1. PLA nanocomposite foam production and solubility determination

PLA nanocomposite films with different concentrations of C30B (0, 5, and 10 % w/w) were successfully obtained by extrusion and subsequently foamed using $scCO_2$ as a blowing agent. During the foaming process, the pressure, temperature, and soaking time were maintained at 25 MPa, 120 °C, and 20 min, respectively, based on previously reported processing conditions by Rojas et al. [19]. The presence of C30B at low concentration (5 % w/w) did not significantly change the expansion ratio (19.71 ± 3.84) and porosity (94.69 ± 0.82 %) of the PLA-nanocomposite foam compared to the values of expansion ratio (12.63 ± 2.59) and porosity (91.91 ± 1.66 %) obtained for the control PLA foam (PLAF). This result is in accordance with the data reported by Rojas et al. [19]. It is well known that the porosity and expansion ratio of PLA foams obtained using $scCO_2$ as a blowing agent depends on the conditions of pressure, temperature, and time, which govern the amount of sorbed $scCO_2$ in the polymer structure, and on the number of nucleation sites inside the polymer for cell formation [53]. Particularly, the promotion of the crystallization of PLA has been used as an effective strategy to improve its foaming ability, *i.e.,* improving the expansion ratio and the porosity of the resulting PLA foams. Namely, crystals reduce the cell nucleation energy barrier by providing numerous heterogeneous nucleation sites [54,55]. In this context, the similar expansion ratios and porosities of PLA foams without the clay and with 5 % w/w C30B were in agreement with the same crystallinity (part 3.4) and an exfoliated structure (part 3.2) of both samples. The exfoliation of C30B at 5 % w/w inside PLA has been previously reported [56–58].

418 **Table 1**. Pore diameters (d), cell density (ρ_c), and impregnation yield (*I*) of EU-PHE cocrystal

Sample	d_{min} (µm)	d_{max} (µm)	d_{aver} (µm)	ρ_c (10^{-8} pores cm^{-3}]	*I* (% w/w)
PLAF (control)	4.22	42.71	22.70 ± 6.65 [a]	2.40	-
PLAF-EU-PHE	3.69	50.85	15.97 ± 6.65[d]	3.31	8.62 ± 0.06[c]
PLAF-5%C30B	4.22	41.21	20.90 ± 6.35 [b]	2.80	-
PLAF-5%C30B/EU-PHE	3.83	33.14	15.55 ± 4.73 [d]	3.65	9.19 ± 0.12[d]
PLAF-10%C30B	3.84	37.16	15.39 ± 3.84 [c]	4.58	-
PLAF-10%C30B/EU-PHE	3.80	61.36	13.58 ± 3.80 [e]	14.06	9.25 ± 0.37[d]

419 Different superscripts indicate statistically significant differences in the crystallinity of the samples.
420

421 **Fig. 2** shows the representative images of PLA nanocomposite foams with different
422 C30B concentrations (0, 5, and 10 % w/w). The foams' average pore diameters (d_{aver}) and
423 cell density (ρ_c) values are presented in **Table 1**. As shown in **Fig. 2**, the incorporation of
424 C30B did not change the closed cell morphology present in the control PLAF. Nevertheless,
425 clay agglomerates were observed in the PLA nanocomposite foam with C30B at 10 % w/w
426 since the nanoparticles were less dispersed inside the polymer (**Fig. 2d**). This phenomenon
427 decreased the porosity (81.69%) and consequently, the expansion ratio (5.47) of the foam
428 with the high C30B concentration compared to the pristine PLA foam. Particularly, nanoclay
429 agglomerations could act as a physical barrier for the polymer expansion during the cell
430 growth stage [19,59], which explained the formation of polymer foams with lower average
431 pore diameter sizes (15.39 ± 3.84 µm) compared to the control PLAF (20.90 ± 6.35 µm) and
432 the foam with 5 % w/w C30B (22.70 ± 6.65 µm). Consequently, the PLA nanocomposite
433 foam with 10 % w/w C30B presented the highest cell density compared with the values
434 obtained for the control PLAF and PLA nanocomposite foam with 5% w/w C30B (**Table 1**).

435

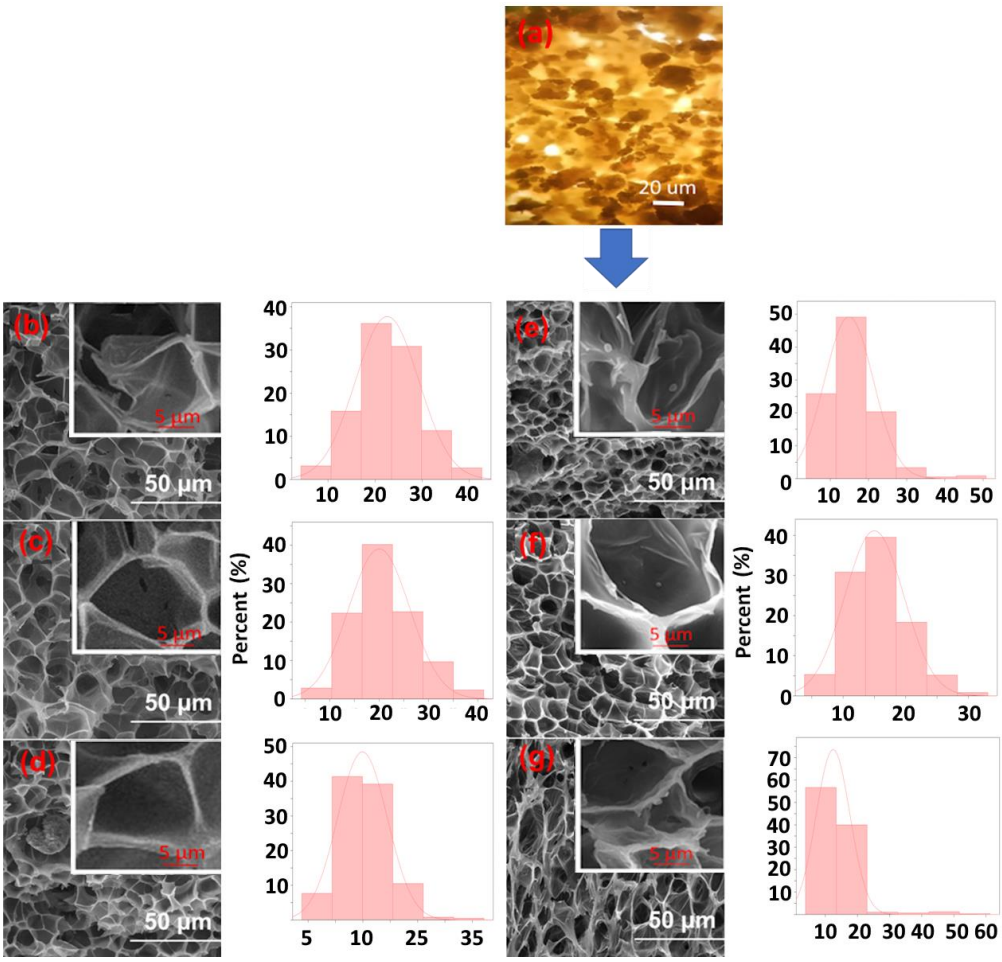

436

437 **Fig. 2.** Optical microscope image of the EU-PHE cocrystal powder (a), SEM images
438 and pore size distribution of PLA foams with 0, 5 and 10 % w/w of C30B (b, c, and d,
439 respectively), and SEM images and pore size distribution of the PLA foams impregnated
440 with EU-PHE cocrystals with 0, 5 and 10 % w/w of C30B (e, f, and g, respectively).

441

442 The experiments in the view cell confirmed the stability of the EU-PHE cocrystal
443 when exposed to $scCO_2$ under the conditions of interest (15 MPa and 60 °C). No phase
444 separation could be observed during the exposure or after the system decompression. The
445 determined solubilities of EU, EU-PHE cocrystal, and PHE in $scCO_2$ at 15 MPa and 60 °C
446 were 0.0370±0.0005, 0.0123±0.0002, and 0.00109±0.00006 g/g_{scCO2}, respectively. The
447 results indicated that the EU solubility in $scCO_2$ was considerably higher than that of PHE.

448 The EU-PHE cocrystal solubility was approximately ten times higher than the solubility of
449 pure PHE and three times lower compared to the EU. In the literature, data on EU solubility
450 in $scCO_2$ are usually derived from supercritical fluid extraction measurements for different
451 $scCO_2$ flow rates and particle sizes [60]. In contrast, the static solubility measurement data
452 are scarce. Chen et al. determined the VLE data for the system $scCO_2$-EU in a semi-flow type
453 apparatus and reported the maximal EU molar fraction value of $0.96x10^{-2}$ (corresponding to
454 0.035 g/g_{scCO2}) at 328.15K & 125.1 bar [61], which is similar to our value. The only report
455 on PHE solubility in $scCO_2$ is the work of Van Alsten et al. [62]. The authors obtained a PHE
456 molar fraction of 0.000225 (corresponding to 0.00092 g/g_{scCO2}) at 14.58 MPa and 50 °C,
457 which is comparable to our result. The determined EU-PHE cocrystal solubility (0.0123
458 g/g_{scCO2}) lies between the values of pure EU and PHE, and it is appropriate (high enough) to
459 allow for an effective SSI.

460 EU and EU-PHE cocrystals were successfully impregnated in PLA nanocomposite
461 foams by SSI under the conditions of 15 MPa and 60 °C and with a decompression rate of
462 0.5 MPa/min. To the best of our knowledge, there is no data on the impregnation of EU in
463 PLA by SSI or another method. The obtained impregnation yield of EU was in the range
464 between 20 to 22 % w/w and slightly increased (from 20 to 22%) with the C30B content.
465 This might be due to the hydrophobic nature of EU and possible interactions with the
466 nanoclay's silicate layers. The same phenomenon has been used to explain the slight impact
467 of C30B on the impregnation yield of cinnamaldehyde in PLA nanocomposite foams [19]
468 and films [63] with C30B content up to 5 % w/w. The impregnation yield of EU for PLA
469 foams obtained in this study is comparable to those reported for other essential oil derivatives.
470 Under similar processing conditions, Torres et al. stated that a thymol loading in PLA films
471 was 20.4% w/w [64].

Recently reported EU-impregnated polymeric materials utilizing $scCO_2$ include linear low-density polyethylene (LLDPE) with EU impregnation yield ranging between 1 and 6 % w/w [65], polyamide fibers with impregnation yield between 8 and 15 % w/w [41], and polyamide dental floss with impregnation yield ranging between 4 and 16 % w/w [42]. It is clear from comparing these studies with our findings that PLA exhibits higher EU impregnation yields than the aforementioned polymers. It is well-known that the SSI of bioactive substances in polymers depends on the balance between the affinity of the bioactive substance towards the polymer and $scCO_2$. Particularly, the high loading of active substances in PLA has been attributed to electrostatic interactions between functional groups of the bioactive substances and free carbonyl groups available in PLA chains. In the case of cinnamaldehyde, hydrogen bonds between the oxygen of the aldehyde belonging to the cinnamaldehyde and the PLA carbonyl group allow for incorporations of up to 13 % w/w [66]. According to reports, notable thymol incorporation in the polymeric matrix (up to 24 % w/w) was caused by a secondary interaction between the phenolic group of thymol and the free PLA's carbonyl groups [6]. In our study, the hydroxyl group of EU and its electrostatic interactions with carbonyl groups of PLA contributed to the high EU loadings.

The obtained impregnation yields for the EU-PHE cocrystal were notably high, ranging from 8.62 to 9.25 % w/w (**Table 1**). The presence of C30B slightly increased the cocrystal loading, similar to the observed with EU. **Fig. 2**. presents the images of EU-PHE cocrystal and neat and impregnated PLA foams along with their pore size distribution. The SEM images revealed a slight decrease in the average pore diameter of PLA nanocomposite foams due to the EU-PHE cocrystal incorporation (**Fig. 2e**, **2f**, and **2g**). This phenomenon has been previously observed for PLA nanocomposite foams impregnated with cinnamaldehyde [19] and starch foams impregnated with carvacrol [67,68]. The phenomenon

was explained by the plasticizing properties of these essential oil derivatives. **Fig. 2a** shows EU-PHE cocrystals generated manually by grinding according to the procedure described in part 2.2. The cocrystals appear as agglomerated granules of diameters up to 25 µm. However, EU-PHE cocrystals appeared inside the PLA nanocomposite foams as isolated spherical shape micrometric particles with an average diameter of around 0.8 µm (**Fig. 2e, f, and g**). Therefore, it can be concluded that the recrystallization of the EU-PHE complex from the supercritical phase occurred. SEM images with EU-PHE recrystallized particles and their dimensions are presented in Fig. S1 (Supplementary material). The micronization or nanonization of solid particles inside polymeric structures by means of the SSI process has been previously reported [43,44]. Ubellitogullary et al. reported the nanonization of phytosterol particles inside nanoporous starch aerogels by decreasing their solubility in $scCO_2$ during the last stage of the SSI process. The authors attributed the formation of isolated nanoparticles to favored nucleation rather than crystal growth during the fast-cooling stage previous to the depressurization of the system [43].

It is well-known that the solvation of solid particles in supercritical fluids involves the formation of clusters or aggregates of solvent molecules around the solute [69,70]. In this way, clusters of CO_2 molecules probably surrounded the EU-PHE cocrystal particles without destabilizing the supramolecular interactions between their components (EU and PHE) during the first stage of the SSI (solvation stage), allowing their dispersion and transport in the supercritical phase towards the polymer in the second stage of the process (diffusion stage). Finally, the incorporation/recrystalization of the EU-PHE cocrystals inside the polymer foam occurred in the third stage by cooling and the subsequent depressurization of the system.

519 It is well-known that $scCO_2$ solvent power is an important factor governing the
520 impregnation of bioactive substances in polymers [17,18]. In this way, the differences
521 between the impregnation yield obtained for EU and the EU-PHE cocrystal could be
522 associated with their different solubilities in $scCO_2$. There is no data in the open literature
523 about the solubility of cocrystallized derivative essential oils in supercritical fluids, and our
524 study is the first report on cocrystal solubility in $scCO_2$. The solubility values determined in
525 this work support the obtained SSI results and the feasibility of the proposed process.
526

527 *3.2. X-ray diffraction*

528 The X-ray diffraction analysis of PLA nanocomposite foams was performed to
529 identify if the nanoclay was exfoliated on the polymer matrix, that is, if C30B was uniformly
530 distributed, allowing correct intercalation of PLA chains in nanoclay sheets. As **Fig. 3a**
531 shows, XRD diffractograms of PLAF and PLAF-5%C30B did not evidence differences,
532 confirming the exfoliation of C30B by PLA [56,71]. On the other hand, a significant
533 difference was observed in the diffractogram of PLAF-10%C30B with the characteristic
534 band of C30B at approximately 5º that confirmed the low exfoliation in the material when
535 the clay was added at high concentration. This nanocomposite presented an agglomeration
536 of C30B consistent with SEM images and the previously explained phenomena related to the
537 porosity and the expansion coefficient. This effect has also been observed through TEM
538 analysis in a previous work that evidenced the agglomeration of C30B in PLA polymeric
539 structure when added at 10 % w/w [72].
540

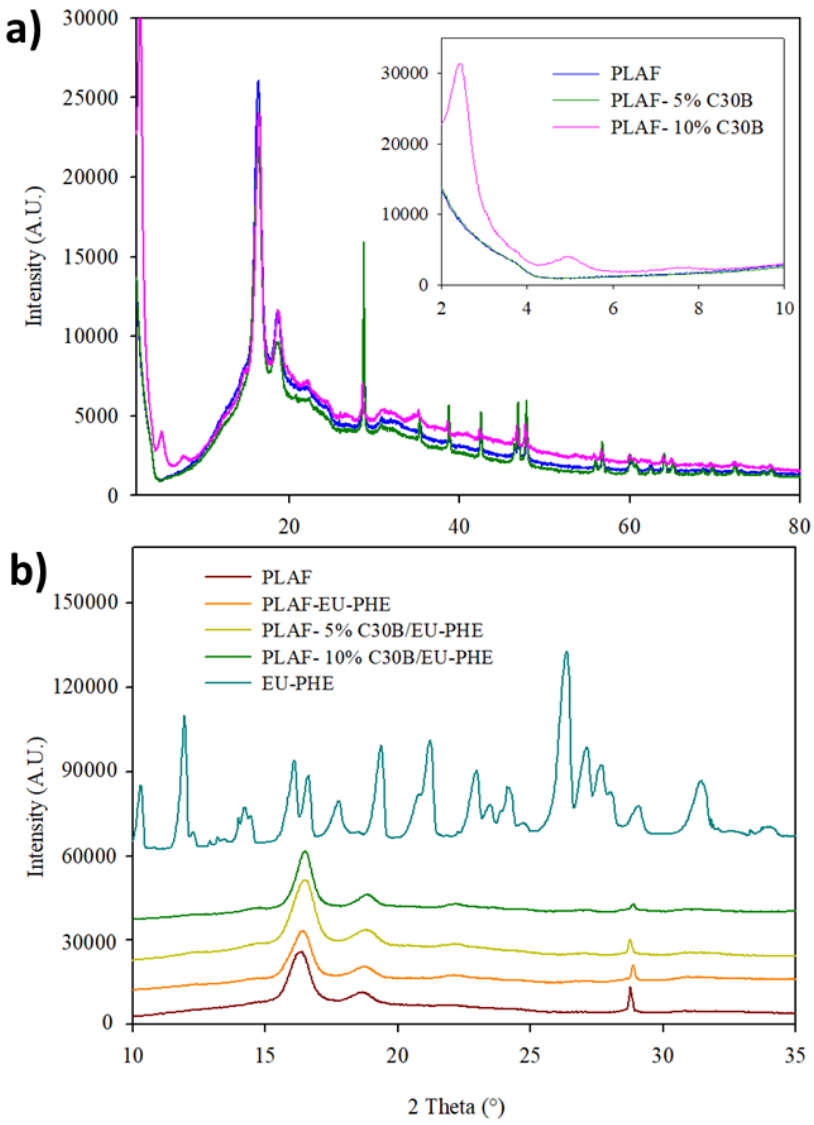

Fig. 3. DRX diffractograms of: a) foamed PLA nanocomposites with 0, 5 and 10 % w/w C30B; b) foamed PLA nanocomposites with 0, 5 and 10 % w/w C30B impregnated with EU/PHE cocrystals.

Fig. 3b presents the XRD diffractograms of foamed PLA nanocomposites impregnated with EU-PHE cocrystals. The diffractogram of EU-PHE confirmed the incorporation of the crystal structure in PLA, in agreement with the XRD previously reported by Mazzeo et al. [25]. The foamed PLA nanocomposites evidenced a shift in the main bands upon incorporating EU-PHE into the polymeric foams, which are present at 16º, 18.6º and

28.75º respectively, indicating an intercalation of EU-PHE with the polymer matrix. No cocrystal agglomeration was detected. New weak bands at 12.3, 22.1, and 27º also appeared upon impregnating the cocrystals, which were attributable to the incorporation/recrystallization of EU-PHE cocrystals in the polymeric matrix.

3.3. FTIR analysis

Fig. 4a shows the spectra of foamed PLA nanocomposites. The main characteristic peaks for PLA can be observed at 1750 and 1082 cm^{-1}, corresponding to the symmetric and asymmetric stretching of the C=O group, respectively; the bands at 1180 and 1127 cm^{-1} are associated to the asymmetric and symmetric stretching of the C-O bond, respectively; the CH_3 bending at 1454 cm^{-1} and the symmetric and asymmetric stretching of the C-H bond of CH_2 are seen as peaks at 1381 and 1360 cm^{-1}, respectively [19,73,74]. Finally, the amorphous and crystalline zones of PLA were observed at 870 and 754 cm^{-1}, respectively [75]. The presence of C30B nanoclay was observed in the range of wavenumbers between 2800 and 3050 cm^{-1}. The bands at 2920 and 2850 cm^{-1} are associated with the asymmetric and symmetric vibrations of the C-H group of the methylene group of C30B, respectively [76].

FTIR spectra of PLA foams impregnated with EU are presented in **Fig. S2** (Supplementary material). Comparing the spectra of neat and EU-impregnated foams, new bands were observed in the impregnated samples, confirming the presence of EU. The new peak at 1511 cm^{-1} is attributed to the stretching of the EU; two new bands at 818 and 793 cm^{-1} are associated with the vibration of the tetra-substituted aromatic ring. The characteristic bands for PLA were detected, and there was no shift in wavenumbers. However, compared to neat foams, a decrease in the absorbance for the characteristic frequencies of the functional

groups C=O and C-O was observed, evidencing an interaction of the hydrogen bond type between these groups and the incorporated EU.

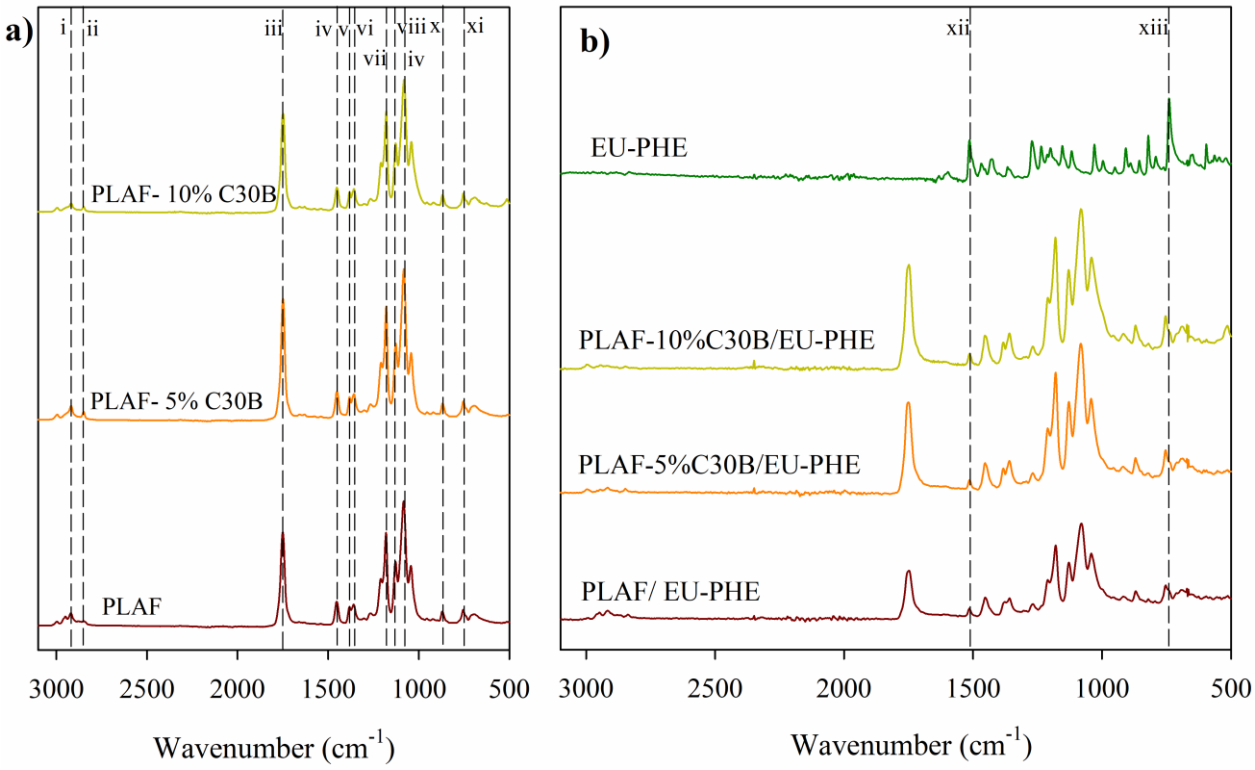

Fig. 4. ATR-FTIR spectra of a) foamed PLA nanocomposites; b) active foamed PLA nanocomposites impregnated with EU-PHE cocrystals.

Fig. 4b shows FTIR spectra of PLA foams impregnated with EU-PHE cocrystals. The PLA characteristic bands were detected, with no shift in wavenumbers. A decrease in the absorbance of the C=O and C-O functional groups was evidenced, showing hydrogen bond interactions between the EU-PHE cocrystals and the PLA polymeric structure [77]. On the other hand, the main peaks of EU-PHE were identified at 1514 cm^{-1}, corresponding to the vibration of the aromatic ring, and at 821 cm^{-1}, associated with the vibration of the tetra-substituted aromatic ring.

3.4. Thermal properties of the impregnated PLA nanocomposite foams

3.4.1. Differential scanning calorimetry

Table 2 shows the thermal properties of pure substances and nanocomposite foams obtained by the DSC analysis. DSC thermograms for EU-PHE cocrystal and PHE, and representative thermograms for the PLA nanocomposite foams, are shown in **Fig. S3** and **Fig. S4** (Supplementary material), respectively. The effective formation of the EU-PHE cocrystal by grinding was evidenced by the appearance of a single melting peak around 52 ºC, revealing that it had a different crystalline structure than that of PHE, which presented a single melting transition at 175 ºC (**Table 2** and **Fig. S3**).

The control PLAF presented a thermal transition at 69 °C associated with the polymer's glass transition temperature. T_g was not detected in PLA foams with EU, EU-PHE cocrystal, and clay, which had higher crystallinity values than the control PLAF. In addition, cold crystallization at 111 °C was registered in PLAF and the active-free PLA nanocomposite foams due to rearrangement of the amorphous regions during the DSC heating, as was reported for pristine PLA foams [78].

Table 2.

Thermal properties of the individual substances and PLA nanocomposite foams.

Sample	T_{cc} (ºC)	ΔH_{cc} (J g^{-1})	T_{m1} (ºC)	T_{m2} (ºC)	T_{m3} (ºC)	ΔH_{m1} (J g^{-1})	ΔH_{m2-3} (J g^{-1})	X_c (%)
PLAF (control)	111	3.8	-	149	-	-	34.6	33 ± 1^{a}
PLAF - EU	-	-	-	104	135	-	33.4	$36 \pm 2^{b,c}$
PLAF - EU-PHE	-	-	33	125	142	0.34	44.2	48 ± 1^{f}
PLAF - 5% C30B	118	5.8	-	150	-	-	32.0	$34 \pm 1^{a,b}$
PLAF - 5% C30B/EU	-	-	-	106	134	-	33.5	38 ± 1^{c}
PLAF - 5% C30B/EU-PHE	-	-	33	126	142	0.25	36.2	41 ± 1^{d}
PLAF - 10% C30B	118	2.1	-	148	157	-	31.0	$34 \pm 2^{a,b}$
PLAF - 10% C30B/EU	-	-	-	107	134	-	27.6	33 ± 1^{a}
PLAF - 10% C30B/EU-PHE	-	-	33	130	143	0.84	37.2	44 ± 1^{e}
EU-PHE	-	-	52	-	-	-	125.1	-
PHE	-	-	-	175	-	-	179.9	-

ANOVA analysis was carried out to find significant differences in the crystallinity values of the samples. Different superscripts indicate statistically significant differences.

The thermograms of PLAF and PLA nanocomposite foams show an endothermic transition at approximately 150 °C, associated with the melting of PLA (**Fig. S4**, Supplementary material). Similar T_m values have been reported for PLA foams obtained by foaming with $scCO_2$ at 147 °C [79] and 150 °C [78]. However, in EU-impregnated PLA foam thermograms (~21 % w/w EU), a broad endothermic transition is observed with two distinct peaks, indicating the melting of two crystalline structures with different degrees of ordering, α' structures less ordered and polymeric structures thermodynamically more stable that melted around 104 °C and 135 °C, respectively (**Fig. S4** and **Table 2**). Similar was observed for PLA foams with different porosities and PLA foams with clay/cinnamaldehyde by Bocz et al. [78] and Rojas et al. [19], respectively. Thermograms of PLAF and its nanocomposite foams impregnated with EU-PHE cocrystal (~9 % w/w of EU-PHE cocrystal) showed a broad melting, which indicated the formation of two crystal structures with different ordering. T_m was shifted to higher temperature values despite the lower proportion of impregnated EU-PHE (compared to EU), reaching values up to 130 °C (T_{m1}) and 143 °C

(T_{m2}) for the PLAF-10%C30B/EU-PHE sample. This is consistent with a more crystalline (41-48%) and stable foam due to EU-PHE cocrystal impregnation compared to those impregnated with EU (33-38%). However, both values were above the crystallinity of the PLAF (33%) (**Table 2**). A crystallinity of 35% was reported for PLA pellets and PLA foams formed by extrusion with 10 % w/w rice husks [80].

The lower melting temperatures (T_{m2} and T_{m3}) of the PLA foams impregnated with EU or EU-PHE cocrystal with respect to those of their corresponding PLA foam controls are explained by a plasticizing effect of the active component. Besides, the melting temperatures of the foams with EU and EU-PHE cocrystal presented differences attributed to the different interactions of the incorporated components with the polymer. For PLAF with EU, hydrogen bond interaction could be established between the hydroxyl group and oxygen of EU and the carbonyl and terminal chains hydroxyl groups of the PLA, obtaining a crystalline structure that was destabilized and melted at lower temperatures than EU-PHE cocrystal-impregnated foams. This result suggested that more stable hydrogen bonding interactions between the pyrazine nitrogen groups and the terminal hydroxyl groups of PLA chains would also be formed. Hydrogen-bonding interactions have been reported in thymol-impregnated polyamide membranes using $scCO_2$ [81]. In addition, in the case of PLA nanocomposite foams, interactions could be formed between the hydroxyl groups of the clay and the organic modifier with EU or EU-PHE molecules. Therefore, a tendency for higher T_m values was observed (**Table 2**). Regarding these observations, Bianchi et al. recently analyzed the inhibition of *Escherichia coli*, *Salmonella* Typhimurium, and *Staphylococcus aureus* using different cocrystals based on carvacrol, thymol, and cinnamaldehyde as essential oils and hexamethylenetetramine and 4-hydroxybenzoic acid as coformers incorporated into the surface of low-density polyethylene (LDPE) films using a chitosan solution. The authors

concluded that the most determining factor for the active compound's stability and time-sustained release is the hydrogen bond's strength between the polymeric matrix and the coformer of the cocrystal [26]. Importantly, PLA foam impregnated with EU-PHE cocrystals showed a low-intensity transition between 30 °C and 50 °C attributed to the melting of the cocrystals, confirming their incorporation into PLAF **(Table 2** and **Fig. S4**).

3.4.2. Thermogravimetric analysis

The results of thermogravimetric analysis are presented in **Table 3** and **Figs. S5-S8** (Supplementary material). PLAF initiated to decompose at 344 °C and had a T_d at 362 °C, similar to that reported in the literature [19,74]. Meanwhile, foams impregnated with EU or EU-PHE presented two degradation stages at T_{d1} and T_{d2}. The first stage was associated with the degradation of the impregnated compound (EU or EU-PHE), whose T_{d1} values were close to that of the individual substances, which confirmed the incorporation of EU and EU-PHE cocrystal in the foams. The second stage was related to PLA degradation (**Table 3** and **Figs. S6** and **S7**).

The T_{onset} and T_d of the PLA foam impregnated with EU-PHE cocrystal, without and with clay, were between the temperature values of the control PLAF and the values obtained for the PLA foam impregnated with EU (**Figs. S5-S8** and **Table 3**). This is in agreement with the higher thermal stability found for the cocrystal compared to the EU but lower with respect to that of the PHE, in terms of the onset decomposition and the maximum degradation rate temperatures (**Table 3**).

Furthermore, it was observed that the nanoclay and EU tended to diminish T_{onset} of the PLA foams, attributed to the lower thermal stability of the organic modifier of the clay and the EU compared to PLA [82,83]. However, the incorporation of EU-PHE cocrystal

673 counteracted this effect and increased the thermal stability of the active foams, which were
674 more crystalline. However, T_d was not significantly modified, similar to the report of Rojas
675 et al., who found that the addition of C30B did not affect the T_d of PLA nanocomposites with
676 cinnamaldehyde [19].

677

678 **Table 3**
679 TGA analysis of the individual substances and the impregnated PLA nanocomposite foams.
680

Sample	T_{onset} (ºC)	T_{d1} (ºC)	T_{d2} (ºC)
PLAF (control)	344 ± 1.0^{a}	362 ± 0.5^{a,b}	-
PLAF - EU	156 ± 1.0^{f}	186 ± 1.0^{f}	362 ± 1.0^{a,b}
PLAF - EU-PHE	165 ± 1.0^{e}	200 ± 1.0^{c,d}	362 ± 1.0^{a,b}
PLAF - 5% C30B	341 ± 1.0^{b}	360 ± 0.5^{a}	-
PLAF - 5% C30B/EU	148 ± 1.0^{g}	186 ± 1.0^{e,f}	357 ± 1.0^{c}
PLAF - 5% C30B/EU-PHE	170 ± 1.0^{d}	202 ± 1.0^{c}	363 ± 1.0^{b}
PLAF - 10% C30B	340 ± 1.0^{b}	362 ± 2.0^{b}	-
PLAF - 10% C30B/EU	156 ± 0.1^{f}	188 ± 0.5^{e}	362 ± 0.5^{a,b}
PLAF - 10% C30B/EU-PHE	172 ± 0.5^{c}	199 ± 0.5^{d}	361 ± 0.5^{a}
EU-PH	172 ± 1.0^{c}	236 ± 1.0	-
PHE	200 ± 1.0	256 ± 1.0	-
EU	103 ± 1.0	186 ± 2.0	-

681 Different superscripts indicated statistically significant differences in the properties among the foams
682 determined by ANOVA analysis.
683

684

685 *3.5. Mechanical assays*

686 The effect of C30B and EU-PHE cocrystal addition on the mechanical properties of
687 PLAF was analyzed following the method described in part 2.5.5. The 10% C30B PLA foam
688 samples were omitted for this analysis because the C30B agglomerated inside the polymer
689 (part 3.2), negatively affecting the materials' physical properties (part 3.1). Therefore, neat
690 PLAF and PLAF with 5% C30B foams (8 x 2.5 cm) were prepared and impregnated with EU
691 and EU-PHE (**Fig. S9**, Supplementary material). In the next step, foams impregnated with

692 EU were excluded from the assays because they hadn't preserved their shape after the
693 impregnation (**Fig. S9**). This phenomenon is due to the extensive plasticizing effect of EU
694 on the polymeric matrix. On the contrary, EU-PHE-impregnated PLA foams maintained their
695 shape and size (**Fig. S9**).

696 Results of tensile modulus, tensile strength, and elongation at break for the non-
697 impregnated foams (PLAF and PLAF - 5% C30B) and the EU-PHE cocrystal impregnated
698 foams (PLAF - EU-PHE and PLAF - 5% C30B/EU-PHE) are shown in Table 4. Uniaxial
699 Stress-strain curves for the materials prepared in this study are shown in **Fig. S10**
700 (Supplementary material). PLAF control presented tensile strength (1.8 MPa) and elongation
701 at break (31.9%) values similar to those reported in the literature for expanded polystyrene
702 [84], which have encouraged the use of PLA foams at the industrial level for food packaging
703 purposes, including its use for the fabrication of cups and trays [85,86]. The presence of
704 C30B or the incorporation of EU-PHE did not significantly alter tensile modulus or tensile
705 strength. Nevertheless, C30B addition at 5% slightly increased the elongation at break of the
706 material from 31.9% (PLAF) to 48.2% (PLAF-5%C30B), which could be related to the full
707 exfoliation of C30B (part 3.2) which probably improved the polymeric matrix cohesion by
708 the electrostatic interactions established between C30B and the polymer chains, consequently
709 improving ductility. This behavior has been previously reported for montmorillonite clays
710 fully exfoliated in a polymeric matrix. Chen et al. reported an increase in the elongation at
711 break from 71.8% to 118% for poly(L-lactide)/poly(butylene succinate) blends using Cloisite
712 25A. The authors attributed the increase in ductility of the films to the electrostatic
713 interactions between C25A and the polymer chains promoted by C25A exfoliation [87].
714 Elongation at break was increased by EU-PHE cocrystal addition from 31.9% (PLAF control)

to 90.3% (PLAF-EU-PHE) due to its plasticizing effect on the polymeric matrix, which increased the material's ductility. This effect has been reported previously for PLA films impregnated with essential oil derivatives such as thymol [64] and cinnamaldehyde [66]. Consequently, the nanocomposite impregnated with the EU-PHE cocrystal (PLAF-5%C30B/EU-PHE) presented the highest elongation at break value (141%) due to the concomitant effect of C30B presence and higher EU-PHE cocrystal incorporation (9.19 % w/w) than in PLAF/EU-PHE (8.62 % w/w).

Table 4
Tensile properties parameters of the materials.

Material Sample	Tensile modulus [MPa]	Tensile Strength [MPa]	Elongation at break [%]
PLAF (control)	14.0 ± 5.3[a]	1.8 ± 0.7[a]	31.9 ± 7.8[a]
PLAF - 5% C30B	17.5 ± 9.3[a]	2.3 ± 0.9[a]	48.2 ± 18.8[a]
PLAF - EU-PHE	18.3 ± 10.4[a]	3.0 ± 1.0[a]	90.3 ± 32.9[b]
PLAF - 5% C30B/EU-PHE	18.4 ± 8.9[a]	4.9 ± 1.2[b]	141.0 ± 25.0[c]

Different superscripts indicate statistically significant differences.

3.6. The release kinetics

The release of EU in its pure and cocrystallized forms from PLAF with different C30B contents was studied through specific migration assays using EtOH 10% as an aqueous food simulant. The partition coefficient of EU ($K_{P/FS}$), a thermodynamic parameter that represents the ratio between the concentration of the bioactive substance in the polymer (P) and the food simulant (FS), was used to express the equilibrium condition. The mathematical modeling employing Korsmeyer-Peppas and Higuchi kinetic models was used to identify the

735 release mechanism of pure EU and cocrystallized EU from the PLA nanocomposite foams.
736 **Table 5** shows the values of the regression coefficient (R^2) obtained from the Higuchi and
737 Korsmeyer-Peppas models. Likewise, the diffusional exponent "n" for the Korsmeyer-
738 Peppas model and the release rate constant "k" were determined. The parameter "n" indicates
739 the type of active substance release mechanism: $n < 0.5$ for a quasi-Fickian diffusion, $n = 0.5$
740 for a Fickian diffusion, and $n > 0.5$ for an anomalous transport [88,89].

741
742 **Table 5.**
743 Partition coefficient ($K_{P/FS}$), regression coefficient (R^2), diffusional exponent (n), and release
744 rate constant (k) of Higuchi and Korsmeyer-Peppas kinetic models.
745

Kinetic Release Models		**Higuchi**			**Korsmeyer-Peppas**		
Sample	**$K_{P/FS}$**	**R^2**	**n**	**k**	**R^2**	**n**	**k**
PLAF-EU	947	0.421	0.5	0.075	0.961	0.055	0.223
PLAF- 5%C30B/EU	1248	0.299	0.5	0.049	0.944	0.033	0.200
PLAF-10%C30B/EU	1017	0.762	0.5	0.073	0.974	0.046	0.188
PLAF-EU-PHE	48	0.990	0.5	0.038	0.994	0.396	0.061
PLAF-5%C30B/EU-PHE	98	0.868	0.5	0.030	0.927	0.293	0.076
PLAF-10%C30B/EU-PHE	131	0.929	0.5	0.042	0.970	0.315	0.085

746

747 The highest R^2 values obtained using the Korsmeyer-Peppas model evidenced its
748 better performance compared to the Higuchi model to fit the experimental release data of EU
749 and EU-PHE cocrystal from the PLA nanocomposite foams. Therefore, the "k" and "n"
750 values determined using the Korsmeyer-Peppas model were used to study the release
751 mechanisms of EU and EU-PHE from PLA foams. **Table 5** shows that the different PLA

752 foams impregnated with EU and EU-PHE showed "n" values lower than 0.5, evidencing that
753 both EU and EU-PHE showed a quasi-Fickian diffusion release mechanism in these
754 materials. Previous studies on active polymeric foams have also reported a quasi-Fickian
755 diffusion mechanism for different substances. For instance, "n" values between 0.14 and 0.31
756 revealed that the release of chloramphenicol from polymeric blended foams based on
757 chitosan followed a quasi-Fickian diffusion-driven sustained release [90]. Likewise, the
758 release of cinnamaldehyde from PLA nanocomposite foams towards EtOH 50% also
759 followed a quasi-Fickian diffusion process since the "n" value was near 0.20 [19]. Spent
760 coffee phenolic compounds also followed a quasi-Fickian diffusion release mechanism from
761 starch foam composites in water and EtOH 10 and 50% as food simulants, with "n" values
762 between 0.18 and 0.49 [91].

763 Most research on designing antimicrobial food packaging materials has been done
764 considering the use of essential oils or some of their derivatives. The main challenge
765 identified so far is decreasing the release rate of these highly volatile compounds from
766 polymeric structures through different strategies [92]. Interestingly, the release kinetics of
767 eugenol from food packaging materials has been scarcely studied [93–95]. **Fig. 5** shows the
768 experimental EU release data from the different PLA foams. **Fig. 5a** indicates EU exhibited
769 a fast release, reaching the equilibrium condition independent of the C30B content after 2 h.
770 A similar fast-release behavior was reported for cinnamaldehyde from PLA nanocomposite
771 foams with different concentrations of C30B using EtOH 50% as food simulant [19]. Fitting
772 the experimental release data using the Korsmeyer-Peppas model showed that the release rate
773 constant (k) for EU in PLAF was 0.223. A similar release rate constant for EU (0.17) was
774 reported for poly (hydroxybutyrate-co-hydroxyvalerate) films and EtOH 10% as a food

775 simulant, evidencing a fast release of EU independent of the polymeric structure used to
776 design the active material [94]. On the contrary, the EU release curves for the PLA foams
777 impregnated with the EU-PHE cocrystal (**Fig. 5b**) exhibited a more prolonged EU release
778 than those impregnated with pure EU. In particular, the time (120 h) necessary to reach the
779 equilibrium condition for the release of cocrystallized EU from PLAF was 60-fold higher
780 than the value for pure EU (2 h). This result confirmed that the EU cocrystallization promoted
781 a prolonged EU release since the diffusion through the porous matrix was carried out in
782 association with a crystalline solid state instead of the liquid state (case of pure EU). In
783 another study, Celebioglu et al. reported a 10-fold decrease in the time necessary to reach the
784 equilibrium condition in water for EU released from pullulan nanofibers due to its
785 encapsulation in cyclodextrins (CDs) [93]. Particularly, the encapsulation of essential oil
786 derivatives in CDs has been one of the most effective reported strategies to prolong their
787 release [96–98]. Therefore, the comparison of the results obtained in this study with the
788 literature data indicates the advantage of cocrystallization engineering over conventional
789 methods to develop antimicrobial polymeric materials with more prolonged release
790 properties. New questions also arose about modifying release kinetic for a specific
791 application regarding the coformer choice, which would influence intermolecular interaction
792 between the coformer and active substance.

793 The sustained release of the EU-PHE cocrystal was also observed in the PLA
794 nanocomposite foams but with less intensity than in PLAF. Nevertheless, the time required
795 to reach the equilibrium condition for the release of the EU-PHE cocrystal decreased with
796 C30B content (**Fig. 5b).** Fitting the experimental release data using the Korsmeyer-Peppas
797 model allowed us to determine that the release rate constants of EU-PHE in PLAF-5%C30B

(0.076) and PLAF-10%C30B (0.085) were 1.25 and 1.39-fold higher than the value obtained for EU-PHE cocrystal in PLAF, respectively. The negative impact of the addition of C30B at 10% on the sustained release of the EU-PHE cocrystals could be associated with the agglomeration of C30B (part 3.2) and the generation of a nanocomposite foam with low porosity and expansion ratio which promoted a shorter release path in comparison with the other materials.

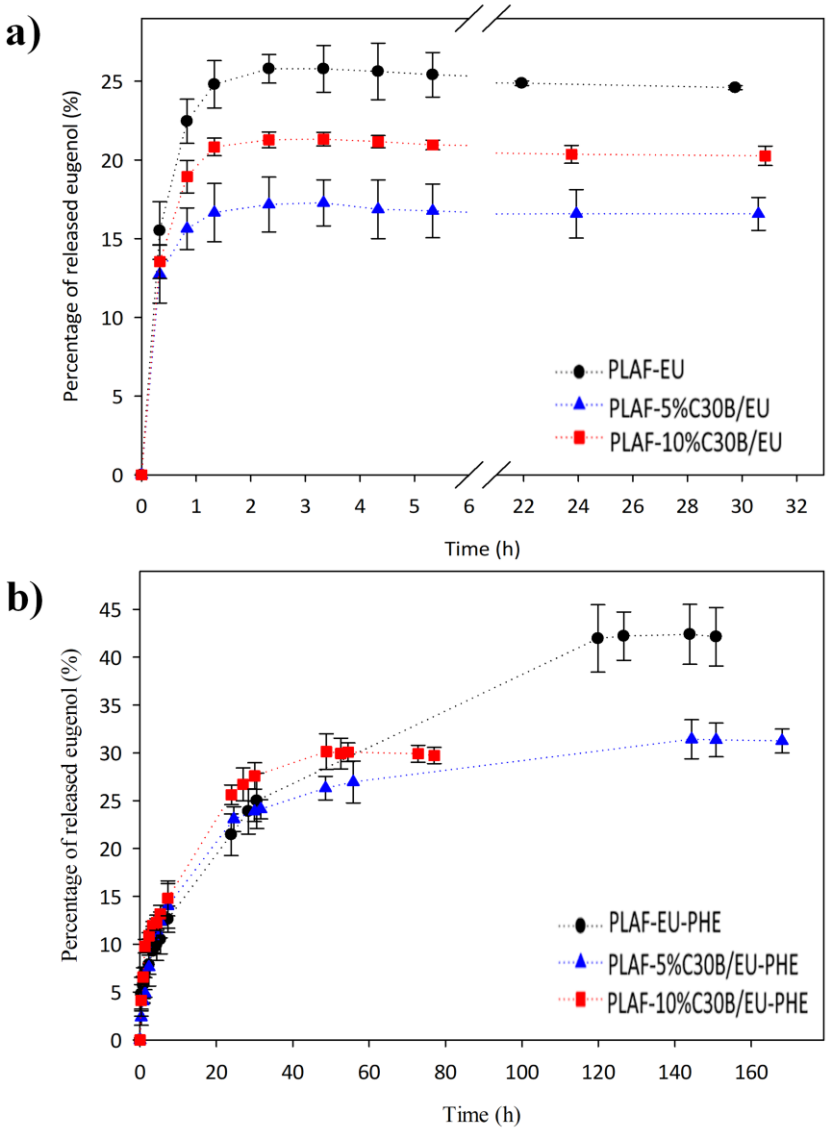

Fig. 5. Release curves of EU from a) EU-impregnated foams and b) EU-PHE cocrystal-impregnated foams towards EtOH 10% at 40 °C.

The sustained release of the EU-PHE cocrystal was also observed in the PLA nanocomposite foams but with less intensity than in PLAF. Nevertheless, the time required to reach the equilibrium condition for the release of the EU-PHE cocrystal significantly decreased with C30B content (**Fig. 5b).** Fitting the experimental release data using the Korsmeyer-Peppas model allowed us to determine that the release rate constants of EU-PHE in PLAF-5%C30B (0.076) and PLAF-10%C30B (0.085) were 1.25 and 1.39-fold higher than the value obtained for EU-PHE cocrystal in PLAF, respectively. The negative impact of the addition of C30B at 10% on the sustained release of the EU-PHE cocrystals could be associated with the agglomeration of C30B (part 3.2) and the generation of a nanocomposite foam with low porosity and expansion ratio, which promoted a shorter release path in comparison with the other materials.

Table 5 also summarizes the distribution coefficients ($K_{P/FS}$) that characterize the equilibrium condition for the release of EU and EU-PHE from the different PLA nanocomposite foams. Among the polymeric foam samples impregnated with pure EU, PLAF showed the lowest $K_{P/FS}$ value, evidencing the highest percent released of EU to the food simulant at the equilibrium condition (**Fig. 5a**). The $K_{P/FS}$ value increased with the concentration of C30B. This fact could be related to the interaction between the free hydroxyl groups of C30B and the EU hydroxyl groups that increased the affinity of EU towards the polymeric phase, decreasing its release to the simulant. The same phenomenon was also observed for the release of thymol from LDPE extruded films with C30B at 5 % w/w [4] and LLDPE extruded films loaded with C20A [99]. In these studies, the high retention of thymol in the polymer was associated to interactions between the nanoclays and the active compounds. In our study, the lowest EU release was obtained from PLA nanocomposite foam

with C30B at 5 % w/w. In this case, the exfoliation of the nanoclays in the foam favored the retention of EU in the foams. Instead, the poor dispersion of the nanoclay sheets in the PLA nanocomposite foam with C30B at 10 % w/w promoted the easier release of the active compound to the food simulant, evidenced by lower $K_{P/FS}$ values than for the PLA nanocomposite foam with C30B at 5 % w/w.

Table 5 shows that the highest percentages of released EU were obtained from PLA foams impregnated with the EU-PHE cocrystal. Particularly, $K_{P/FS}$ values for the release of EU from PLAF impregnated with the EU-PHE were 20-fold lower than the value obtained for the PLAF impregnated with pure EU. This fact is related to the lower initial EU content (4.14 % w/w) in the samples impregnated with EU-PHE cocrystal compared to the initial EU content (20 % w/w) in the PLAF impregnated with pure EU. As was obtained for the EU-impregnated samples, the $K_{P/FS}$ for EU increased by the C30B presence due to the interactions developed between C30B and the EU-PHE cocrystal.

3.7. Microbiological studies

The obtained MIC value of EU for *L. monocytogenes* and *S. Enteritidis* was 1.25%. The obtained MIC values of PHE and the EU-PHE cocrystal were >5%.

The log CFU/cm^2 reduction values of the anti-attachment assay on *L. monocytogenes* compared to the PLAF control are shown in **Fig. 6**. *L. monocytogenes* growth expressed as CFU/cm^2 is displayed in **Table S1** (Supplementary material). Total attachment inhibition of *L. monocytogenes* occurred after 24 h on PLA-5%C30B/EU-PHE, PLAF-5%C30B/EU, PLAF-10%C30B/EU, PLAF-EU/PHE, and PLAF-EU with zero attached cells (**Fig. 6a)**.

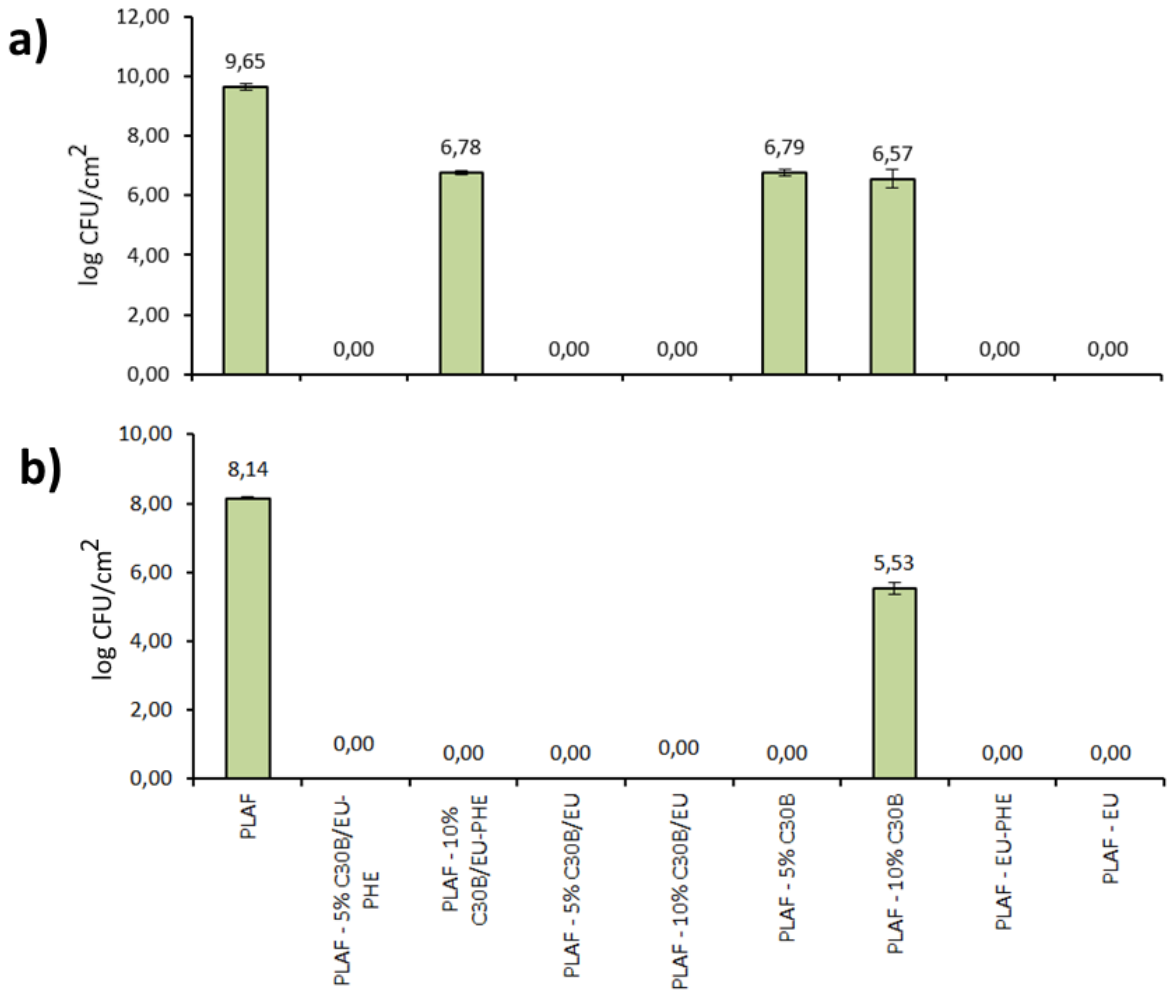

Fig. 6. Inhibition of adhesion of *L. monocytogenes* on PLAF nanocomposite foams after a) 24 h and b) 48 h of incubation in TSB with 1 % glucose. Legend: The results were expressed as log CFU/cm^2 of attached cells.

The tested strain, after 24 h, successfully attached to the PLAF control surface with a total number of 9.65±0.13 log CFU/cm^2, and to the PLA nanocomposite foams surfaces (PLAF-5%C30B and PLAF-10%C30B) in a number of 6.79±0.12 log CFU/cm^2 and 6.50±0.30 log CFU/cm^2, respectively. Regardless of the successful attachment to PLAF-5%C30B and PLAF-10%C30B, the significant logarithmic reduction between 2.87 – 3.0 log CFU/cm^2 ($p<0,05$) in the number of attached *Listeria* is noticeable in comparison with the

865 control PLAF (**Table S1**). The antibacterial activity of C30B against *L. monocytogenes* has
866 been reported previously for LDPE/C30B films [100] and polyethylene)/thermoplastic
867 starch/C30B films [101], and it has been attributed to the action of the quaternary ammonium
868 cations in the C30B silicate layers. In our study, the detected number of attached *L.*
869 *monocytogenes* of 6.78±0.07 log CFU/cm^2 to PLAF-10%C30B-EU-PHE was similar to log
870 CFU values detected on non-impregnated nanocomposites, PLAF-5%C30B and PLAF-
871 10%C30B (**Fig. 6a**), which indicated that during the first 24 h of incubation, the EU-PHE
872 cocrystal was still not available to exert an additional antibacterial activity against *L.*
873 *monocytogenes*. This result could be explained in terms of the higher retention capacity of
874 the EU cocrystal as the C30B content increases, as evidenced by the release assays using a
875 food simulant.

876 A prolonged incubation period of 48 h provided a complete adhesion inhibition of *L.*
877 *monocytogenes* on the surface of all tested PLAF samples, except the control PLAF and
878 PLAF-10% C30B, where the strain attached in the number of 8.14±0.07 log CFU/cm^2 and
879 5.53±0.16 log CFU/cm^2, respectively (**Fig. 6b**). Particularly, the weaker anti-attachment
880 activity of PLAF-10%C30B, compared with the activity of PLAF-5%C30B, could be
881 associated with the thermal degradation of its quaternary ammonium modifiers during the
882 extrusion process [100]. This degradation phenomenon was evidenced by XRD only for the
883 PLA nanocomposite foam sample with C30B at 10% and not for the nanocomposite foam
884 with C30B at 5%.

885

886 The log CFU/cm^2 reduction values obtained in the anti-attachment assay of *S.*
887 Enteritidis compared to the PLAF control are shown in **Figure 7**. *S.* Enteritidis growth
888 expressed as CFU/cm^2 is shown in **Table S2**.
889

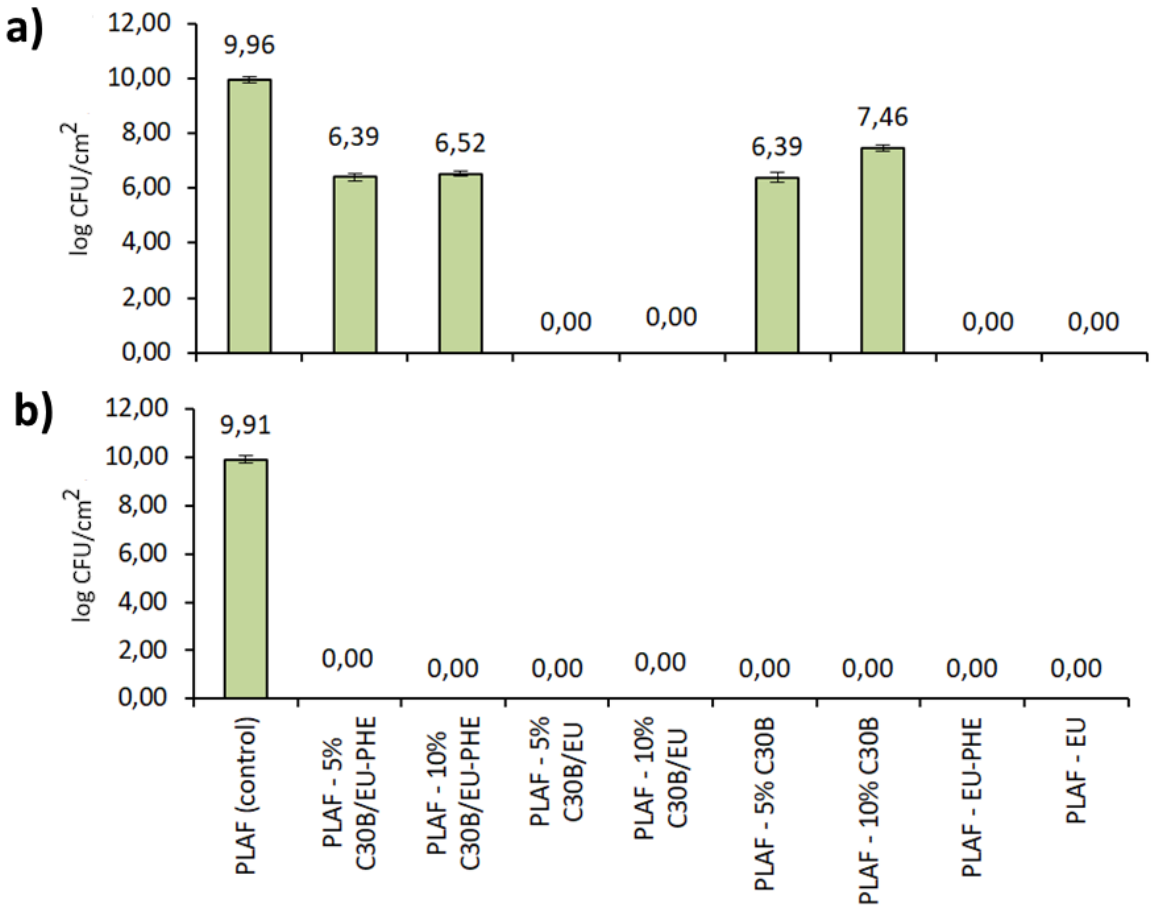

890

891 **Fig. 7.** Inhibition of adhesion of *S.* Enteritidis on PLAF nanocomposite foams after a) 24 h
892 and b) 48 h of incubation in TSB with 1% glucose. Legend: The results are expressed as log
893 CFU/cm^2 of attached cells.
894

After 24 h of incubation, total adhesion inhibition of *S.* Enteritidis occurred on PLAF-5%C30B/EU, PLAF-10%C30B/EU, PLAF-EU-PHE, and PLAF-EU, (>9,0 log CFU reduction compared to PLAF control, $p<0.05$) (**Table 2S**). *S.* Enteritidis showed stronger resistance to contact inhibition compared to *L. monocytogenes* and after 24 hours it successfully attached to the PLAF control and to the PLA nanocomposite foams impregnated with the EU-PHE cocrystal (PLAF-5%C30B/EU-PHE and PLAF-10%30B/EU-PHE) in a total number of 9.96 ±0.10 log CFU/cm^2, 6.39±0.15 log CFU/cm^2, 6.52±0.10 log CFU/cm^2, respectively (**Fig. 7a**). These results could be related, to the higher MIC values of the EU-PHE cocrystal compared with the pure EU. Also, C30B retains the cocrystal in the PLAF structure better than PLAF without C30B. This was evidenced from the release assays using a food simulant (part 3.6) through the 3-fold increase for the cocrystal distribution coefficient due to the presence of 10%C30B compared with the cocrystal distribution coefficient for the PLAF without C30B. As expected, *S.* Enteritidis successfully attached to PLAF-5%C30B and PLAF-10%C30B, in a total number of 6.39±0.18 log CFU/cm^2, 7.46±0.11 log CFU/cm^2, respectively. Despite the successful attachment, both nanocomposite PLA foams significantly reduced the total number of attached cells compared to the PLAF control (log CFU/cm^2 reduction 2.49 -3.45, $p<0.05$) (**Table 2S**).

After 48 hours of incubation, all impregnated PLAF films exhibited a complete adhesion inhibition effect on *S.* Enteritidis, with zero cells detected on the surface of the films, which is a 100% reduction compared to the PLAF control ($p<0.05$) (**Fig. 7b**). These results show that C30B did not reduce the antimicrobial potential of the EU-PHE cocrystal but slowed down its manifestation. PLAF with C30B alone (without impregnated EU or EU-PHE cocrystal) also exhibited antimicrobial activity against *S.* Enteritidis due to the release of quaternary ammonium cations from C30B silicate layers.

Regarding the determination of killing effect (KE), bacterial growth control ($A_{control}$), and culture with PLAF non-impregnated polymer ($A_{control\ PLAF}$) had very similar OD values (statistically and microbiologically, the differences were insignificant), which was expected for PLAF to be microbiologically inert. Therefore, due to the easier and clearer presentation of the results, in **Table 6** and **Table 7**, results are presented as % of the growth of *Listeria* and *Salmonella*, respectively, in the broth with impregnated foams compared to their growth with the control PLAF which was taken as a 100% growth.

Table 6
Killing effect [KE%] during 96 h incubation of *Listeria monocytogenes.*

Sample	KE [%]			
	After 24h	After 48h	After 72h	After 96h
PLAF - 5% C30B/EU-PHE	99.24 ± 0.06	48.71 ± 0.30	103.70 ± 0.45	95.34 ± 0.46
PLAF - 10% C30B/EU-PHE	98.88 ± 0.06	65.44 ± 1.23	81.91. ± 0.31	80.31 ± 0.01
PLAF - 5% C30B/EU	95.42 ± 0.05	108.73 ± 0.53	78.85 ± 0.28	95.91 ± 0.35
PLAF - 10% C30B/EU	95.79 ± 0.11	64.71 ± 0.36	87.45 ± 0.49	78.28 ± 0.04
PLAF - 5% C30B	99.97 ± 0.06	83.90 ± 0.07	102.74 ± 0.49	111.81 ± 0.01
PLAF - 10% C30B	99.34 ± 0.15	109.39 ± 0.01	100.09 ± 0.27	71.84 ± 0.05
PLAF - EU-PHE	99.41 ± 0.10	85.40 ± 0.44	96.83 ± 0.30	69.31 ± 0.21
PLAF - EU	95.82 ± 0.05	95.48 ± 0.53	93.42 ± 0.18	50.12 ± 0.03
PLAF	100.00 ± 0.00	100.00 ± 0.00	100.00 ± 0.00	100.00 ± 0.00

Legend: Percentage of bacterial growth in the presence of impregnated PLAF films compared to the PLAF control, which was taken as 100% growth.

The broth killing effect results, which were directly proportional to the release of the active substances into the environment, indicated that the release of the antimicrobial substances from all the foams needed to be triggered by the previous soaking of the PLA foams in a liquid medium for approximately 24 h. This result is very relevant for antibacterial food packaging because the antibacterial substances need to be released to the food only when it is necessary, i.e., once the food is packaged and not before, by means of a trigger

937 mechanism for the release of the antimicrobial substances, such as the water vapor emitted
938 from some foods, such as fruits and vegetables, to the package headspace [92,102,103].
939 After 48 h of contact, all active PLA foams, except PLAF-10%C30B and PLAF-
940 5%C30B-EU, showed antibacterial activity against *L. monocytogenes*, reducing the growth
941 between 4.52% and 51.29%. Particularly, PLAF impregnated with EU manifested only
942 4.52% growth reduction of *L. monocytogenes*, which could be related to the low solubility of
943 EU in an aqueous medium. The growth reduction of *L. monocytogenes* slightly increased to
944 6.58% after 72 h and 49.88% after 96 h
945 A significantly higher growth reduction of *L. monocytogenes* was obtained for the
946 PLAF impregnated with the EU-PHE cocrystal (14.6%) after 48 h. This result is very
947 interesting, considering that phenazine (the other component of the cocrystal) itself didn't
948 exert strong antibacterial activity against *L. monocytogenes.* Moreover, the initial amount of
949 EU-PHE cocrystal in PLAF-EU-PHE (8.62% w/w) was lower than the initial content of EU
950 in PLAF-EU (21% w/w), which implied a lower active compound concentration gradient for
951 the release of the cocrystal compared with EU. Considering both facts, the notable increase
952 in the capacity of EU to inhibit the growth of *L. monocytogenes* could be related to the
953 synergistic antibacterial activity between EU and PHE in the broth culture and to the
954 improvement of the EU solubility in the aqueous medium due to its cocrystallization.
955 Different solutes have been found to become more soluble in aqueous media thanks to their
956 cocrystallization [89,104,105].
957 Probably the highest solubility of EU in its cocrystallized form allowed the PLAF-
958 EU-PHE sample to reach the maximal growth reduction of *L. monocytogenes* (30.69%) after
959 96 h, not so far from the growth reduction reached by PLAF-EU (49.88%), even considering
960 the notable differences in the initial amount of EU between PLAF-EU (21% w/w) and PLAF-

EU-PHE (4.14 % w/w). This is a relevant result because the design of antibacterial food packaging materials should consider the use of minimal amounts of essential oil derivatives to exert the desired antibacterial effect on food with minimal impact on the physical properties of the plastic films [106,107] and the organoleptic properties and food quality [88,108].

Interestingly, after 48 h, both nanocomposite PLAF samples impregnated with the EU-PHE cocrystal, PLAF-5%C30B-EU-PHE, and PLAF-10%C30B-EU-PHE, showed stronger *L. monocytogenes* growth reduction values (51.29% and 34.56%, respectively) comparing to the sum of the individual growth reduction rates obtained for PLAF-5%C30B (16.1%), PLAF-10%C30B (0%) and PLAF-EU-PHE (14.6%), indicating that C30B and EU-PHE had synergistic antibacterial activity against *L. monocytogenes*. Particularly, the lower inhibition growth of PLAF-10%C30B-EU-PHE compared with the activity of PLAF-5%C30B-EU-PHE, which agrees with the attachment inhibition assay results for *L. monocytogenes* obtained using both samples, could be associated with the decrease of the C30B antibacterial activity due to partial thermal degradation of its quaternary ammonium modifiers during the extrusion process and to the lower amount of EU-PHE cocrystal released from the PLAF sample with the highest C30B content after 48 h. Considering that both nanocomposite foams presented a similar initial amount of EU-PHE cocrystal, the lower release of the cocrystal from PLAF-10%C30B could be related to the increase in the cocrystal retention capacity of PLAF as C30B content increased, which even allowed the PLAF-10%C30B-EU-PHE sample to supply cocrystal to the broth culture after 96 h in a controlled manner to exert an approximately 20% growth reduction of *L. monocytogenes*. Meanwhile, PLAF-5%C30B-EU-PHE loses completely its antibacterial properties against *L. monocytogenes* between 48 h and 72 h due to its lower EU-PHE cocrystal retention capacity.

The high EU-PHE retention capacity for the nanocomposite PLAF with the highest C30B content was evidenced from the release assays using a food simulant (part 3.5) through the 1.34-fold increase in the cocrystal distribution coefficient by the increase in C30B content from 5% to 10%.

Table 7
Killing effect [KE%] during 96h incubation of ***Salmonella*** **Enteritidis.**

Samples	KE [%]			
	After 24h	After 48h	After 72h	After 96h
PLAF - 5% C30B/EU-PHE	97.98 ± 0.13	68.91 ± 1.52	94.11 ± 0.80	94.80 ± 0.02
PLAF - 10% C30B/EU-PHE	92.07 ± 0.04	84.40 ± 2.14	96.27 ± 0.31	90.49 ± 0.04
PLAF - 5% C30B/EU	59.52 ± 0.08	49.41 ± 1.30	83.99 ± 0.28	90.13 ± 0.06
PLAF - 10% C30B/EU	67.95 ± 0.06	54.56 ± 1.18	56.76 ± 0.41	68.87 ± 0.17
PLAF - 5% C30B	99.42 ± 0.08	38.36 ± 0.92	100.66 ± 0.76	99.16 ± 0.42
PLAF - 10% C30B	101.58 ± 0.14	62.71 ± 1.45	102.07 ± 0.47	101.04 ± 0.04
PLAF - EU-PHE	91.02 ± 0.08	20.59 ± 0.46	92.49 ± 0.52	94.89 ± 0.00
PLAF - EU	77.35 ± 0.05	19.45 ± 0.46	82.67 ± 0.51	88.04 ± 0.04
PLAF	100.00 ± 0.00	100.00 ± 0.00	100.00 ± 0.00	100.00 ± 0.00

Legend: Percentage of bacterial growth in the presence of experimental, impregnated PLAF films compared to the PLAF control, which was taken as 100% growth.

Table 7 shows that the samples impregnated with EU were more effective than EU-PHE cocrystal-impregnated samples to inhibit the growth of *S.* Enteritidis. In the first 24 h. PLAF-5%C30B/EU. PLAF-10%C30B/EU and PLAF-EU showed a relatively strong killing effect, reducing the growth of *S.* Enteritidis by approximately 40%, 30%, and 25%, respectively. Meanwhile. in the first 24 h. the nanocomposite PLAF samples (PLAF-5%C30B and PLAF-10%C30B) did not reduce the growth of *S.* Enteritidis.

All polymers strongly reduced the growth of *Salmonella* after 48h, of which PLAF-EU and PLAF-EU-PHE were particularly strong, reducing growth by 80%, while PLAF-5%C30B. PLAF-5%C30B/EU and PLAF-10%C30B/EU were also relatively strong with a

reduction in growth of approximately 45-60%. Particularly, the weaker growth inhibition of *Salmonella* using PLAF with C30B could be the effect of increasing the retaining EU and EU-PHE capacity with the simultaneous increase in C30B content, which reduced the release of both substances into the broth culture. This was also evidenced by the release assays using a food simulant (part 3.6). Unlike in antibacterial assays against *L. monocytogenes*, where several foams showed the strongest killing effect after 96 h, only PLAF-10%C30B/EU retained the killing effect against *Salmonella* Enteritidis in the 96th hour (with approximately 30% growth reduction) due to more prolonged release of EU from this sample.

3.8. Relevance of the obtained results and future prospective

3.8.1. Relevance for the food industry

Unlike most infectious diseases that have been eradicated or suppressed significantly in the last few decades, *salmonellosis* and *listeriosis* are continuously present in all countries, regardless of the region's geographical, cultural, and climate characteristics [109,110]. In recent decades, parallel to the development of molecular research methods, there is more and more evidence that certain *L. monocytogenes* strains and *Salmonella* serovars can persist for months and even years in food production facilities. Equipment and all kinds of surfaces made of plastic, stainless steel, wood, glass, and gum may be a substrate for successful surface adherence of *S.* Enteritidis and *L. monocytogenes* and for the development of biofilms that become a source of repeated contamination of final food products [111]. According to data from the *European Food Safety Authority* (EFSA), in 2019, there were 87,923 cases of *salmonellosis* recorded in the territory of European countries, the source of which was food [112]. The incidence of *listeriosis* is significantly lower and amounted to 0.46 and 0.24 cases per 100,000 population in 2015 in the European Union and the United States, respectively

[111]. Despite the reduced incidence during the last decade, cases of *salmonellosis* and *listeriosis* are still relatively frequent, leading to a certain number of deaths and high economic costs for hospitalized affected consumers [113]. There is also the perspective of the significant economic losses of the food industry, which, after the outbreaks of *salmonellosis* or *listeriosis,* is obliged to withdraw from the sale and destroy all contaminated products or to stop production completely.

Based on the obtained results, in theory, materials developed in this study that showed the strongest antimicrobial activity and significantly reduced the total number of *Salmonella* and *Listeria* (such as PLAF-EU-PHE, which reduced the total number of *Salmonella* by approximately 80%) would significantly reduce the incidence of *salmonellosis* and *listeriosis* if applied on the industrial level. Besides the envisaged application to substitute PS trays, we should not rule out the possible use of obtained materials for packaging food for animals, especially for intensively breeding animals on farms. The animal food can also be contaminated with *Salmonella* and lead to outbreaks of diseases in farms with substantial economic consequences. We should not forget that the initial number of microorganisms in our study was very high, 10^8 CFU/mL. In comparison, the number of *Salmonella* and *Listeria* in contaminated food can be significantly lower (10^3 CFU/mL, 10^2 CFU/mL, or even smaller). Therefore, the actual effect of the *in situ* PLAF material in which the contaminated food is packed could be increased to 100%.

From the microbiological point of view, a new question arose. Is it possible to design an active food packaging aimed at protection from a target bacterial strain? We reported obviously different (individual) degrees of sensitivity of *Salmonella* and *Listeria* to the same material designed in this study. Therefore, a new hypothesis was developed that designing

specialized active packaging with the maximal antimicrobial activity against *Listeria* or *Salmonella* was possible.

3.8.2. Relevance for the pharmaceutical industry

The crystallization to obtain the smallest possible crystals of active pharmaceutical ingredients (API) with improved bioavailability is very important for the pharmaceutical industry. Consequently, micronization techniques have been developed applying $scCO_2$ as a green solvent or antisolvent [114]. As mentioned in the introduction, cocrystallization has gained tremendous importance in the pharmaceutical industry because of its ability to fine-tune the physicochemical properties of crystalline drugs without modifying their molecular structure [115]. There are reports and efforts to establish API cocrystallization from the $scCO_2$ phase [116,117]. The proposed process (CSS - cocrystallization from supercritical solution) is based on the dissolution of pure API and conformer in $scCO_2$ and their posterior cocrystallization from the supercritical phase during the cooling and decompression. However, the main limitation of this process is the necessity of similar solubilities of the API and conformer in $scCO_2$ [117]. In this study, we demonstrated a possibility to overcome this limitation. We produced micronized EU-PHE cocrystals (average diameter of 0.8 μm) in an environmentally friendly manner without organic solvents, though EU and PHE have significantly different solubilities in $scCO_2$ (0.037 and 0.00109 g/g_{scCO2}, respectively). We introduced the re-cocrystallization (or cocrystal recrystallization) based on the dissolution of previously formed large cocrystals in $scCO_2$ (average diameter of 25 μm) with the subsequent micronization from the supercritical phase. The prerequisites for this process are cocrystal stability (*e.g.*, no liquid EU separation from the cocrystal when exposed to $scCO_2$) and good solubility in $scCO_2$. To our knowledge, this study is the first report on re-cocrystallization

from the $scCO_2$. Therefore, the obtained results are relevant for the pharmaceutical industry as well.

4. Conclusions

The EU-PHE cocrystal was produced by a simple mechanical method. The cocrystal was stable in $scCO_2$ under the conditions of interest, with the solubility in $scCO_2$ approximately ten times larger than the cofomer's solubility (PHE). Nanocomposite PLA films with 0, 5, and 10 % w/w of nanoclay were produced by extrusion. In the next step, the films were foamed by $scCO_2$. The foams were successfully impregnated with EU (impregnation yields from 20 to 22 % w/w) and EU-PHE cocrystal (impregnation yields from 8.62 to 9.25 % w/w) via SSI. The presence of C30B and cocrystal improved the mechanical properties of PLA foams. The SEM, DCS, TGA, and XRD analyses confirmed the EU-PHE cocrystal re-crystallization within the PLA foams. Consequently, the foams impregnated with PHE-EU cocrystal had significantly slower release kinetics of the active compound than EU-impregnated ones. The impregnated foams completely inhibited the attachment of *Listeria monocytogenes* and *Salmonella* Enteritidis strains. PLAF-EU-PHE sample reduced the total number of *Salmonella* in broth by approximately 80% after 48 h. PLAF - 5% C30B/EU-PHE and PLAF-10% C30B/EU-PHE foams showed the strongest reduction of *Listeria monocytogenes* in 48 h. The release and microbiological assays showed that PLAF-C30B/EU-PHE polymeric foams had prolonged EU release and extended bioactivity.

This study proposes a green approach to designing antimicrobial food packaging materials based on the coupling of the concepts of supercritical fluid technology and cocrystallization engineering. The successful EU-PHE cocrystal micronization by $scCO_2$ is of interest to materials engineering and pharmaceutical technology.

CRediT authorship contribution statement

Adrián Rojas: Conceptualization. Methodology. Formal analysis. Supervision. Writing original draft. Writing– review & editing. Project administration. Funding acquisition. **Dusan Misic:** Methodology. Investigation. Formal analysis. Writing original draft. Writing– review & editing. **Irena Zizovic**: Methodology. Investigation. Writing original draft. Writing– review & editing. **Carol López de Dicastillo:** Formal analysis. Writing original draft. Writing– review. **Aleksandra Rajewska:** Methodology. Investigation. Formal analysis. **Eliezer Velásquez:** Formal analysis. Writing original draft. Writing– review & editing. **Bastián Rozas:** Investigation. Formal analysis. **Luciano Catalán:** Investigation. Formal analysis. **Cristian Vidal Patiño:** Writing original draft.. **Abel Guarda:** Supervision. Resources. **María José Galotto:** Supervision. Resources. Project administration. Funding acquisition.

Declaration of Competing Interest

The authors declare that they have no known competing financial interests or personal relationships that could have appeared to influence the work reported in this paper.

Acknowledgment

M.J. Galotto and A. Rojas thank the support of Agencia Nacional de Investigación y Desarrollo through the Fondecyt regular Project N°1201301 and to the "Programa de Financiamiento Basal para Centros Científicos y Tecnológicos de Excelencia" (Project AFB220001). A. Rojas thanks the support of the University of Santiago de Chile through the Postdoctoral Fellowship DICYT Código 082371GL_Postdoc. C. López de Dicastillo acknowledges the "Ramon y Cajal" Fellowship RYC2020-029874-I/AEI/10.13039/501100011033 financed by the Spanish Ministry of Science and Innovation. D. Misic and I. Zizovic thank the support of Narodowe Centrum Nauki. (Poland), Grant number 2019/35/B/NZ9/02774.

References

[1] B. Malhotra, A. Keshwani, H. Kharkwal, Antimicrobial food packaging: Potential and pitfalls, Front Microbiol. 6 (2015) 1–9. https://doi.org/10.3389/fmicb.2015.00611.

[2] X. Chen, M. Chen, C. Xu, K.L. Yam, Critical review of controlled release packaging to improve food safety and quality, Crit Rev Food Sci Nutr. 59 (2019) 2386–2399. https://doi.org/10.1080/10408398.2018.1453778.

[3] L. Kuai, F. Liu, B. Sen Chiou, R.J. Avena-Bustillos, T.H. McHugh, F. Zhong, Controlled release of antioxidants from active food packaging: A review, Food Hydrocoll. 120 (2021) 106992. https://doi.org/10.1016/J.FOODHYD.2021.106992.

[4] A. Rojas, A. Torres, A. Añazco, C. Villegas, M.J. Galotto, A. Guarda, J. Romero, Effect of pressure and time on scCO<inf>2</inf>-assisted incorporation of thymol into LDPE-based nanocomposites for active food packaging, Journal of CO2 Utilization. 26 (2018) 434–444. https://doi.org/10.1016/j.jcou.2018.05.031.

[5] A. Rojas, A. Torres, F. Martínez, L. Salazar, C. Villegas, M.J. Galotto, A. Guarda, J. Romero, Assessment of kinetic release of thymol from LDPE nanocomposites obtained by supercritical impregnation: Effect of depressurization rate and nanoclay content, Eur Polym J. 93 (2017). https://doi.org/10.1016/j.eurpolymj.2017.05.049.

[6] N. Alvarado, J. Romero, A. Torres, C. López de Dicastillo, A. Rojas, M.J. Galotto, A. Guarda, Supercritical impregnation of thymol in poly(lactic acid) filled with electrospun poly(vinyl alcohol)-cellulose nanocrystals nanofibers: Development an active food packaging material, J Food Eng. 217 (2018). https://doi.org/10.1016/j.jfoodeng.2017.08.008.

[7] M.S. Razavi, A. Golmohammadi, A. Nematollahzadeh, C. Rovera, S. Farris, Cinnamon Essential Oil Encapsulated into a Fish Gelatin-Bacterial Cellulose Nanocrystals Complex and Active Films Thereof, Food Biophys. 17 (2022) 38–46. https://doi.org/10.1007/s11483-021-09696-6.

[8] M. Li, F. Zhang, Z. Liu, X. Guo, Q. Wu, L. Qiao, Controlled Release System by Active Gelatin Film Incorporated with β-Cyclodextrin-Thymol Inclusion Complexes, Food Bioproc Tech. 11 (2018) 1695–1702. https://doi.org/10.1007/s11947-018-2134-1.

[9] A. Adjali, A.R.N. Pontillo, E. Kavetsou, A. Katopodi, A. Tzani, S. Grigorakis, S. Loupassaki, A. Detsi, Clove Essential Oil–Hydroxypropyl-β-Cyclodextrin Inclusion Complexes: Preparation, Characterization and Incorporation in Biodegradable Chitosan Films, Micro. 2 (2022) 212–224. https://doi.org/10.3390/micro2010014.

[10] M. Krepker, C. Zhang, N. Nitzan, O. Prinz-Setter, N. Massad-Ivanir, A. Olah, E. Baer, E. Segal, Antimicrobial LDPE/EVOH layered films containing carvacrol fabricated by multiplication extrusion, Polymers (Basel). 10 (2018) 3–4. https://doi.org/10.3390/polym10080864.

[11] W. Zhang, C. Shu, Q. Chen, J. Cao, W. Jiang, The multi-layer film system improved the release and retention properties of cinnamon essential oil and its application as coating in inhibition to penicillium expansion of apple fruit, Food Chem. 299 (2019) 125109. https://doi.org/10.1016/J.FOODCHEM.2019.125109.

[12] G. Mensitieri, Supercritical fluids, Supercritical Fluid Science and Technology. 9 (2021) 55–68. https://doi.org/10.1016/B978-0-444-63724-6.00004-4.
[13] Ž. Knez, M. Škerget, M. Knez Hrnčič, D. Čuček, Chapter 2 - Particle Formation Using Sub- and Supercritical Fluids, in: V. Anikeev, M.B.T.-S.F.T. for E. and E.A. Fan (Eds.), Elsevier, Boston, 2014: pp. 31–67. https://doi.org/https://doi.org/10.1016/B978-0-444-62696-7.00002-2.
[14] E. Weidner, Impregnation via supercritical CO2–What we know and what we need to know, J Supercrit Fluids. 134 (2018) 220–227. https://doi.org/10.1016/J.SUPFLU.2017.12.024.
[15] G.A. Sutil, K.S. Andrade, E.A. Rebelatto, M. Lanza, Effects of incorporation of pure or multicomponent active agents in biopolymers for food packaging using supercritical CO2, Trends Food Sci Technol. 120 (2022) 349–362. https://doi.org/10.1016/J.TIFS.2022.01.025.
[16] N.D. Machado, J.E. Mosquera, R.E. Martini, M.L. Goñi, N.A. Gañán, Supercritical CO2-assisted impregnation/deposition of polymeric materials with pharmaceutical, nutraceutical, and biomedical applications: A review (2015–2021), J Supercrit Fluids. 191 (2022) 105763. https://doi.org/10.1016/J.SUPFLU.2022.105763.
[17] A. Rojas, A. Torres, M.J. Galotto, A. Guarda, R. Julio, Supercritical impregnation for food applications: a review of the effect of the operational variables on the active compound loading, Crit Rev Food Sci Nutr. 60 (2020) 1290–1301. https://doi.org/10.1080/10408398.2019.1567459.
[18] M. Champeau, J.M. Thomassin, T. Tassaing, C. Jérôme, Drug loading of polymer implants by supercritical CO2 assisted impregnation: A review, Journal of Controlled Release. 209 (2015) 248–259. https://doi.org/10.1016/J.JCONREL.2015.05.002.
[19] A. Rojas, A. Torres, C.L. de Dicastillo, E. Velásquez, C. Villegas, S. Faba, P. Rivera, A. Guarda, J. Romero, M.J. Galotto, Foaming with scCO2 and Impregnation with Cinnamaldehyde of PLA Nanocomposites for Food Packaging, Processes. 10 (2022). https://doi.org/10.3390/pr10020376.
[20] A. Satpayeva, A. Rojas, M. Tyrka, E. Ksepko, M.J. Galotto, I. Zizovic, Supercritical Foaming and Impregnation of Polycaprolactone and Polycaprolactone-Hydroxyapatite Composites with Carvacrol, Processes. 10 (2022) 482. https://doi.org/10.3390/pr10030482.
[21] S. Milovanovic, D. Markovic, A. Mrakovic, R. Kuska, I. Zizovic, S. Frerich, J. Ivanovic, Supercritical CO 2 - assisted production of PLA and PLGA foams for controlled thymol release, Materials Science and Engineering C. 99 (2019) 394–404. https://doi.org/10.1016/j.msec.2019.01.106.
[22] M. Guo, X. Sun, J. Chen, T. Cai, Pharmaceutical cocrystals: A review of preparations, physicochemical properties and applications, Acta Pharm Sin B. 11 (2021) 2537–2564. https://doi.org/10.1016/J.APSB.2021.03.030.
[23] J.L. Dias, M. Lanza, S.R.S. Ferreira, Cocrystallization: A tool to modulate physicochemical and biological properties of food-relevant polyphenols, Trends Food Sci Technol. 110 (2021) 13–27. https://doi.org/10.1016/J.TIFS.2021.01.035.

[24] H. Zu, R.F. Henry, G.G.Z. Zhang, L.R. MacGillivray, Inhibiting Sublimation of Thymol by Cocrystallization, J Pharm Sci. 112 (2023) 350–353. https://doi.org/10.1016/J.XPHS.2022.10.019.
[25] P.P. Mazzeo, C. Carraro, A. Monica, D. Capucci, P. Pelagatti, F. Bianchi, S. Agazzi, M. Careri, A. Raio, M. Carta, F. Menicucci, M. Belli, M. Michelozzi, A. Bacchi, Designing a Palette of Cocrystals Based on Essential Oil Constituents for Agricultural Applications, ACS Sustain Chem Eng. 7 (2019) 17929–17940. https://doi.org/10.1021/acssuschemeng.9b04576.
[26] F. Bianchi, F. Fornari, N. Riboni, C. Spadini, C.S. Cabassi, M. Iannarelli, C. Carraro, P.P. Mazzeo, A. Bacchi, S. Orlandini, S. Furlanetto, M. Careri, Development of novel cocrystal-based active food packaging by a Quality by Design approach, Food Chem. 347 (2021) 129051. https://doi.org/10.1016/J.FOODCHEM.2021.129051.
[27] H. Services, 54960 Federal Register / Vol . 81 , No . 159 / Wednesday , August 17 , 2016 / Rules and Regulations AGENCY : ACTION :, 81 (2016) 54960–55055.
[28] E. Orlo, C. Nerín, M. Lavorgna, M. Wrona, C. Russo, M. Stanzione, R. Nugnes, M. Isidori, Antioxidant activity of coatings containing eugenol for flexible aluminium foils to preserve food shelf-life, Food Packag Shelf Life. 39 (2023) 101145. https://doi.org/10.1016/J.FPSL.2023.101145.
[29] M.T. Yilmaz, W.S. Hassanein, A.S. Alkabaa, Z. Ceylan, Electrospun eugenol-loaded gelatin nanofibers as bioactive packaging materials to preserve quality characteristics of beef, Food Packag Shelf Life. 34 (2022) 100968. https://doi.org/10.1016/J.FPSL.2022.100968.
[30] J. Cheng, H. Wang, S. Kang, L. Xia, S. Jiang, M. Chen, S. Jiang, An active packaging film based on yam starch with eugenol and its application for pork preservation, Food Hydrocoll. 96 (2019) 546–554. https://doi.org/10.1016/J.FOODHYD.2019.06.007.
[31] L. Lin, C. Mei, C. Shi, C. Li, M.A. Abdel-Samie, H. Cui, Preparation and characterization of gelatin active packaging film loaded with eugenol nanoparticles and its application in chicken preservation, Food Biosci. 53 (2023) 102778. https://doi.org/10.1016/J.FBIO.2023.102778.
[32] R. Scaffaro, A. Maio, F.E. Gulino, C. Di Salvo, A. Arcarisi, Bilayer biodegradable films prepared by co-extrusion film blowing: Mechanical performance, release kinetics of an antimicrobial agent and hydrolytic degradation, Compos Part A Appl Sci Manuf. 132 (2020) 105836. https://doi.org/10.1016/J.COMPOSITESA.2020.105836.
[33] R. Scaffaro, E.F. Gulino, M.C. Citarrella, A. Maio, Green Composites Based on Hedysarum coronarium with Outstanding FDM Printability and Mechanical Performance, Polymers (Basel). 14 (2022) 1198. https://doi.org/10.3390/polym14061198.
[34] R. Scaffaro, L. Settanni, E.F. Gulino, Release Profiles of Carvacrol or Chlorhexidine of PLA/Graphene Nanoplatelets Membranes Prepared Using Electrospinning and Solution Blow Spinning: A Comparative Study, Molecules. 28 (2023) 1967. https://doi.org/10.3390/molecules28041967.
[35] T.A. Swetha, A. Bora, K. Mohanrasu, P. Balaji, R. Raja, K. Ponnuchamy, G. Muthusamy, A. Arun, A comprehensive review on polylactic acid (PLA) – Synthesis,

processing and application in food packaging, Int J Biol Macromol. 234 (2023) 123715. https://doi.org/10.1016/J.IJBIOMAC.2023.123715.
[36] Goodao ©, PLA Trays and Containers, (2017) 1. https://www.gl-bz.com/new-environmentally-friendly-pla-material-biodegradable-trays-and-containers-for-packing-fruit-meat-food-product/.
[37] S. Punia Bangar, W.S. Whiteside, V. Chaudhary, P. Parambil Akhila, K.V. Sunooj, Recent functionality developments in Montmorillonite as a nanofiller in food packaging, Trends Food Sci Technol. 140 (2023) 104148. https://doi.org/10.1016/J.TIFS.2023.104148.
[38] D. Cheikh, H. Majdoub, M. Darder, An overview of clay-polymer nanocomposites containing bioactive compounds for food packaging applications, Appl Clay Sci. 216 (2022) 106335. https://doi.org/10.1016/J.CLAY.2021.106335.
[39] L.R. Beuchat, Listeria monocytogenes: incidence on vegetables, Food Control. 7 (1996) 223–228. https://doi.org/10.1016/S0956-7135(96)00039-4.
[40] F.M. Sánchez-Vargas, M.A. Abu-El-Haija, O.G. Gómez-Duarte, Salmonella infections: An update on epidemiology, management, and prevention, Travel Med Infect Dis. 9 (2011) 263–277. https://doi.org/10.1016/J.TMAID.2011.11.001.
[41] J.E. Mosquera, M.L. Goñi, R.E. Martini, N.A. Gañán, Mass transfer kinetics of CO2 and eugenol in the supercritical impregnation of polyamide fibers: Experimental data and modeling, J Supercrit Fluids. 166 (2020) 105030. https://doi.org/10.1016/J.SUPFLU.2020.105030.
[42] J.E. Mosquera, M.L. Goñi, R.E. Martini, N.A. Gañán, Supercritical carbon dioxide assisted impregnation of eugenol into polyamide fibers for application as a dental floss, Journal of CO2 Utilization. 32 (2019) 259–268. https://doi.org/10.1016/J.JCOU.2019.04.016.
[43] A. Ubeyitogullari, O.N. Ciftci, Generating phytosterol nanoparticles in nanoporous bioaerogels via supercritical carbon dioxide impregnation: Effect of impregnation conditions, J Food Eng. 207 (2017) 99–107. https://doi.org/10.1016/j.jfoodeng.2017.03.022.
[44] A. Ubeyitogullari, O.N. Ciftci, Phytosterol nanoparticles with reduced crystallinity generated using nanoporous starch aerogels, RSC Adv. 6 (2016) 108319–108327. https://doi.org/10.1039/c6ra20675a.
[45] F. Muratore, M.L. Goñi, M.C. Strumia, S.E. Barbosa, N.A. Gañan, R.E. Martini, Eugenol As An Active Component In Food Packaging Materials, Eugenol: Biosynthesis, Toxicity and Uses. (2019) 1–48.
[46] S. Milovanovic, M. Stamenic, D. Markovic, M. Radetic, I. Zizovic, Solubility of thymol in supercritical carbon dioxide and its impregnation on cotton gauze, J Supercrit Fluids. 84 (2013) 173–181. https://doi.org/10.1016/J.SUPFLU.2013.10.003.
[47] José Aniceto, Supercritical carbon dioxide density and viscosity calculation, (2023). https://www.egichem.com/tools/calculators/carbon-dioxide/.
[48] C. Simoneau, Guidelines on testing conditions for articles in contact with foodstuffs (with a focus on kitchenware) - EUR 23814 EN 2009, 2015.
[49] CLSI, Clinical and Laboratory Standards Institute Methods for Dilution Antimicrobial Susceptibility Tests for Bacteria That Grow Aerobically Standard,, Approval CDM-A.;,

M07 Methods for Dilution Antimicrobial Susceptibility Tests for Bacteria That Grow Aerobically. (2018) 91.
[50] G. Donelli, Microbial Biofilms Methods and Protocols, 2014. https://doi.org/10.1007/978-1-4939-0467-9_3.
[51] ISO:7218, Microbiology of food and animal feeding stuffs — General requirements and guidance for microbiological examinations, Iso. 2013 (2013). www.iso.org.
[52] M. Tyrka, M. Nowak, D. Misic, T. Półbrat, S. Koter, A. Trusek, I. Zizovic, Cellulose Acetate Membranes Modification by Aminosilane Grafting in Supercritical Carbon Dioxide towards Antibiofilm Properties, Membranes (Basel). 12 (2021) 33. https://doi.org/10.3390/membranes12010033.
[53] E. Di Maio, E. Kiran, Foaming of polymers with supercritical fluids and perspectives on the current knowledge gaps and challenges, J Supercrit Fluids. 134 (2018) 157–166. https://doi.org/10.1016/J.SUPFLU.2017.11.013.
[54] B. Li, G. Zhao, G. Wang, L. Zhang, J. Gong, Fabrication of high-expansion microcellular PLA foams based on pre-isothermal cold crystallization and supercritical CO2 foaming, Polym Degrad Stab. 156 (2018) 75–88. https://doi.org/10.1016/J.POLYMDEGRADSTAB.2018.08.009.
[55] P. Xiang, L. Gou, Y. Zou, B. Chen, S. Bi, X. Chen, P. Yu, A facile strategy for preparation of strong tough poly(lactic acid) foam with a unique microfibrillated bimodal micro/nano cellular structure, Int J Biol Macromol. 199 (2022) 264–274. https://doi.org/10.1016/J.IJBIOMAC.2021.12.187.
[56] F.B. Ali, A.S. Azmi, H. Anuar, J. Jamaluddin, Characterization of Polylactic Acid/Organoclay Nanocomposites BT - Advances in Nanotechnology and Its Applications, in: A.T. Jameel, A.Z. Yaser (Eds.), Springer Singapore, Singapore, 2020: pp. 107–114. https://doi.org/10.1007/978-981-15-4742-3_7.
[57] J. Trifol, D. Plackett, C. Sillard, O. Hassager, A.E. Daugaard, J. Bras, P. Szabo, A comparison of partially acetylated nanocellulose, nanocrystalline cellulose, and nanoclay as fillers for high-performance polylactide nanocomposites, J Appl Polym Sci. 133 (2016). https://doi.org/https://doi.org/10.1002/app.43257.
[58] W. Chávez-Montes, G. González-Sánchez, E. López-Martínez, P. de Lira-Gómez, L. Ballinas-Casarrubias, S. Flores-Gallardo, Effect of Artificial Weathering on PLA/Nanocomposite Molecular Weight Distribution, Polymers (Basel). 7 (2015) 760–776. https://doi.org/10.3390/polym7040760.
[59] M. Keshtkar, M. Nofar, C.B. Park, P.J. Carreau, Extruded PLA/clay nanocomposite foams blown with supercritical CO2, Polymer (Guildf). 55 (2014) 4077–4090. https://doi.org/https://doi.org/10.1016/j.polymer.2014.06.059.
[60] N.H. Arsad, N.R. Putra, Z. Idham, N.S.M. Norodin, M.A. Che Yunus, A.H. Abdul Aziz, Solubilization of eugenol from Piper betle leaves to supercritical carbon dioxide: Experimental and modelling, Results in Engineering. 17 (2023) 100914. https://doi.org/10.1016/J.RINENG.2023.100914.
[61] K.W. Cheng, S.J. Kuo, M. Tang, Y.P. Chen, Vapor–liquid equilibria at elevated pressures of binary mixtures of carbon dioxide with methyl salicylate, eugenol, and diethyl phthalate, J Supercrit Fluids. 18 (2000) 87–99. https://doi.org/10.1016/S0896-8446(00)00056-5.

[62] J. G. Van Alsten, C. A. Eckert, Effect of entrainers and of solute size and polarity in supercritical fluid solutions, Journal of Chemical & Engineering Data. 38 (2002) 605–610. https://doi.org/10.1021/je00012a034.
[63] C. Villegas, M.P. Arrieta, A. Rojas, A. Torres, S. Faba, M.J. Toledo, M.A. Gutierrez, E. Zavalla, J. Romero, M.J. Galotto, X. Valenzuela, PLA/organoclay bionanocomposites impregnated with thymol and cinnamaldehyde by supercritical impregnation for active and sustainable food packaging, Compos B Eng. 176 (2019) 107336. https://doi.org/10.1016/j.compositesb.2019.107336.
[64] A. Torres, E. Ilabaca, A. Rojas, F. Rodríguez, M.J. Galotto, A. Guarda, C. Villegas, J. Romero, Effect of processing conditions on the physical, chemical and transport properties of polylactic acid films containing thymol incorporated by supercritical impregnation, Eur Polym J. 89 (2017). https://doi.org/10.1016/j.eurpolymj.2017.01.019.
[65] M.L. Goñi, N. Gañan, V. A., Q. N., A. A., R. Martini, Supercritical carbon dioxide impregnation of LLDPE films with eugenol. Influence of process conditions and film characterization, 2016.
[66] C. Villegas, A. Torres, M. Rios, A. Rojas, J. Romero, C.L. de Dicastillo, X. Valenzuela, M.J. Galotto, A. Guarda, Supercritical impregnation of cinnamaldehyde into polylactic acid as a route to develop antibacterial food packaging materials, Food Research International. 99 (2017) 650–659. https://doi.org/10.1016/j.foodres.2017.06.031.
[67] F. Lopresti, L. Botta, R. Scaffaro, V. Bilello, L. Settanni, R. Gaglio, Antibacterial biopolymeric foams: Structure–property relationship and carvacrol release kinetics, Eur Polym J. 121 (2019) 109298. https://doi.org/https://doi.org/10.1016/j.eurpolymj.2019.109298.
[68] R. Gaglio, L. Botta, G. Garofalo, A. Miceli, L. Settanni, F. Lopresti, Carvacrol activated biopolymeric foam: An effective packaging system to control the development of spoilage and pathogenic bacteria on sliced pumpkin and melon, Food Packag Shelf Life. 28 (2021) 100633. https://doi.org/https://doi.org/10.1016/j.fpsl.2021.100633.
[69] K.W. Cheng, M. Tang, Y.P. Chen, Calculations of solid solubility in supercritical fluids using a simplified cluster solvation model, Fluid Phase Equilib. 214 (2003) 169–186. https://doi.org/10.1016/S0378-3812(03)00350-9.
[70] C.J. Benmore, B.L. Tomberli, The structure of carbon dioxide around naphthalene investigated using H/D substitution in neutron diffraction, Ind Eng Chem Res. 39 (2000) 4491–4495. https://doi.org/10.1021/ie000150i.
[71] E.J. Velásquez, L. Garrido, A. Guarda, M.J. Galotto, C. López de Dicastillo, Increasing the incorporation of recycled PET on polymeric blends through the reinforcement with commercial nanoclays, Appl Clay Sci. 180 (2019) 105185. https://doi.org/10.1016/J.CLAY.2019.105185.
[72] M. Pluta, M.-A. Paul, M. Alexandre, P. Dubois, Plasticized polylactide/clay nanocomposites. I. The role of filler content and its surface organo-modification on the physico-chemical properties, J Polym Sci B Polym Phys. 44 (2006) 299–311. https://doi.org/https://doi.org/10.1002/polb.20694.

[73] P.A. Ulloa, J. Vidal, C. Dicastillo, F. Rodriguez, A. Guarda, R.M.S. Cruz, M.J. Galotto, Development of poly(lactic acid) films with propolis as a source of active compounds: Biodegradability, physical, and functional properties, J Appl Polym Sci. 136 (2019) 47090. https://doi.org/10.1002/app.47090.
[74] E. Velásquez, A. Rojas, C. Piña, M.J. Galotto, C.L. de Dicastillo, Development of bilayer biodegradable composites containing cellulose nanocrystals with antioxidant properties, Polymers (Basel). 11 (2019) 1945. https://doi.org/10.3390/polym11121945.
[75] M. Przybysz-Romatowska, J. Haponiuk, K. Formela, Poly(ε-Caprolactone)/Poly(Lactic Acid) Blends Compatibilized by Peroxide Initiators: Comparison of Two Strategies, Polymers (Basel). 12 (2020) 228. https://doi.org/10.3390/polym12010228.
[76] J.M. Cervantes-Uc, J. V. Cauich-Rodríguez, H. Vázquez-Torres, L.F. Garfias-Mesías, D.R. Paul, Thermal degradation of commercially available organoclays studied by TGA–FTIR, Thermochim Acta. 457 (2007) 92–102. https://doi.org/10.1016/J.TCA.2007.03.008.
[77] S.G. Kazarian, G.G. Martirosyan, Spectroscopy of polymer/drug formulations processed with supercritical fluids: in situ ATR–IR and Raman study of impregnation of ibuprofen into PVP, Int J Pharm. 232 (2002) 81–90. https://doi.org/10.1016/S0378-5173(01)00905-X.
[78] K. Bocz, T. Tábi, D. Vadas, M. Sauceau, J. Fages, G. Marosi, Characterisation of natural fibre reinforced PLA foams prepared by supercritical CO2 assisted extrusion, Express Polym Lett. 10 (2016) 771–779. https://doi.org/10.3144/expresspolymlett.2016.71.
[79] L. Wei, H. Shicheng, Z. Hongfu, Effect of octa(epoxycyclohexyl) POSS on thermal, rheology property, and foaming behavior of PLA composites, J Appl Polym Sci. 135 (2018) 46399. https://doi.org/https://doi.org/10.1002/app.46399.
[80] R. Mort, E. Peters, G. Curtzwiler, S. Jiang, K. Vorst, Biofillers Improved Compression Modulus of Extruded PLA Foams, Sustainability. 14 (2022) 5521. https://doi.org/10.3390/su14095521.
[81] I. Zizovic, A. Trusek, M. Tyrka, I. Moric, L. Senerovic, Functionalization of polyamide microfiltration membranes by supercritical solvent impregnation, Journal of Supercritical Fluids. 174 (2021). https://doi.org/10.1016/j.supflu.2021.105250.
[82] D. Matykiewicz, K. Skórczewska, Characteristics and Application of Eugenol in the Production of Epoxy and Thermosetting Resin Composites: A Review, Materials. 15 (2022) 4824. https://doi.org/10.3390/ma15144824.
[83] E. Velásquez, S. Espinoza, X. Valenzuela, L. Garrido, M.J. Galotto, A. Guarda, C. López de Dicastillo, Effect of Organic Modifier Types on the Physical–Mechanical Properties and Overall Migration of Post-Consumer Polypropylene/Clay Nanocomposites for Food Packaging, Polymers . 13 (2021) 1502. https://doi.org/10.3390/polym13091502.
[84] S. Doroudiani, M.T. Kortschot, Polystyrene foams: II. Structure-impact properties relationships, J Appl Polym Sci. 90 (2003) 1421–1426. https://doi.org/10.1002/app.12805.

[85] Ivheeco, Supermarket Biodegradable Disposable Take Away Customized Tray Food Grade Cornstarch Frozen Food Packaging Container, Ivheeco. (2023). https://www.lvheeco.com/Plate/supermarket-biodegradable-disposable-take-away-customized-tray-food-grade-cornstarch-frozen-food-packaging-container?gclid=CjwKCAiAvoqsBhB9EiwA9XTWGSXn-uHzQvtb0e74GCVP726_Qp8fhiVtMUhjaUwWTBGNQlTFcQgmsBoCSvgQAvD_BwE.
[86] J.H. Schut, Foamed PLA shows promise in biodegradable meat trays, Plastics Technology. 53 (2007) 39–43. https://www.ptonline.com/articles/foamed-pla-shows-promise-in-biodegradable-meat-trays.
[87] G.X. Chen, H.S. Kim, E.S. Kim, J.S. Yoon, Compatibilization-like effect of reactive organoclay on the poly(l-lactide)/poly(butylene succinate) blends, Polymer (Guildf). 46 (2005) 11829–11836. https://doi.org/10.1016/j.polymer.2005.10.056.
[88] A.R. Mukurumbira, R.A. Shellie, R. Keast, E.A. Palombo, S.R. Jadhav, Encapsulation of essential oils and their application in antimicrobial active packaging, Food Control. 136 (2022) 108883. https://doi.org/10.1016/J.FOODCONT.2022.108883.
[89] J.Y. Chen, H. Wu, C.Y. Guo, B. Zhu, G. Bin Ren, Enhancing the solubility of natural compound xanthotoxin by modulating stability via cocrystallization engineering, Int J Pharm. 572 (2019) 118776. https://doi.org/10.1016/J.IJPHARM.2019.118776.
[90] G. Michailidou, E. Christodoulou, S. Nanaki, P. Barmpalexis, E. Karavas, S. Vergkizi-Nikolakaki, D.N. Bikiaris, Super-hydrophilic and high strength polymeric foam dressings of modified chitosan blends for topical wound delivery of chloramphenicol, Carbohydr Polym. 208 (2019) 1–13. https://doi.org/10.1016/J.CARBPOL.2018.12.050.
[91] K. Trongchuen, A. Ounkaew, P. Kasemsiri, S. Hiziroglu, W. Mongkolthanaruk, R. Wannasutta, U. Pongsa, P. Chindaprasirt, Bioactive Starch Foam Composite Enriched With Natural Antioxidants from Spent Coffee Ground and Essential Oil, Starch - Stärke. 70 (2018) 1700238. https://doi.org/10.1002/star.201700238.
[92] A. Rojas, D. Misic, C.L. de Dicastillo, I. Zizovic, E. Velásquez, D. Gutiérrez, G. Aguila, C.P. Vidal, A. Guarda, M.J. Galotto, A review on thymol-based bioactive materials for food packaging, Ind Crops Prod. 202 (2023) 116977. https://doi.org/10.1016/J.INDCROP.2023.116977.
[93] A. Celebioglu, T. Uyar, Electrohydrodynamic encapsulation of eugenol-cyclodextrin complexes in pullulan nanofibers, Food Hydrocoll. 111 (2021) 106264. https://doi.org/10.1016/J.FOODHYD.2020.106264.
[94] R. Requena, M. Vargas, A. Chiralt, Release kinetics of carvacrol and eugenol from poly(hydroxybutyrate-co-hydroxyvalerate) (PHBV) films for food packaging applications, Eur Polym J. 92 (2017) 185–193. https://doi.org/10.1016/J.EURPOLYMJ.2017.05.008.
[95] M.L. Goñi, N.A. Gañán, M.C. Strumia, R.E. Martini, Eugenol-loaded LLDPE films with antioxidant activity by supercritical carbon dioxide impregnation, J Supercrit Fluids. 111 (2016) 28–35. https://doi.org/10.1016/J.SUPFLU.2016.01.012.
[96] F. Velázquez-Contreras, N. García-Caldera, J.D.P. de la Rosa, D. Martínez-Romero, E. Núñez-Delicado, J.A. Gabaldón, Effect of pla active packaging containing

monoterpene-cyclodextrin complexes on berries preservation, Polymers (Basel). 13 (2021). https://doi.org/10.3390/polym13091399.
[97] M.I. Rodríguez-López, M.T. Mercader-Ros, J.A. Pellicer, V.M. Gómez-López, D. Martínez-Romero, E. Núñez-Delicado, J.A. Gabaldón, Evaluation of monoterpene-cyclodextrin complexes as bacterial growth effective hurdles, Food Control. 108 (2020) 106814. https://doi.org/10.1016/j.foodcont.2019.106814.
[98] C. Shen, M. Wu, C. Sun, J. Li, D. Wu, C. Sun, Y. He, K. Chen, Chitosan/PCL nanofibrous films developed by SBS to encapsulate thymol/HPβCD inclusion complexes for fruit packaging, Carbohydr Polym. 286 (2022). https://doi.org/10.1016/j.carbpol.2022.119267.
[99] A. Torres, C.L. De Dicastillo, M. Ríos, I. Bastias, A. Guarda, M.J. Galotto, Effect of organoclay incorporation on thermal, physical and morphological properties of LLDPE nanocomposites for active food packaging applications, Journal of the Chilean Chemical Society. 59 (2015) 2681–2685. https://doi.org/10.4067/s0717-97072014000400011.
[100] S.I. Hong, J.W. Rhim, Preparation and properties of melt-intercalated linear low density polyethylene/clay nanocomposite films prepared by blow extrusion, LWT - Food Science and Technology. 48 (2012) 43–51. https://doi.org/10.1016/J.LWT.2012.03.009.
[101] S.I. Hong, L.F. Wang, J.W. Rhim, Preparation and characterization of nanoclays-incorporated polyethylene/thermoplastic starch composite films with antimicrobial activity, Food Packag Shelf Life. 31 (2022) 100784. https://doi.org/10.1016/J.FPSL.2021.100784.
[102] W. Zhang, R. Liu, X. Sun, H. An, T. Min, Z. Zhu, Y. Wen, Leaf-stomata-inspired packaging nanofibers with humidity-triggered thymol release based on thymol/EVOH coaxial electrospinning, Food Research International. 162 (2022) 112093. https://doi.org/10.1016/J.FOODRES.2022.112093.
[103] Z. Wang, F. Zhan, D. Zhang, Y. Wang, Y. Qiu, J. Zhang, L. Wang, L. Zhao, Relative humidity-triggered polyamide 4/Cinnamaldehyde core-shell nanofibers for antibacterial packaging, J Food Eng. 357 (2023) 111635. https://doi.org/10.1016/J.JFOODENG.2023.111635.
[104] J. Pantwalawalkar, H. More, D. Bhange, U. Patil, N. Jadhav, Novel curcumin ascorbic acid cocrystal for improved solubility, J Drug Deliv Sci Technol. 61 (2021) 102233. https://doi.org/10.1016/J.JDDST.2020.102233.
[105] P. Roy, N. Pandey, N. Kumari, R. Baidya, Y.S. Mary, Y.S. Mary, A. Ghosh, Development of sulfamethoxazole-succinimide cocrystal by mechanochemical cocrystallization – An insight into spectroscopic, electronic, chemical conformation and physicochemical properties, Chemical Engineering Research and Design. 185 (2022) 446–457. https://doi.org/10.1016/J.CHERD.2022.07.012.
[106] A. Rojas, E. Velásquez, C.P. Vidal, A. Guarda, M.J. Galotto, C.L. de Dicastillo, Active PLA packaging films: Effect of processing and the addition of natural antimicrobials and antioxidants on physical properties, release kinetics, and compostability, Antioxidants. 10 (2021). https://doi.org/10.3390/antiox10121976.

[107] E. Velásquez, C. Patiño Vidal, A. Rojas, A. Guarda, M.J. Galotto, C. López de Dicastillo, Natural antimicrobials and antioxidants added to polylactic acid packaging films. Part I: Polymer processing techniques, Compr Rev Food Sci Food Saf. 20 (2021) 3388–3403. https://doi.org/10.1111/1541-4337.12777.
[108] S. Sharma, S. Barkauskaite, A.K. Jaiswal, S. Jaiswal, Essential oils as additives in active food packaging, Food Chem. 343 (2021) 128403. https://doi.org/10.1016/J.FOODCHEM.2020.128403.
[109] S. Report, Salmonellosis, (2022) 1–9.
[110] S. Report, Listeriosis. AER 2021, (2022).
[111] P. Rodríguez-López, J. Rodríguez-Herrera, D. Vázquez-Sánchez, M. López Cabo, Current Knowledge on Listeria monocytogenes Biofilms in Food-Related Environments: Incidence, Resistance to Biocides, Ecology and Biocontrol, Foods. 7 (2018) 85. https://doi.org/10.3390/foods7060085.
[112] P. Korzeniowski, P. Śliwka, M. Kuczkowski, D. Mišić, A. Milcarz, M. Kuźmińska-Bajor, Bacteriophage Cocktail Can Effectively Control Salmonella Biofilm in Poultry Housing, Front Microbiol. 13 (2022) 1–11. https://doi.org/10.3389/fmicb.2022.901770.
[113] A.W.M. Suijkerbuijk, M. Bouwknegt, M.J.J. Mangen, G.A. De Wit, W. Van Pelt, P. Bijkerk, I.H.M. Friesema, The economic burden of a Salmonella Thompson outbreak caused by smoked salmon in the Netherlands, 2012-2013, Eur J Public Health. 27 (2017) 325–330. https://doi.org/10.1093/eurpub/ckw205.
[114] A. Martín, M.J. Cocero, Micronization processes with supercritical fluids: Fundamentals and mechanisms, Adv Drug Deliv Rev. 60 (2008) 339–350. https://doi.org/10.1016/J.ADDR.2007.06.019.
[115] S.N. Madanayake, A. Manipura, R. Thakuria, N.M. Adassooriya, Opportunities and Challenges in Mechanochemical Cocrystallization toward Scaled-Up Pharmaceutical Manufacturing, Org Process Res Dev. 27 (2023) 409–422. https://doi.org/10.1021/ACS.OPRD.2C00314.
[116] L. Padrela, M.A. Rodrigues, S.P. Velaga, H.A. Matos, E.G. de Azevedo, Formation of indomethacin–saccharin cocrystals using supercritical fluid technology, European Journal of Pharmaceutical Sciences. 38 (2009) 9–17. https://doi.org/10.1016/J.EJPS.2009.05.010.
[117] L. MacEachern, A. Kermanshahi-Pour, M. Mirmehrabi, Supercritical carbon dioxide for pharmaceutical co-crystal production, Cryst Growth Des. 20 (2020) 6226–6244. https://doi.org/10.1021/acs.cgd.0c00571.

Declaration of Interest Statement

No conflicts of interest